Natural Resources Canada | Ressources naturelles Canada

GEOLOGICAL SURVEY OF CANADA
OPEN FILE 7771

Till and bedrock heavy mineral signatures of the Kiggavik uranium deposits, Nunavut

S.V.J. Robinson, C.W. Jefferson, R.C. Paulen,
D. Layton-Matthews, B. Joy, and D. Quirt

2016

Canada

GEOLOGICAL SURVEY OF CANADA
OPEN FILE 7771

Till and bedrock heavy mineral signatures of the Kiggavik uranium deposits, Nunavut

S.V.J. Robinson[1], C.W. Jefferson[2], R.C. Paulen[2], D. Layton-Matthews[1], B. Joy[1], and D. Quirt[3]

[1]Queen's University, Kingston, Ontario
[2]Geological Survey of Canada, Ottawa, Ontario
[3]AREVA Resources Canada Inc., Saskatoon, Saskatchewan

2016

doi:10.4095/297563

This publication is available for free download through GEOSCAN (http://geoscan.nrcan.gc.ca/)

Recommended citation

Robinson, S.V.J., Jefferson, C.W., Paulen, R.C., Layton-Matthews, D., Joy, B., and Quirt, D., 2016. Till and bedrock heavy mineral signatures of the Kiggavik uranium deposits, Nunavut; Geological Survey of Canada, Open File 7771, 1 zip file. doi:10.4095/297563

Publications in this series have not been edited; they are released as submitted by the author.

Contribution to the Geological Survey of Canada's Geo-mapping for Energy and Minerals (GEM) Program (2008–2013)

TABLE OF CONTENTS

Figures

Tables

Till and bedrock heavy mineral signatures of the Kiggavik uranium deposits, Nunavut

S.V.J. Robinson[1], C.W. Jefferson[2], R,C. Paulen[2], D. Layton-Matthews[1], B. Joy[1], and D. Quirt[3]

[1]Department of Geological Sciences, Queen's University, Kingston, Ontario K7L 3N6
[2]Geological Survey of Canada, 601 Booth Street, Ottawa, Ontario K1A 0E8
[3]AREVA Resources Canada Inc., 817 45th Street West, Saskatoon, Saskatchewan S7L 5X2

ABSTRACT

In 2010, a drift prospecting study was initiated over the Kiggavik uranium (U) deposit under the Geomapping for Energy and Minerals (GEM) Program. The objective of this study was to document the till geochemical and heavy mineral signatures of the Kiggavik U deposit and to identify potential applications of those characteristics in future exploration for drift-covered, basement-hosted, unconformity-related U deposits. The study area is within the zone affected by the migration of the Keewatin Ice Divide of the Laurentide Ice Sheet. Mineralized and non-mineralized bedrock and near-surface till samples (n = 71) were collected directly overlying, up-ice, and at various distances (50 m, 100 m, 200 m, 500 m, 1 km, 2 km, 3 km, 5 km, and 10 km) in a fan-shaped pattern down-ice from the deposit with respect to the dominant north-northwest, northwest, and west ice-flow directions.

Detailed microscopy and microprobe analysis of ore samples from drill core reaffirmed uraninite and coffinite as the dominant ore minerals at the Kiggavik U deposit, with accessory galena, pyrite and very minor native gold associations. These minerals are predominantly very fine-grained and rarely exceed 100 μm in diameter, with the exception of rare massive crystalline uraninite.

Examination of the sand-size heavy mineral concentrate (HMC) from till yielded no U-rich or directly associated accessory ore minerals, reflecting the overall fine-grained nature and instability of these minerals in oxidizing conditions such as those found in near-surface till. This ultimately limits the utility of these minerals as empirical indicators of U deposits.

Native gold grains in till samples collected in this study are, however, more abundant than those in regional background samples. Elevated counts were found up to 3 km down-ice of the Kiggavik Main Zone (KMZ) in a west-northwest direction. The sample containing the highest gold grain count in till was collected directly overlying the KMZ, suggesting local provenance and the applicability of native gold as an indicator mineral for Kiggavik-style unconformity-type U deposits. Moreover, Pb-rich fluorapatite grains (up to 8% PbO), from the alteration zone around the KMZ U deposit, are of particular interest due to their uniqueness, stability under near-surface weathering conditions, and thus their potential to be an indicator mineral for such deposits. However the fluorapatite grains are very finely crystalline, as are the main U-bearing phases observed in ore samples, therefore a new technique to separate, collect, and identify the finer fraction of the HMC needs to be developed.

INTRODUCTION

Mineral exploration in Canada and Fennoscandia has successfully utilized till geochemistry for Au (e.g. Averill, 1988; McClenaghan, 2001), base metals (e.g. Kaszycki et al., 1996; Parkhill and Doiron, 2003), and rare earth elements (e.g. McConnell and Batterson, 1987). Most of the published case studies that document the geochemical dispersal signatures from U deposits (e.g. Earle, 2001; Campbell, 2009) are from the Athabasca Basin, and very little has been published on drift prospecting from other basins in northern Canada. However, Robinson et al. (2014) and Robinson (2015) built on studies by Aylsworth and Shilts (1989), Aylsworth et al. (1990), Grunsky et al. (2006, 2009), McMartin and McClenaghan (2001), McMartin and Henderson (2004), McMartin and Dredge (2005), and McMartin et al. (2006, 2008) to refine ice-flow directions and document the till geochemical signatures of the Kiggavik uranium (U) exploration camp, which flanks the northeastern part of the Thelon Basin. The Kiggavik camp, located in the Kivalliq Region of Nunavut (Figs. 1, 2), is an ideal location for drift prospecting studies because several of the mineral occurrences subcrop beneath glacial cover and collaborative work with geoscientist conducting bedrock mapping under the GEM Program (e.g. Jefferson et al., 2011c) provides an up-to-date bedrock context for these surficial studies.

This study is the second part of a thesis project completed by Robinson (2015) to understand the metallic, oxide, and silicate indicator minerals associated with U minerals and alteration of the Kiggavik deposits, as well as the mineral abundances, their spatial distributions, grain morphologies, and respective transport distances down-ice. To achieve these objectives, representative samples were taken of mineralized zones,

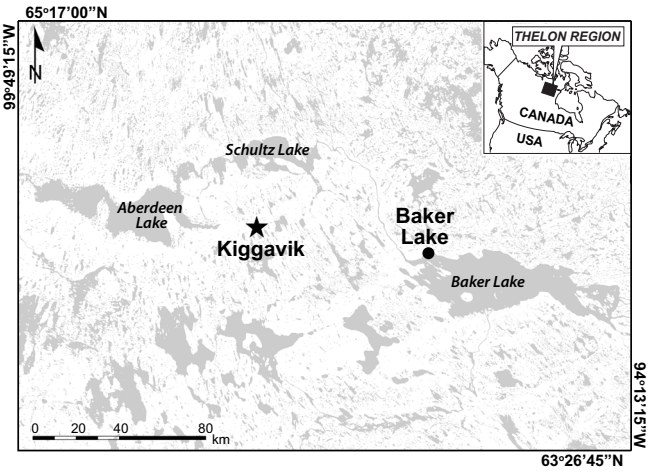

Figure 1. General geographic setting of the Kiggavik study area in the central Kivalliq Region of Nunavut. The broad sweep of elongate lakes trending northwesterly at Baker Lake through north-northeasterly over Aberdeen Lake reflects surficial landforms created by a major Quaternary ice flow direction.

hydrothermally altered and least-altered host rocks from the Kiggavik Main and Centre zones, and from outcrops at both camp-and regional-scales. An additional 71 bulk till samples were collected and processed to isolate a heavy mineral concentrates (HMC) which were compared to the mineralogical compositions of the bedrock samples. Thin section petrography, binocular microscopy, heavy mineral picking, scanning electron microscopy, and microprobe analysis documented the heavy mineral concentrate from the bulk till samples to develop an indicator mineral suite of buried, drift-covered U deposits.

Project location and physiography

Uranium deposits in the Kiggavik exploration camp are located in the central Kivalliq Region of Nunavut, in the Schultz Lake topographic map sheet (NTS 66A/05; Fig. 1). The Kiggavik Main Zone (KMZ) trench is approximately 80 km west of the community of Baker Lake at 64º26'32" north and 97º38'50" west (UTM easting 565119, northing 7146985; Datum NAD83, zone 14). The study area lies on the northern edge of the Kazan Upland, at the intersection of the Thelon Plain, Back Lowland, and Wager Plateau physiographic divisions of the Kazan Region of the Canadian Shield (Bostock, 1970). The region is underlain by continuous permafrost with the depth of the active layer varying from 15 to 200 cm, depending on the sediment type and drainage conditions (McMartin et al., 2006). The vegetation is characteristic of open tundra (dwarf trees, shrubs, sedges, and grasses). In the study area around Kiggavik, the relief is low and glacially streamlined, bogs are thinly developed, and the abundant shallow-water bodies range from 25 m ponds to 5 km lakes. These freeze solid in winter, with the exception of the deeper lakes that are greater than 1–2 km in diameter (McMartin et al., 2006). Regional Quaternary ice-flow directions are summarized by McMartin and Henderson (2004) and McMartin and Dredge (2005), with details of the Kiggavik U camp provided in Robinson et al. (2014).

Exploration history of the Kiggavik uranium camp

Exploration for U in Proterozoic supracrustal successions within the Churchill structural province was initiated after reconnaissance bedrock mapping during the 1950s by Wright (1955) and subsequent stratigraphic work by Donaldson (1965). With the discovery of the high-grade Rabbit Lake U deposit in the Athabasca Basin, U exploration in and around the late Paleoproterozoic Thelon Basin began due to its geological similarities (Miller and LeCheminant, 1985). Exploration in the vicinity of the KMZ (initially named the Lone Gull deposit) has been ongoing since the 1970s, when Urangesellschaft Canada Limited (UGC) selected this area for its similarity to the eastern part of the Athabasca Basin (Fuchs et al., 1985). In 1974, much of the Thelon Formation and the adjacent basement rocks were systematically explored using lake sediment, water, and airborne radiometric surveys. This program led to the discovery of a strong geochemical anomaly hosted in radioactive frost boils overlying the KMZ (Reilly, 1997). Drilling in the late 1970s outlined significant U in structurally controlled zones within what was then termed "dirty quartzite" (Griep, 1978).

Follow-up gravimetric, EM-16 VLF, and resistivity surveys, overburden drilling, and geochemical soil sampling took place in the late 1970s and lead to the discovery of two smaller deposits, which subcrop beneath glacial sediments approximately 600 m and 1200 m east-northeast of the KMZ (Griep et al., 1980). These deposits are now called the Centre (CZ) and East (EZ) zones. The 1970s drilling, which encompassed over 25,000 m in 200 diamond drill holes, outlined the two cigar-shape bodies of the KMZ and CZ zones. Also discovered were additional radiometric anomalies to the west and southwest of the KMZ at approximately 6 and 15 km, respectively. In 1988, open pit mining was proposed for both the KMZ and CZ, with minable reserve estimates of 14,307 tonnes U at 0.424% (Beak Consultants Limited, 1988).

Mineralogical, petrographic, and structural studies of the Kiggavik deposits were undertaken during the late 1980s and early 1990s (Fuchs et al., 1985; Weyer et al., 1989; Weyer, 1992). By 1985, regional programs were terminated and UGC focussed on the KMZ. With the addition of venture partners Daewoo and PNC, airborne geophysical surveys using the Dighem IV

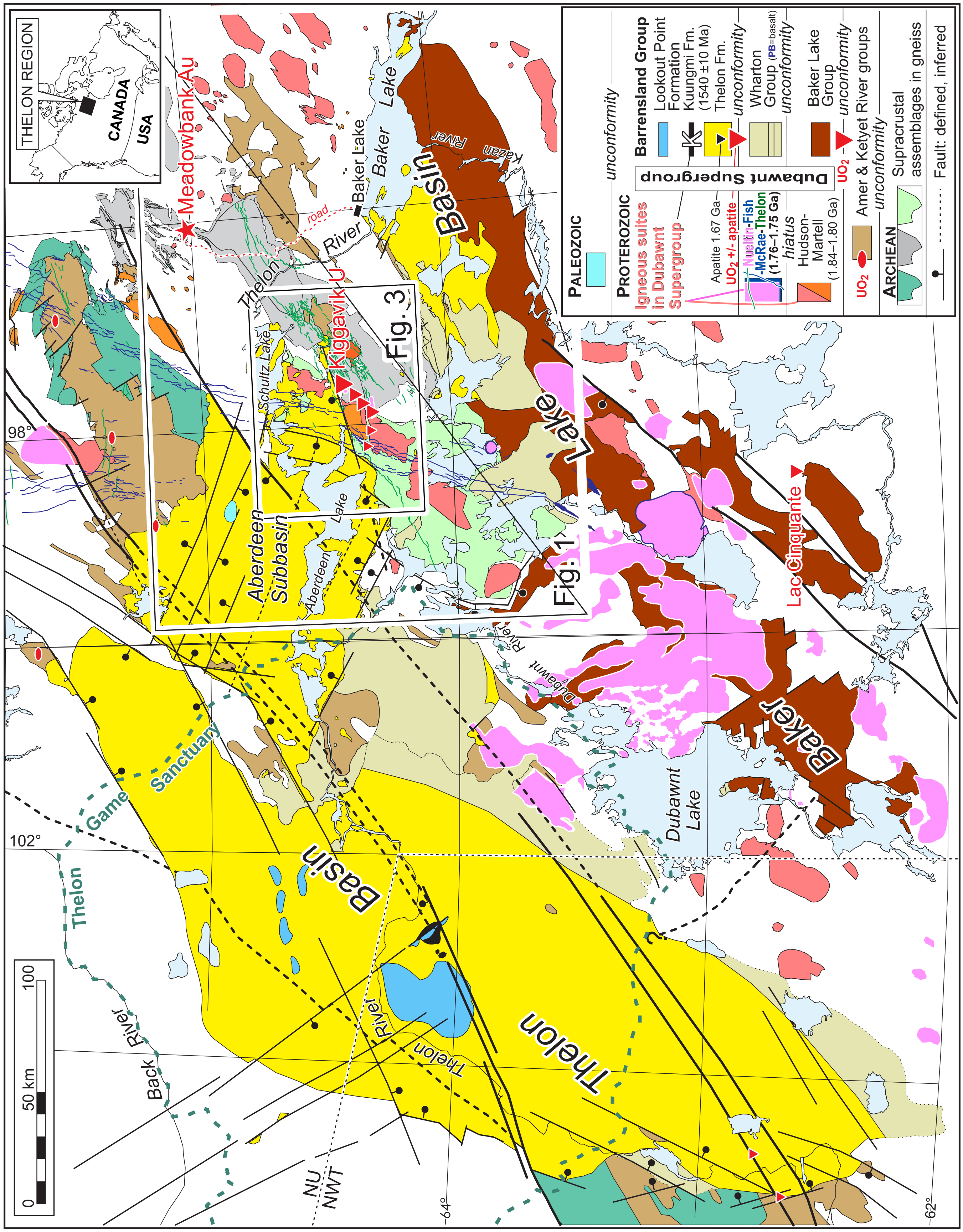
THELON REGION
CANADA
USA
Meadowbank Au
Kiggavik U
Fig. 3
Fig. 1
Lac Cinquante
Baker Lake
Baker Lake Basin
Thelon Basin
Aberdeen Subbasin
Schultz Lake
Aberdeen Lake
Dubawnt Lake
Thelon River
Back River
Kazan River
Dubawnt River
Thelon Game Sanctuary
road
NU
NWT
0 50 km 100
98°
102°
64°
62°
PALEOZOIC
unconformity
PROTEROZOIC
Igneous suites in Dubawnt Supergroup
Barrensland Group
Lookout Point Formation
Kuungmi Fm. (1540 ±10 Ma)
Thelon Fm.
unconformity
Apatite 1.67 Ga
UO2 +/- apatite
Nueltin-Fish -McRae-Thelon (1.76–1.75 Ga)
Wharton Group (PB=basalt)
unconformity
hiatus
Hudson-Martell (1.84–1.80 Ga)
Baker Lake Group
unconformity
Dubawnt Supergroup
UO2
Amer & Ketyet River groups
unconformity
ARCHEAN
Supracrustal assemblages in gneiss
Fault: defined, inferred

system soon discovered resistivity and ground gravity lows along the east-northeast-trending Judge Sissons Fault, which led to the discovery of two additional buried deposits (Andrew Lake and End Grid deposits) located 15 to 17 km southwest of KMZ (Reilly, 1997).

In 1993, COGEMA Incorporated (COGEMA) became the operator of the project by acquiring 69% of Urangesellschaft. Detailed petrographic studies were completed on the host rocks, alteration, and ore mineralogy of the Kiggavik deposits (Pacquet, 1993; Reyx, 1994). No further exploration took place and little work was done on the Kiggavik deposits until late 1997 when J.H. Reedman and Associated Limited conducted a pre-feasibility study on behalf of COGEMA (Morrison, 2009).

Between 1997 and 2006, partial rehabilitation and field inspection/assessment work removed the most derelict of the original Lone Gull camp buildings and radioactive core was relocated to a nearby enclosed site. Cleanup of the exploration camp continued until work began in mid-2006 to prepare for future feasibility studies on the Kiggavik, End Grid, and Andrew Lake deposits (Morrison, 2009). During the 2008 summer drilling program, COGEMA changed its name to AREVA Resources Canada and expanded exploration outside of the main deposits to identify prospective areas (Morrison, 2009). This program added 19 diamond drill holes through the Kiggavik, Andrew Lake, and End Grid deposits, primarily for geotechnical and/or metallurgical purposes, and an additional 10 holes to evaluate the Bong and Granite Grid prospects (D. Quirt, pers. comm., 2012) (Fig. 3).

Bedrock geology

The late Paleoproterozoic Thelon Basin was much larger than the current erosional and structural remnants, as supported by the presence of sandstone outliers beyond the present extents and westerly paleocurrents of the Thelon Formation preserved in both the Thelon Basin and the Baker Lake Basin to the east (Hiatt et al., 2003; Rainbird et al., 2003; R. Hunter, oral presentation, Nunavut Mining Symposium, April 2011; Jefferson et al., 2011a–c). The Thelon Basin refers to the area occupied by part of the Barrensland Group that is west of the Baker Lake Basin and has been subdivided (Tschirhart et al., 2011) into two subbasins: 1) the 500 by 200 km main western basin, and 2) the ~100 by 110 km northeastern portion, termed the Aberdeen subbasin (Fig. 2).

The Kiggavik U deposits are interpreted to have formed beneath a much broader primary Aberdeen subbasin, and as such are classified as basement-hosted, unconformity-related deposits (Fuchs et al., 1985; Miller and LeCheminant, 1985; Fuchs and Hilger, 1989; Jefferson et al., 2007, 2011c, 2013). The prospective deposits are located in basement terrane, just southeast of the preserved Aberdeen subbasin, separated from the southeast corner of the subbasin by the Thelon Fault (Fig. 3). The basement rocks are dominantly metasedimentary, with subordinate metavolcanic and intrusive rocks. The Neoarchean and early Paleoproterozoic metasedimentary and minor metavolcanic rocks are highly deformed but weakly metamorphosed, interfolded, and thrust-repeated (Jefferson et al., 2011c, 2013b).

The Neoarchean-Paleoproterozoic structural package was intruded by late-orogenic granite sills, laccoliths, and localized plugs of the Hudson Suite and numerous ultrapotassic mafic to felsic dykes, all ca.1.83 Ga (Peterson et al., 2002; Scott et al., 2015). The first major sequence of the Dubawnt Supergroup is the Baker Lake Group, deposited from 1.84 to 1.81 Ga in the Baker Lake and related basins to the south and east of Kiggavik (Fig. 2; Rainbird et al., 2003). The Baker Lake Group comprises intercalated conglomerate and sandstone of the Kazan and South Channel formations intercalated with ultrapotassic bimodal volcanic rocks of the Christopher Island Formation (CIF) within a deep strike-slip basin. The CIF intrusive equivalents in the Kiggavik camp include the Martell syenite (mingled with the Hudson granite) and abundant minette (lamprophyre) plus bostonite (microsyenite) dykes that transect the camp. These intrusions were altered near and within U deposits as part of the ore-forming process but are essentially barren of U oxide mineral phases (Figs. 2, 3). The Kunwak Formation conglomerate filled late extensional basins at the top of the Baker Lake Group.

The region was peneplaned, deeply weathered, and unconformably overlain by aeolian to alluvial sandstone and conglomerate of the Amarook Formation, which is the lower part of the Wharton Group and begins the middle sequence of the Dubawnt Supergroup. Shortly after deposition of the Amarook Formation, the region was impacted by undeformed bimodal products of the 1.77–1.74 Ga Kivalliq Igneous Suite (KIS) (Peterson et al., 2014, 2015a,b), which comprise volcanic and epiclastic rocks of the Pitz Formation (upper Wharton Group) and multiple intrusive components: the Nueltin Granite, Mallery Gabbro

Figure 2 opposite page. Regional geology of the Baker Lake and Thelon basins, the Dubawnt Supergroup, and the older supracrustal belts (after Jefferson et al., 2011c, 2013). Uranium showings and occurrences are annotated by red triangles, the Andrew Lake and Kiggavik deposits being the largest. Baker Lake community is denoted by a black rectangle. The locations of Figures 1 and 3 are outlined.

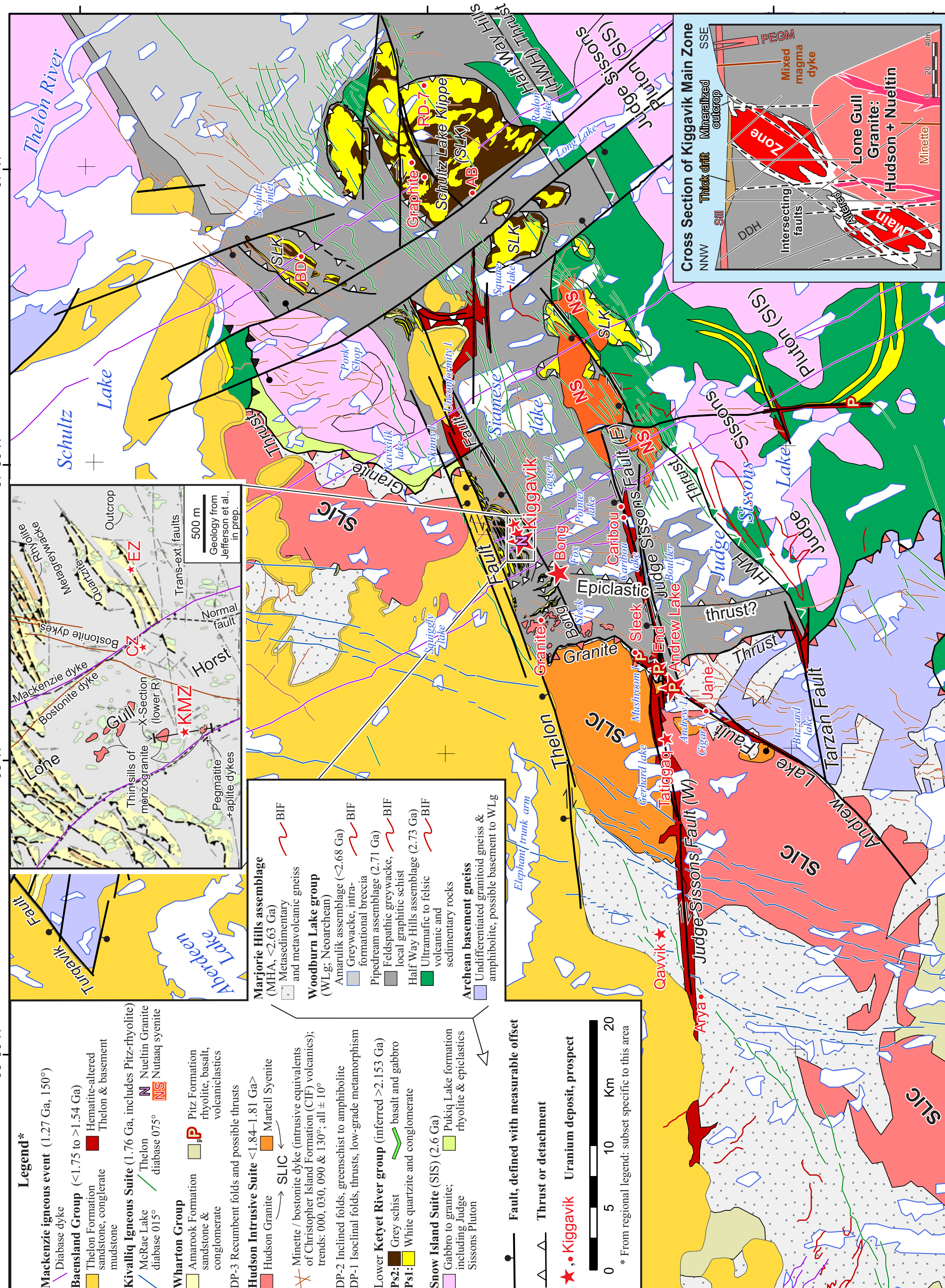
Legend*
Mackenzie igneous event (1.27 Ga, 150°)
Diabase dyke
Baensland Group (<1.75 to >1.54 Ga)
Thelon Formation sandstone, conglomerate mudstone
Hematite-altered Thelon & basement
Kivalliq Igneous Suite (1.76 Ga, includes Pitz-rhyolite)
McRae Lake diabase 015°
Thelon diabase 075°
Nueltin Granite
Nutaaq syenite
Wharton Group
Amarook Formation sandstone & conglomerate
Pitz Formation rhyolite, basalt, volcaniclastics
DP-3 Recumbent folds and possible thrusts
Hudson Intrusive Suite <1.84–1.81 Ga>
Hudson Granite
Martell Syenite
SLIC
Minette / bostonite dyke (intrusive equivalents of Christopher Island Formation (CIF) volcanics); trends: 000, 030, 090 & 130°; all ± 10°
DP-2 Inclined folds, greenschist to amphibolite
DP-1 Isoclinal folds, thrusts, low-grade metamorphism
Lower Ketyet River group (inferred >2.153 Ga)
Ps2: Grey schist
Ps1: White quartzite and conglomerate
basalt and gabbro
Snow Island Suite (SIS) (2.6 Ga)
Gabbro to granite; including Judge Sissons Pluton
Pukiq Lake formation rhyolite & epiclastics
Fault, defined with measurable offset
Thrust or detachment
Uranium deposit, prospect
Km
0 5 10 20
* From regional legend: subset specific to this area
Marjorie Hills assemblage (MHA, <2.63 Ga)
Metasedimentary and metavolcanic gneiss
BIF
Woodburn Lake group (WLg, Neoarchean)
Amarulik assemblage (<2.68 Ga)
Greywacke, intra-formational breccia
Pipedream assemblage (2.71 Ga)
Feldspathic greywacke, local graphitic schist
Half Way Hills assemblage (2.73 Ga)
Ultramafic to felsic volcanic and sedimentary rocks
Archean basement gneiss
Undifferentiated granitoid gneiss & amphibolite, possible basement to WLg
98°30'W
98°W
97°30'W
97°W
64°45'N
64°30'N
64°15'N
Thelon River
Schultz Lake
Aberdeen Lake
Turqavik Fault
Elephant trunk arm
Thelon Fault
Half Way Hills (HWH) Thrust
Judge Sissons Pluton (SIS)
Schultz Lake Klippe (SLK)
Judge Sissons Fault (F)
Judge Sissons Fault (W)
Judge Sissons Lake
Andrew Lake Fault
Tarzan Fault
Siamese lake
Kiggavik
Bong
Caribou
Granite
Sleek
End
Andrew Lake
Jane
Tatiggaq
Qavvik
Arya
Graphite
RD-7
AB
BD
SLIC
NS
Epiclastic
thrust?
Thrust
Lone Gull
Horst
KMZ
EZ
Cz
Mackenzie dyke
Bostonite dyke
Bostonite dykes
Rhyolite
Metagreywacke
Quartzite
Outcrop
Trans-ext. faults
Normal fault
Thin sills of monzogranite
X-Section (lower R)
Pegmatite +aplite dykes
500 m
Geology from Jefferson et al., in prep.
Cross Section of Kiggavik Main Zone
NNW
SSE
Sill
Thick drift
Mineralized outcrop
DDH
Intersecting faults
Main Zone
PEGM
Mixed magma dyke
Lone Gull Granite: Hudson + Nueltin
Minette
0 20 40m

(anorthositic), and two sets of diabase dykes — the 015° McRae Lake and 075° Thelon River swarms. The Amarook Formation and KIS were in turn block faulted, peneplaned, deeply weathered, and unconformably overlain in the study area by the three major sequences of the Barrensland Group: conglomerate, red mudstone, and pale pink sandstone of the Thelon Formation, ultrapotassic mafic flows of the Kuungmi Formation, and carbonate strata of the Lookout Point Formation (Gall et al., 1992) (Fig. 3).

Urangesellschaft's detailed bedrock mapping and drilling of the Kiggavik deposit area (Fuchs et al., 1985; Miller and LeCheminant, 1985; Fuchs and Hilger, 1989) concluded that the most prospective U prospects is hosted in Neoarchean quartzofeldspathic metasedimentary rock with minor iron formation, although a portion of the KMZ is hosted by the Lone Gull granitoid intrusion (Fuchs et al., 1985; Weyer et al., 1989; Reyx, 1994). Detailed mapping and drilling by AREVA Resources Canada Inc., and regional to targeted mapping in and around the camp by Pehrsson et al. (2010, 2013), Jefferson et al. (2011c, 2015), McEwan et al. (2011), and Scott et al. (2015) have corroborated the early rock types and interpreted them in a modern stratigraphic, structural, and geochronological context. The host rocks include 2.7 Ga metagreywacke with schistose metapelite partings, 2.6 Ga rhyolite and thinly bedded epiclastic rocks of the Pukiq Lake Formation, and marginal zones of the Lone Gull plug. Quartzite is common within and overlying the deposits but is not mineralized. All depositional layering is transposed parallel to S_1 schistose foliation, which dips gently north in the area of the deposits. Layers of greywacke, rhyolite-epiclastic and quartzite are structurally intercalated multiple times in an east-west panel flanking the south side of the Thelon Fault and in a north-south-trending panel west of the Bong deposit (Fig. 3). Details of these rock types are provided in the Bedrock Petrology section and linked appendices of this report.

Outcrops of the Thelon Formation closest to the Kiggavik U camp are on the north side of the Thelon Fault, 2 km north of the KMZ (Fuchs and Hilger, 1989). The Ayra occurrence, one of the new discoveries by Cameco Corp. (R. Hunter, oral presentation, Nunavut Mining Symposium, April 5, 2011), is located 40 km to the west-southwest of Kiggavik and is overlain by an outlier of the Thelon Formation, supporting the unconformity association for deposits of the Kiggavik camp. The border phases of the complex Lone Gull granite intrusion also are clay-altered and host disseminated uraninite. This intrusion comprises dominantly equigranular Hudson granite dated at 1.83 Ga and was invaded and metasomatized by hypabyssal Nueltin granite that is part of the 1.77–1.74 Ga KIS (Scott, 2012; Peterson et al., 2015a,b; Scott et al., 2015).

The host rocks of the Kiggavik deposits were overprinted by hydrothermal alteration that is most strongly developed along steeply dipping, intersecting, brittle fault zones. Two of the most prominent regional faults are the east-northeast-trending Thelon Fault, ~2 km north of Kiggavik, and the Judge Sissons Fault, ~8.5 km to the south (Fig. 3). These are the best exposed parts of an interpreted array of such faults (Jefferson et al., 2011c), one or more of which trend directly through the Kiggavik deposits. The Kiggavik deposits are localized by intersections of these faults with northeast- and northwest-trending faults. The existence and importance of these fault systems have long been recognized by exploration geologists (Fuchs and Hilger, 1989; R. Hunter, oral presentation, Nunavut Mining Symposium, April 5, 2011).

Three separate deposits have been drilled in the immediate Kiggavik area, the following descriptions of which are summarized from Fuchs et al. (1985), and Fuchs and Hilger (1989), and Weyer et al. (1989) except where noted. The Main and Center zones (KMZ and CZ) are approximately 600 m apart and both are on a 065º-trending fault zone. The East zone (EZ) is 500 m east of the CZ (Campbell and Clark, 2009). The KMZ is the largest, comprising two major subparallel en echelon lenses within the same fault zone. These lenses are elongate, plunging to the east-northeast at 25º to a depth of 150–190 m, and are hosted by both metagreywacke and the border phase of the Lone Gull granite. Most of the KMZ subcrops beneath <10 m of glacial till but a small part of it is exposed on the surface, where it was trenched during initial exploration and sampled by this study. The CZ also comprises two defined lenses; these are hosted by metagreywacke and metarhyolite, which sandwich a barren quartzite unit that dips shallowly to the north. The EZ, located approximately 150 m along strike, is similar to the CZ in that the disseminated uraninite is restricted to within 100 m of the surface.

The U deposits are enclosed by intense alteration haloes, which are characterized by dequartzification and conversion of feldspar and mica to clay minerals, dominantly illite and sericite (Fuchs and Hilger, 1989;

Figure 3 opposite page. Bedrock geology of the Kiggavik camp in the western Schultz Lake and eastern Aberdeen Lake map areas (NTS 66A, B, respectively). Details of the Kiggavik Main Zone (KMZ) deposit are shown in the inset map at the top and the cross section at the bottom-right (modified from Scott et al., 2015 by including new knowledge from auriferous sample 10PTA-R047, which was collected at the southeast corner of the map area).

Table 1. List of U-bearing and associated minerals in the Kiggavik deposits (Fuchs et al., 1985; Weyer et al., 1989; Pacquet, 1993; Reyx, 1994; this study).

Mineral	Chemical Formula
Uraninite	UO_2
Coffinite	$(U^{4+},Th)(SiO_4)_{1-x}(OH)_{4x}$
Uranophane	$Ca(UO_2)_2[HSiO_4]_2 \cdot 5H_2O$
Gold	Au
Molybdenite	MoS_2
Fluoroapatite	$Ca_5(Pb)(PO_4)_3(F,Cl,OH)$
Rutile / Anatase	TiO_2
Pyrite / Marcasite	FeS
Hematite	Fe_2O_3
Limonite	$FeO(OH) \cdot nH_2O$
Galena	PbS
Chalcopyrite	$CuFeS_2$
Bismuthinite	Bi_2S_3
Electrum	(Au,Ag)
Brannerite (U-rich)	$(U^{4+}REE,Th,Ca)(Ti,Fe^{3+},Nb)_2(O,OH)_6$
Covellite	CuS
Digenite	Cu_9S_5
Bi-Ag tellurides-sulphates	Bi_2Te_3; Ag,Au,Te_2; (Au_2Bi+Bi+Bi_7Te_3)

Pacquet, 1993). The main ore minerals are uraninite and coffinite; minor uranophane is present in weathered rock at surface (Fuchs et al., 1985). The ore minerals are fine-grained (<100 μm) and disseminated predominantly along foliation planes and/or in veinlets parallel to the foliation, as well as in fill fractures (Fuchs and Hilger, 1989; Weyer et al., 1989; Reyx, 1994), and form vermiform micro roll-front textures. The metallic minerals include subordinate pyrite, marcasite, galena, and hematite/limonite with common calcite stringers. Additional trace minerals and elements are listed in Table 1. Of interest as potential geochemical tracers are fine-grained native gold (<50 μm), molybdenite, and Bi-Ag telluride group minerals (Reyx, 1994).

The KMZ and CZ zones contain inferred resources of 12,383 and 3992 tonnes of U metal grading 0.48% and 0.50% U, respectively (Berthet and Osorio, 2011a,b). The EZ contains a bulk historical resource of ~495 tonnes of U, grading 0.05% U (Jefferson et al., 2007). Additional resources have been identified in the Kiggavik Camp at the Andrew Lake and End Grid deposits, located about 15 km south-southwest of the KMZ, with inferred resources of 20,003 and 14,696 tonnes U, grading 0.50 and 0.40%, respectively (recalculated from Berthet (2011) and Osorio (2011), respectively). The Bong deposit, located about 3.9 km southwest of the KMZ, has an historical bulk resource of approximately 1650 tonnes U, grading 0.23% (Jefferson et al., 2007).

Surficial geology

The Kiggavik deposit is located within the Keewatin Ice Divide of the Laurentide Ice Sheet (Aylsworth and Shilts, 1989; McMartin and Henderson, 2004). Located in the central part of the Keewatin Sector of the Laurentide Ice Sheet, this area was constantly ice-covered from the beginning of the Wisconsin (Dyke et al., 2002) through the Late Wisconsin Maximum (18–13 ^{14}C ka BP) with complete deglaciation only between 7.2 and 6.0 ^{14}C ka BP (Dyke, 2004).

Surficial features in the Keewatin region (e.g. eskers, ribbed moraines, streamlined landforms) form a distribution pattern that is roughly concentric around the Keewatin Ice Divide (Aylsworth and Shilts, 1989). Surficial geology near Kiggavik is dominated by low hummocky moraine and undulating plains that are, in part, a discontinuous veneer of till over bedrock. Eskers and ribbed moraines are absent around the Kiggavik deposit and in the Schultz Lake area (Aylsworth and Shilts, 1989).

The Schultz Lake map area is described as a well developed glacial landscape with numerous drumlins, striations, and chatter marks of older subglacial erosion on bedrock, which suggests wet-based, erosive conditions during the last glaciation (McMartin et al., 2006). The land surface surrounding the Kiggavik deposit is commonly streamlined in different directions (Aylsworth and Shilts, 1989). Thin till veneer (<2 m) partially covers bedrock highs (resistant rocks), whereas low-lying areas, especially where underlain by less resistant metasedimentary and sedimentary rocks, are typically covered by till blankets (2–25 m) and hummocky till (Fig. 4). Sections along the Thelon River (McMartin et al., 2006), diamond drill holes drilled by Urangesellschaft in the 1980s (cf. Pacquet, 1993), and surficial mapping (Aylsworth et al., 1990; McMartin et al., 2008) indicate that till is the dominant surficial material.

During deglaciation, the retreating ice mass, centred approximately 60 km to the southeast of the Kiggavik deposit, blocked the drainage of the ancestral Thelon River. This inundated the region and resulted in deposition of lake sediments in low-lying areas, which are now known as the Thelon River Valley and Princess Mary Lake basin, between 7 and 6 ^{14}C ka BP (Dyke, 2004; McMartin et al., 2006). Post-glacial marine and/or glaciolacustrine sediments occur solely in poorly drained, low-lying areas and glaciofluvial sediments are non-existent. Minor outwash sediments, consisting of boulders, glaciofluvial and mixed strata, are located immediately to the southeast and east of the Kiggavik deposit. Lacustrine wave-washed erosional stepped benches are common with sandy raised beaches in places. Bedrock outcrops make up less than 5% of the land surface (Figs. 3, 4) and are exposed mainly in wave-washed outcrops around gentle hills that are dominated by Proterozoic quartzite and Mesoarchean

to Early Proterozoic granitoid rocks. These exposures, particularly the Proterozoic quartzite units north of the Kiggavik deposit, preserve faceted and striated surfaces that record multiple ice-flow trajectories.

Ice-flow indicators

In 1893, Tyrrell (1897) was the first to measure glacial striae in the Schultz Lake map area documenting several striations sets that recorded opposing ice-flow directions between Schultz Lake and Baker Lake. Cunningham and Shilts (1977) mapped ice-flow directions based on striations and streamlined landforms in the region between Baker and Schultz lakes and postulated that the Keewatin Ice Divide migrated to the south and east during the latter stages of deglaciation. Shilts et al. (1979) re-evaluated the Keewatin sector of the Laurentide Ice Sheet, and returned to Tyrrell's (1898) concept of an ice centre in central Keewatin. More recent work conducted by Aylsworth and Shilts (1989) and Aylsworth et al. (1990), which was based mainly airphoto interpretation of landforms, indicate that the area surrounding the Kiggavik deposit was dominated by a northwesterly glacial ice-flow event with local evidence of later and lesser ice flow toward the west.

A regional till sampling and surficial mapping project of the Schultz Lake area undertaken by McMartin et al. (2006) observed that faceted and striated bedrock surfaces and palimpsest streamlined landforms record multiple ice flows. A total of nine sets of ice-flow sequences were recorded by McMartin and Dredge (2005) that include (oldest to youngest): west-southwest, south-southwest, south-southeast, southeast (first occurrence), north-northwest, northwest, west-northwest, west, and southeast (second occurrence) (Fig. 5).

Previous till geochemical studies

Although Robinson et al. (2014) were the first to publish detailed studies of the surficial geochemistry of the Kiggavik deposit, a number of regional surficial geochemistry surveys provided guidance. In the 1970s, the GSC published a number of studies focused on techniques to track U and base metal transport by ice in the Kivalliq Region of central Nunavut (then Keewatin District of Northwest Territories) (Shilts and Klassen, 1976; Klassen and Shilts, 1977a,b; Shilts and Cunningham, 1977; Dilabio, 1979). In the Kaminak Lake and Baker Lake areas (~300 km south-southeast and 80 km east of Kiggavik) Klassen and Shilts (1977a) observed that U was preferentially partitioned into the <0.002 mm (clay) fraction of till, with higher concentrations found in wet clay. Klassen and Shilts (1977a) noted that 75% of till samples over Aphebian metasedimentary basins near Kaminak Lake contain background U, suggesting that U ore potential in such rocks is reflected by U concentrations in till. The Baker Lake study (Klassen and Shilts, 1977a) found that bedrock U occurrences do not correspond to U content in till samples and concluded that dispersion would be difficult to track unless a very small sampling grid was utilized. Elevated U contents (>20 ppm U) in till from northeast of Baker Lake (Klassen and Shilts, 1977b; Shilts and Cunningham, 1977) were determined to be associated with elevated natural background compositions of the underlying felsic volcanic rocks and were not necessarily sites of U occurrences. McMartin et al. (2006) also reported similar findings, concluding that higher U contents in till are commonly associated with felsic granitoid rocks and Archean gneiss and are rarely guides to U occurrences.

A focused study on drift prospecting around U and base-metal occurrences south of Baker Lake reported small dispersal trains of U originating from a site of pitchblende-bearing fracture fillings in gneiss (Dilabio, 1979). This dispersal train, defined by the <0.002 mm fraction of till, displayed U levels of up to 280 ppm as well as high amounts of Mo and Pb (Dilabio, 1979). These findings had been missed by the earlier reconnaissance-scale survey (~1.6 km sample spacing) of Klassen and Shilts (1977a).

In 2004, McMartin et al. (2006) carried out a regional survey of till composition and provenance in parts of the Shultz Lake map area (NTS Zone 66A1 to 66A8, inclusive). The Kiggavik exploration camp is in the mid-west section of that survey area (Fig. 4). Sample spacing was, on average, 10 to 15 km. The authors reported samples with higher U contents, in addition to equivalent U (*e*U) and equivalent Th (*e*Th) (concentrations determined indirectly from daughter products ^{214}Bi and ^{208}Tl and are assumed to be in equilibrium with their parents isotopes), were collected from the northeast portion of the map area (75 km northeast of Kiggavik) and are associated with Archean gneiss, supracrustal rocks, and Proterozoic granitic bodies. The most proximal sample to the Kiggavik deposit was collected 4 km to the west-northwest and displayed low to moderate metal contents, with a U concentration of 2.6 ppm U. Over the entire survey area, the U concentrations in till ranged from 0.25 to 6.9 ppm U, with an average of 2.5 ppm.

Indicator mineral exploration in glaciated terrain, particularly for uranium

Indicator mineral exploration in glaciated terrain uses the presence of diagnostic minerals in glacial and fluvial sediments to indicate the presence of a specific type of mineral occurrence, alteration, or lithology derived from bedrock sources. For a mineral to be utilized as an indicator mineral it should be present in sufficient quantity and be easily detected, coarse grained (silt to sand sized), visually distinctive (colourful,

a)

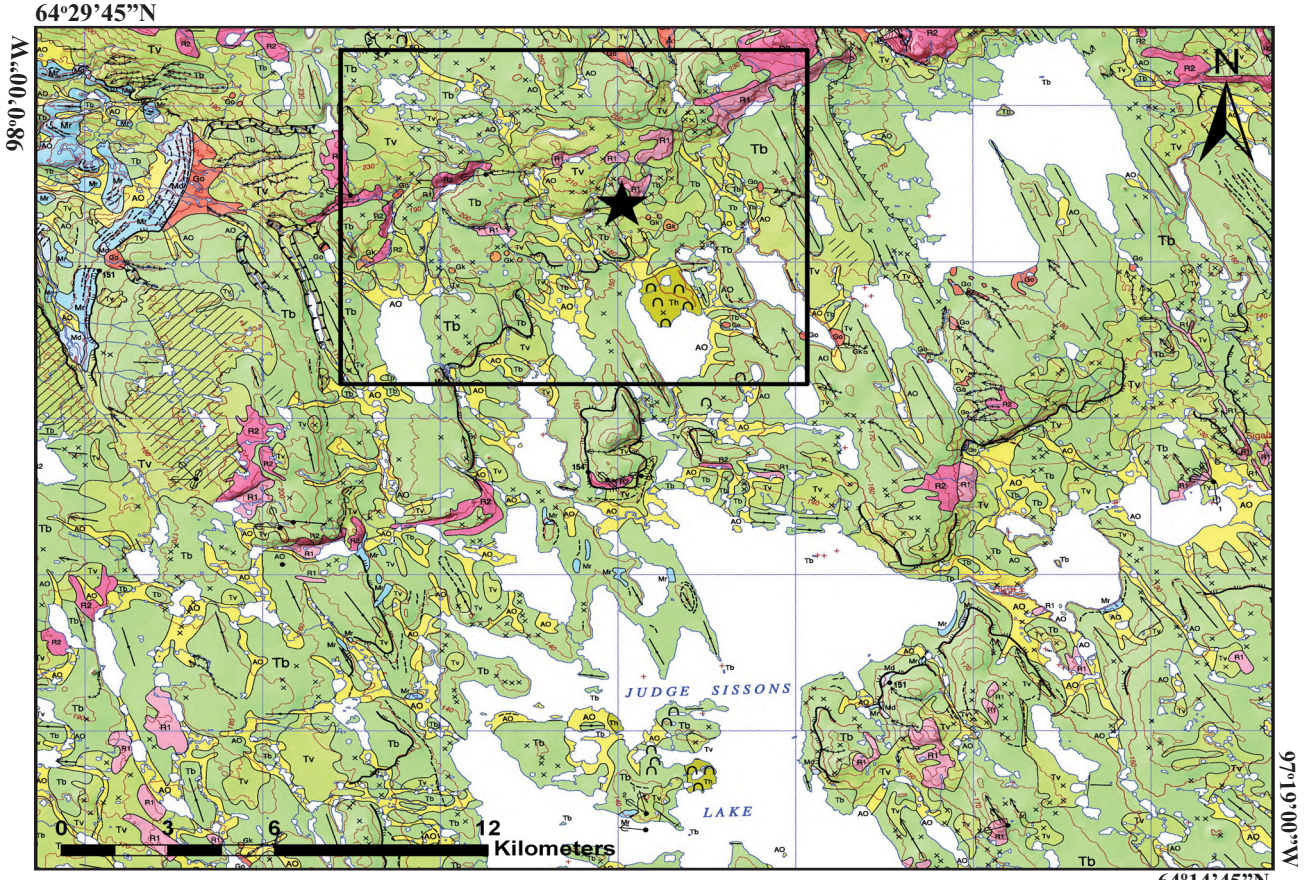
64°29'45"N
98°0'00"W
97°19'00"W
64°14'45"N
JUDGE SISSONS
LAKE
0 3 6 12
Kilometers
N

b)

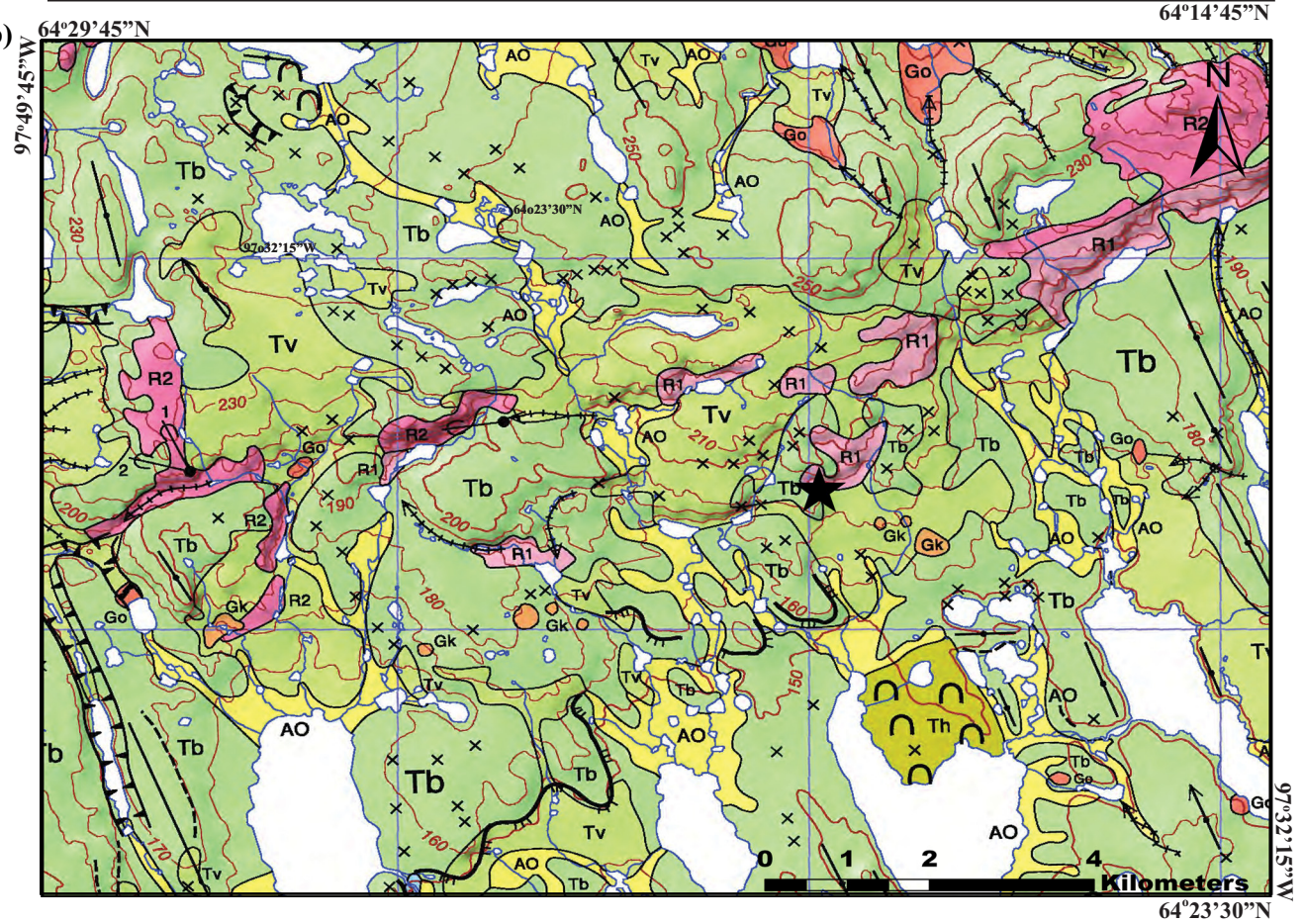
64°29'45"N
97°49'45"W
97°32'15"W
64°23'30"N
64o23'30"N
97o32'15"W
0 1 2 4
Kilometers
N

LEGEND

QUATERNARY

POST-LAST GLACIATION

ALLUVIAL DEPOSITS: stream-deposited material within active drainage systems formed since the retreat of the postglacial sea, proglacial lakes, or glacial ice; 1 m to several metres thick

A — **Alluvium:** sand, gravel, and cobbles; 1–10 m thick; deposited in channels and on floodplains, or as deltaic sediments where modern streams enter lakes

AO — **Alluvium and marine outwash sediments, undifferentiated:** sand or silt, minor gravel; 1–5 m thick; modern alluviam mixed with fine-grained sediments washed from till slopes by wave action, or with glaciofluvial outwash sediments in stream valleys or abandoned channels above marine limit; occurs in topographic lows or on gently sloping surfaces; commonly covered by a thin organic mat; high water table and rare ice-wedge polygons

MARINE DEPOSITS: materials deposited in the postglacial Tyrell Sea from 6500 +500 BP to about 500 years ago; mainly derived from reworking of glacial deposits by wave and current action during marine regression; 1 m to several

Md — **Deltaic sediments:** sand, pebbly sand, gravel; 2–20 m thick; deposited by glacial or nonglacial draining into the sea

Mr — **Littoral sediments:** generally well sorted sand, gravel, cobbles, or boulders; 1–5 m thick; deposited as beaches, bars, spits, and shore ice-push ridges derived from the rewoking of upload surficial deposits

LAST GLACIATION

GLACIOFLUVIAL DEPOSIT: generally well sorted material deposited by meltwater streams behind, at, and in front of the ice margin; 2 m to several metres thick

Gk — **Ice-contact sediments:**poorly stratified sand and gravel; 5–15 m thick; deposited in, or, over, or around ice or in subglacial ice tunnels; forming isolate kame terraaces near marine limit

Go — **Outwash sediments:** stratified sand and gravel; 2–15 m thick; deposited in a proglacial environment by subaerial meltwater streams in areas above local sea level as valley trains, terraces, and fans; surfaces locally terraced, hummocky, and kettled; grading to deltaic sediment near marine limit

GLACIAL DEPOSITS: poorly sorted seiments with distinctive forms deposited directly by glacial ice; 1 m to several metres thick; lithic composition genally reflects a local provenance and a net transport direction to the northwest, except in the southeast extermity of the map area where the youngest flow was to the southeast. Till located mainly southwest of the Thelon River has a reddish matrix and a significant Dubawnt Supergroup clast content, till composition northeast to the river generally reflects underlying bedrock types.

TM — **Till and marine sediments, undifferentiated:** till and marine diamictons mised with patches of marine offshore and sublittoral sediments; 1–5 marine thick; forming till-cored landforms vaneered by marine silt and silty sand, or marine deposits in depressions among till landforms; includes areas of till reworked from marine and current action; may occur anywhere below marine limit, but distribution is patchy above 50 m a.s.l.

Tb — **Till blanket:** glacial diamicton; 2–25 m thick; deposted mainly in a subglacial environment; forming gently undulating till plains or stream-lined landforms; includes areas of boulder lags as a result of wave-washing or meltwater erosion

Tv — **Till veneer:** glacial diamicton; 1–2 m thick; discontinuous cover mimicking underlying bedrock topography; includes numerous small bedrock outcrops and boulder fields

Tr — **Ribbed moraine:** generally bouldery till, in places sand and gravel; forming straight to sinuous ridges; less than 1 km long and 2–10 m high; ridges generally oriented at right angles to direction of ice flow

Th — **Hummocky till:** gracial diamicton, occuring as 5–20 m high rounded hummocks; surfaces lack significant boulder cover

PRE-QUATERNARY

BEDROCK: Archean to Paleoproterozoic supracrustal and instrusive igneous and metamorphic rocks; red volcanic rocks, and unmetamorphosed sediments; surface comprises more than 80% outcrop

R1 — **Polydeformed and metamorphosed supracrustal and intrusive rocks:** Neoarchean metasedimentary and metavolcanic supracrustal rocks of the Woodburn Group, and late Archean granitoid complexes; Paleoproterozoic, clastic-dominated supracrustal rocks of the Ketyet River Group; minor Mesoarchean gneissic remnants of the basement to the Woodburn Group

R2 — **Paleoproterozoic Dubawnt Supergroup rocks:** underformed and unmetamorphosed red volcanic and sedimentary rocks; include distrinctive quartz sandstone and conglomerate units of the Thelon Formation, and red volcanic rocks of the Pitz and Christopher Island formations

Figure 4. Overall **(a)** and expanded view **(b)** of the surficial geology of the Kiggavik U exploration camp in the northwestern part of the Schultz Lake map area (parts of NTS 66A5, A6). From McMartin et al. (2008). The black star shows the location of the Kiggavik Main Zone; the black rectangle on (a) outlines the area expanded in (b).

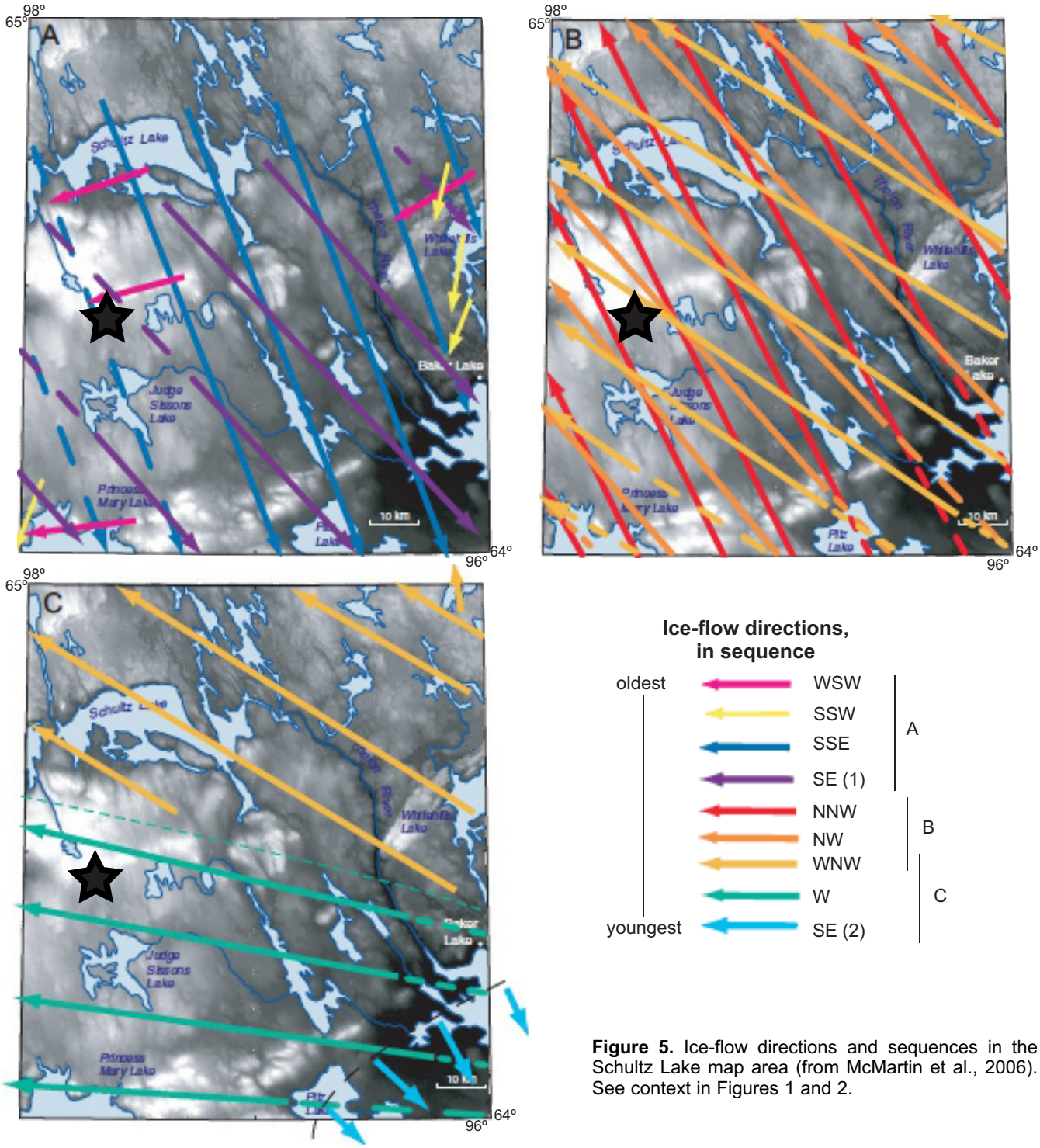

Figure 5. Ice-flow directions and sequences in the Schultz Lake map area (from McMartin et al., 2006). See context in Figures 1 and 2.

uniquely textured, altered, or fractured), be sufficiently dense for further concentration by gravity means (SG > 3.2 g/cm^3), and be relatively resistant to weathering (Averill, 2001; McClenaghan, 2005).

Heavy mineral abundances in till have been successfully applied to mineral exploration, the most notable being kimberlite indicator minerals (KIM) in diamond exploration (Carlson et al., 1999; McClenaghan and Kjarsgaard, 2007). Indicator mineral techniques have also been used for Au (McClenaghan, 2001; Averill, 2013), base metals (Averill, 2001; Hicken et al., 2012; McClenaghan, 2013) and W exploration (McClenaghan et al., 2014). However, only a few publications discuss the use of indicator minerals for U exploration (e.g. Dilabio, 1979; Geddes, 1982; Corriveau et al., 2007).

Till samples near Vixen Lake, northern Saskatchewan, revealed U-Ni anomalies in HMC obtained by reverse circulation (RC) drilling (Geddes, 1982). These anom-

alies were attributed to the presence of small grains of niccolite (NiAs) containing black intergrowths believed to be pitchblende. Detailed geochemical analysis, comparing the U-Ni ratio of the till to local deposits and prospects, concluded that the till containing these anomalous heavy minerals had undergone a relatively long distance of transport and was separated from its source, the Collins Bay "B" zone, by several kilometres. More recently, Corriveau et al. (2007) remarked that the application of indicator mineral methods for U-rich iron oxide-copper-gold (IOCG) exploration is nearly non-existent, however there remains much potential that minerals such as uraninite may be possible indicators. The mineralogy of the HMC can help define the type of U deposit source, as described by Campbell (2009), who concluded that the relative and absolute abundances of hematite, zircon, and rutile versus garnet, amphiboles, pyroxene, and pyrite can point to either sandstone- or basement-hosted U deposits in the Athabasca Basin. Furthermore, Campbell (2009) noted that the identification of U-bearing ore minerals, such as coffinite, ramberzite, and uraninite (including pitchblende), in addition to pathfinder minerals, such as niccolite, arsenopyrite, chalcopyrite, and sphalerite, can complement till matrix geochemistry for U exploration.

METHODS USED IN THE PRESENT STUDY

Geologists from the GSC and Queen's University collected till and rock samples from hand-dug pits, outcrops, and diamond drill core at the Kiggavik deposit during the summer of 2010. Till samples were collected around the KMZ and drill core was sampled from previously drilled holes in both the KMZ and the CZ (Fig. 6). These till samples were also processed and analyzed for geochemistry of the <0.063 mm and <0.002 mm fractions, as reported by Robinson et al. (2014).

Ice-flow measurements

The glacial history within the study area was observed by noting till compositions at sample sites and by measuring the orientations of ice-flow indicators, which ranged from large glacially streamlined till landforms to fine-scale, erosionally sculpted, striated, and grooved bedrock outcrops (Robinson et al., 2014). Glacial landforms encompass drumlins and flutings ranging in scale from 100s of metres to 10s of kilometres that are evident on aerial photographs and interpreted as subglacial constructional bedforms. Landform orientation data were supplemented and calibrated by other investigations, such as detailed striation mapping, because the ice-flow phase indicated by glacial landforms may differ from the effective sediment transport path, which in this area is a result of multiple ice flows due to the migrating ice divide (e.g. McMartin et al., 2006; Stea et al., 2009).

Outcrop locations for striation measurements were selected based upon accessibility by foot or helicopter traverses and the potential for striae preservation. Striations on hard, fine-grained bedrock weather more slowly and are better defined than on coarse-grained granitic rocks. Striations were measured on relatively flat outcrop surfaces and care was taken to ensure unbiased data collection by preferentially measuring sites on stoss slopes created by the last major ice flow (Stea et al., 2009). Relative ages of striated facets were determined wherever possible by evaluating their relative positions on an outcrop according to the criteria defined by Lundqvist (1990) and McMartin and Paulen (2009). A total of 24 outcrops were visited in a 320 km^2 region proximal to the Kiggavik deposit. Of these, 21 exposed multiple striation azimuths with crosscutting relationships. Striation site locations and measurements are given in Robinson et al. (2014).

Field sampling of till

Based on known ice-flow patterns throughout the area, which had been determined by previous work and observations made during this field program a fan-shaped pattern of sample sites was designed, extending to the west and northwest of the Kiggavik deposit (Fig. 6), to test the range of down-ice glacial transport directions .Till samples were collected from hand-dug holes (15–45 cm deep) in active and inactive frost boils up-ice, overlying, and down-ice of the deposit by foot and helicopter traverses. Frost boils (Fig. 7) were selected as the sample medium because the area experiences continuous permafrost with an active layer in the summer. The resulting freeze-thaw conditions generate diapiric frost boils, which bring up fresh deep till that over time mixes with surface till and soil. Thus soil profiles in frost-boil terrane are poorly developed (Shilts, 1973, 1978; McMartin and McClenaghan, 2001; McMartin and Campbell, 2009). During sampling, the surface of each frost boil was scraped clean of organic material, rocks, and other potentially contaminating debris prior to collection, and the pits were centred on the upwelling diaper to obtain the freshest possible till.

A total of 71 bulk till (5–15 kg) samples were collected. Of these, 61 were collected from 7 fan-shaped transects at 0.25, 0.5, 1, 2, 3, 5, and 10 km down-ice of the Kiggavik Camp, to maximize data for the dominant ice-flow directions (Fig. 6). Three till samples (10-PTA-035, -036, and -037), were collected ~5 km down-ice of Kiggavik, proximal to the mineralized Granite Grid showing (P. Wollenberg, pers. comm., 2010) for comparison with samples collected proximal to the

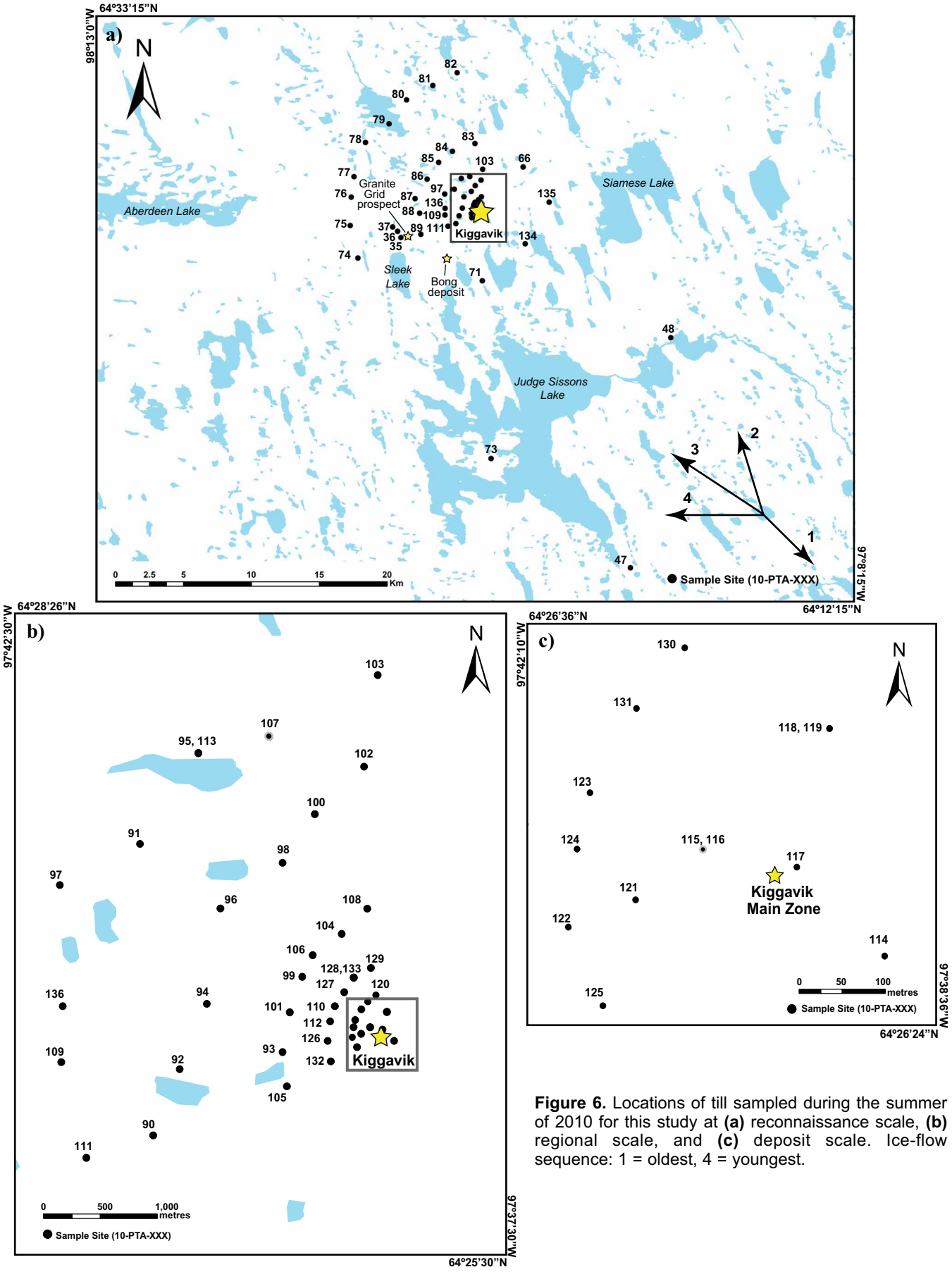

Figure 6. Locations of till sampled during the summer of 2010 for this study at **(a)** reconnaissance scale, **(b)** regional scale, and **(c)** deposit scale. Ice-flow sequence: 1 = oldest, 4 = youngest.

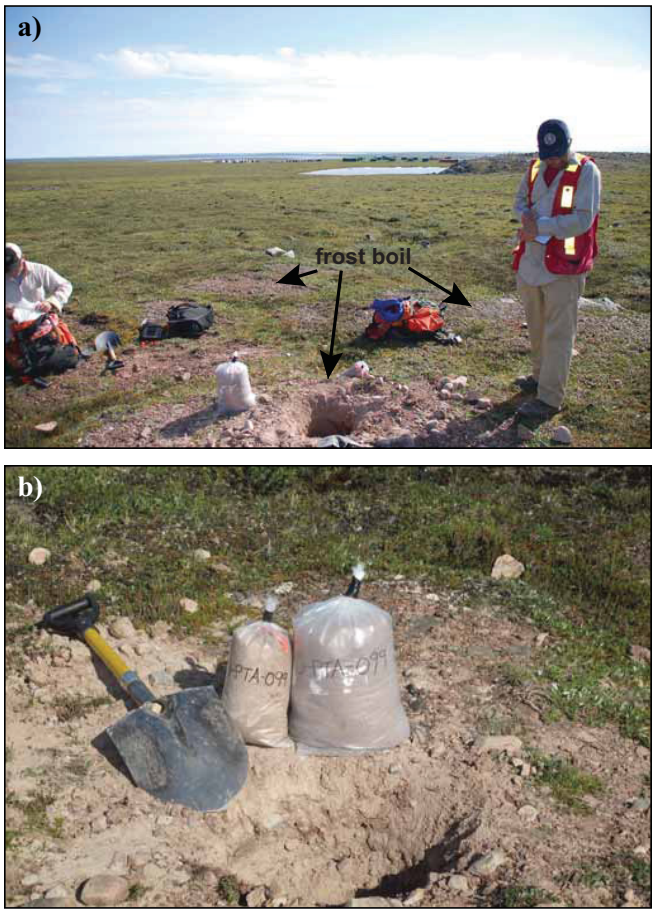

Figure 7. a) Photograph of the site where till sample 10-PTA-099 was collected at one of multiple frost boils in a till veneer plain northeast of Kiggavik Main Zone (KMZ). **b)** Photograph of the sample pit in frost boil illustrating the dominant sandy texture encountered in till pits dug around the KMZ.

KMZ. The remaining 5 till samples were collected to record the heavy mineral content of local (samples 10-PTA-066, -135, and -136) and regional (10-PTA-047 and -048) up-ice samples (Fig. 6). Three field duplicates collected to test sediment heterogeneity and quality control during the laboratory separation and mineral identification procedures (Plouffe et al., 2013): sample 10-PTA-113 is a field duplicate of 10-PTA-095, 10-PTA-119 is a duplicate of 10-PTA-118, and 10-PTA-133 is a duplicate of 10-PTA-128. Samples 10-PTA-115 and 10-PTA-116 were collected at different depths within the same dug-out pit. Till sample locations are listed in Appendix A1 of this report; field descriptions and site photographs of are in Appendix A of Robinson et al. (2014).

Sampling and processing of bedrock samples

A total of 42 rock samples were collected around the Kiggavik Camp in the summer of 2010 from outcrop and drill core (Table 2; Appendix A2). The term "outcrop" is used here to include solid outcrop, frost-heaved outcrop, and monolithological felsenmere that clearly represents the local bedrock. Samples were collected to document the petrology of the most important rock units, especially their mineralogy, both regionally and within the Kiggavik Camp (Table 2). The sample locations were chosen up- and down-ice of the Kiggavik U deposit, taking into consideration that the net transport direction was toward the northwest (Scott et al., 2015). The goal was to characterize the mineralogy of the fresh to highly altered (including those with abundant uraninite) main rock units that could have contributed material to till in the project area. Part of that goal was to separate and characterize potential heavy mineral indicators with potential for glacial transport and to document their primary shapes, sizes, and densities.

Outcrop and hand specimen photographs of 39 of the rock samples are presented in Appendix B of this report. Binocular microscope descriptions of 18 samples, contributed by Stu Averill of Overburden Drilling Management (Appendix C), provided a preliminary, yet still relevant guide to further analyses, as well as hand-sample context for the thin section petrography that was completed by Robinson (2015). Petrography, lithological descriptions and discussions, and the nomenclature of map units reported herein were significantly revised by the second author (Appendix D) based on new knowledge from other components of the northeast Thelon project, as well as from new mapping and core logging by Johnstone (2015).

Sample processing and indicator mineral picking of till and bedrock samples

The 71 bulk till samples were sent to Overburden Drilling Management (ODM) for processing and the production of a HMC for indicator mineral picking. To limit cross-contamination, samples were ranked and processed based on their potential to contain indicator minerals. Five background sample standards, ranging in size from 9 to 13.2 kg and containing no heavy minerals of interest, were labeled and submitted with the field samples (see section "Quality control of till duplicates and background till samples".

The <2.0 mm material was first passed over a shaking table and the HMC recovered directly from the table was micro-panned (commonly termed "pan concentrate") to recover uraninite, coffinite, native gold, and sulphide and platinum group minerals using tweezers and/or steel pick with adhesive. Relatively coarse-grained heavy minerals picked from the pan concentrate were counted, and the size and shape characteristics of gold grains recorded (Appendix E).

With the remaining pan concentrate was recombined with the table HMC and was then sieved to >0.25 mm. The <0.25 mm portion of the table HMC was archived. A heavy liquid separation (methylene iodide diluted to

Table 2. Samples collected from drill core at the Kiggavik deposit and grab samples from local and regional outcrops and float occurrences. Simplified from Appendix A1, which also includes coordinates. Note: U = uraninite +/- coffinite.

Sample ID	Sample site	Lithology and unit name	U	HMs picked	EMPA
10-PTA-R005	Outcrop	Metagreywacke, mylonitic, hematitized, along Judge Sissons Fault: Pipedream assemblage	Nil	Yes	No
10-PTA-R009A -R009B	Outcrop	Metagreywacke (A): Pipedream assemblage cut by sheet of Granite (B): Hudson	Nil	No	No
10-PTA-R010	Outcrop	Quartzite: Ketyet River group	Nil	No	No
10-PTA-R012	Outcrop	Rhyolite, quartz-feldspar porphyritic, highly foliated: Pukiq Lake Formation	Nil	Yes	No
10-PTA-R016	Outcrop	Sandstone, feldspathic, silicified: possibly Amarook Formation, south side Thelon Fault	Nil	No	No
10-PTA-R018	Outcrop	Litharenite, hematitized, clay-altered, feldspathic: Thelon Formation	Nil	No	No
10-PTA-R020	Outcrop	Litharenite, hematitized, clay-altered, feldspathic: Thelon Formation	Nil	Yes	No
10-PTA-R021	Float	Metapelite, grey, highly foliated: Pipedream assemblage	Nil	No	No
10-PTA-R022	Float	Quartzite: basal Ketyet River group	Nil	No	No
10-PTA-R024	Outcrop	Litharenite, quartz pebbly + conglomerate; illitized, hematitized: Thelon Formation	Nil	No	No
10-PTA-R026 -R026B	Outcrop	(A) Mafic Martell Syenite, (B) Hudson Granite: both Schultz Lake Intrusive Complex (SLIC)	Nil	No	No
10-PTA-R028	Outcrop	Granite, rusty weathering: Hudson, SLIC	Nil	No	No
10-PTA-R030	Outcrop	Granite plug: gossanous, minor aplite + pegmatite: Hudson Suite east of SLIC	Nil	No	No
10-PTA-R032	Outcrop	Metagreywacke, medium-grained, thick-bedded: Pipedream assemblage	Nil	Yes	No
10-PTA-R033	Outcrop	Red mudstone, interbed between conglomerate beds: basal Thelon Formation	Nil	No	No
10-PTA-R040	Outcrop	Quartzite: basal Ketyet River group	Nil	No	No
10-PTA-R041	Core	Granite, Lone Gull plug: Hudson + Nueltin	Nil	Yes	No
10-PTA-R042	Core	Granite, Lone Gull plug: Hudson + Nueltin	Nil	No	No
10-PTA-R043	Core	Metagreywacke, relatively fresh, excellently graded beds: Pipedream assemblage	Nil	No	No
10-PTA-R044	Core	Metagreywacke, slightly clay-altered: Pipedream assemblage	Nil	No	No
10-PTA-R045	Core	Epiclastic rock or pelitic metagreywacke, highly clay-altered: Pukiq Lake Formation or Pipedream assemblage	Minor	No	Yes
10-PTA-R046	Core	Rhyolite, porphyritic, highly foliated, clay-altered, uranophane: Pukiq Lake Formation	Minor	No	Yes
10-PTA-R047	Outcrop	Rhyolite, brecciated and silicified by cherty and drusy quartz, southwest of Judge Sissons Lake, follows N-S fault, ***contains native Au***: Pitz Formation, Wharton Group	Nil	Yes	No
10-PTA-R048	Outcrop	Metagreywacke, foliated, fresh: Pipedream assemblage	Nil	Yes	No
10-PTA-R050	Core	Epiclastic, porphyritic, highly foliated, clay- and hematite-altered: Pukiq Lake Formation	Minor	No	Yes
10-PTA-R051	Core	Rhyolite or epiclastic, porphyritic, highly foliated, clay-altered: Pukiq Lake Formation	Minor	No	Yes
10-PTA-R052	Core	Minette dyke (lamprophyre): Christopher Island Formation (CIF)	Nil	No	No
10-PTA-R053	Core	Epiclastic or pelitic metagreywacke, extremely altered, elevated gamma ray counts: Pukiq Lake Formation / Pipedream assemblage	Minor	No	Yes

Table 2 continued.

Sample ID	Sample site	Lithology and unit name	U	HMs picked	EMPA
10-PTA-R054	Core	Quartzite cut by hematitic quartz veins: basal Ketyet River group, extensional veins	Nil	Yes	No
10-PTA-R055	Core	Syenite, porphyritic, alkali: Martell Syenite	Nil	No	No
10-PTA-R056	Core	Metagreywacke, moderately altered: Pipedream assemblage	Nil	Yes	No
10-PTA-R057	Core	Minette dyke (lamprophyre): Christopher Island Formation (CIF)	Nil	Yes	No
10-PTA-R058	Core	Epiclastic rock, chloritic, possibly metapelite: Pukiq Lake Formation or Pipedream assemblage?	Nil	No	No
10-PTA-R059	Core	Epiclastic rock, or possibly metapelite, clay- and chlorite-altered: Pukiq Lake Formation or Pipedream assemblage?	Nil	No	No
10-PTA-R060	Core	Leucogranite, weakly porphyritic: Hudson Granite and possibly Nueltin Granite	Nil	Yes	No
10-PTA-R061	Core	Mingled granite and minette (lamprophyre): Hudson Suite and CIF	Nil	No	No
10-PTA-R062	Core	Epiclastic/metapelite highly altered to clay & U oxides: Pukiq Lake Formation or Pipedream assemblage	Nil	Yes	No
10-PTA-R063	Core	Epiclastic/metapelite, heavily altered, U oxides disseminated: Pukiq Lake Formation or Pipedream assemblage	Major	No	Yes
10-PTA-R064	Core	Epiclastic/metapelite, heavily altered, U oxides disseminated: Pukiq Lake Formation or Pipedream assemblage	Major	No	Yes
10-PTA-R065	Outcrop	Diabase: Mackenzie Dyke	Nil	Yes	No
10-PTA-R072a	Outcrop	Agmatite, volcano-sedimentary fragments in quartz-diorite matrix: Judge Sissons Pluton, Snow Island Suite	Nil	Yes	No
10-PTA-R027b	Outcrop	Quartz diorite to granodiorite: Judge Sissons Pluton, Snow Island Suite	Nil	Yes	No
10-PTA-R073	Outcrop	Iron formation, banded sulphide-magnetite-silicate facies: Half Way Hills assemblage, Woodburn Lake group	Nil	Yes	No
10-PTA-R137	Core	Granitic aplite with molybdenite seams: Hudson Granite plus Nueltin metasomatism	Nil	Yes	No
10-PTA-R138	Core	Bostonite (microsyenite) dyke, altered: CIF	Nil	Yes	No
10-PTA-R139	Core	Epiclastic/metapelite, clay-altered + disseminated hematite, Pukiq Lake Formation/Pipedream assemblage	Nil	No	No
10-PTA-R140	Core	Epiclastic rock, porphyritic; clay- and hematite-altered: Pukiq Lake Formation	Nil	No	No
10-PTA-R141	Core	Rhyolite, quartz porphyritic, highly strained and clay-altered: Pukiq Lake Formation	Nil	No	No
10-PTA-R142	Core	Rhyolite, porphyritic, highly strained and clay-altered: Pukiq Lake Formation	Nil	No	No
10-PTA-R143	Core	Rhyolite or epiclastic rock; intensely foliated, altered; minor U; tectonically interleaved (cm scale) with quartzite: Pukiq Lake Formation and basal Ketyet River group	Minor	No	No
10-PTA-R144	Core	Metagreywacke, lithic, fresh: Pipedream assemblage	Nil	No	No
10-PTA-R145	Outcrop	Pegmatite and aplite, northerly trending dyke above and southwest of KMZ: Hudson Granite	Nil	No	No
Bong rhyolite	Core	Rhyolite, quartz-feldspar porphyritic, foliated, relatively fresh: Pukiq Lake Formation	Nil	No	No

a specific gravity of 3.2 g/cm3) was then applied to the 0.25 to 2.0 mm fraction of the table HMC. The ferromagnetic fraction of the heavy liquid separate, which consists of magnetite and pyrrhotite, was then removed using a hand magnet and set aside for picking of pyrrhotite. The non-ferromagnetic HMC was sieved into three size fractions: 0.25–0.5, 0.5–1.0, and 1.0–2.0 mm. The 0.25–0.5 mm fraction was passed though further paramagnetic separation to facilitate the picking and eventual identification of fine-grained heavy minerals. Potential indicator minerals were picked using tweezers, steel pick, or water pipette from the 0.25–0.5, 0.5–1.0, and 1.0–2.0 mm till HMCs, and their counts were normalized to a 10 kg sample weight (Fig. 8, Appendix F).

Eighteen bedrock samples selected for heavy mineral characterization involving disaggregation were first described using a binocular microscope by Stu Avril of ODM (Appendix C). Samples with U oxide minerals were not disaggregated as the sample size was too small and disaggregating such samples may have led to safety issues. Representative portions of the chosen samples, which ranged in weight from 245 to 340 g, were processed at Queen's University using a selFrag™ high-voltage pulse power fragmentation instrument (Appendix E1). The first stage of selFrag™ disaggregation uses a high-voltage electric pulse (150–200 kV) within a 3 litre vessel of water. Subsequent ongoing electric pulses (5 Hz) through the sample preferentially propagate fractures along grain boundaries (Cabri et al., 2008; Shi et al., 2014). The resulting individually liberated heavy mineral grains were then concentrated using the tabling, micro-panning, and heavy liquid methods described above (Fig. 9). For quality control, cross contamination was limited and monitored by processing a 250 g quartz blank (QB, Appendix E1) at the beginning of the series and between every sample (Figs. 9, 10). The 3 litre vessel and the selFrag™ chamber were thoroughly washed between each run to further reduce cross-contamination. For quality assessment, data for quartz blanks are reported as sample numbers containing QBlk; the results of the processed samples can be found in Appendix E2. The <2.0 mm fraction of each disaggregated bedrock sample was then processed at ODM (Fig. 9) using the same procedures as outlined above for the bulk till samples to produce first a table HMC and then a heavy-liquid HMC, which was sieved into three size fractions from which the heavy minerals were picked.

Petrographic methods

Detailed petrography of 36 thin sections, which were prepared from the 54 bedrock samples that were collected, utilized both reflected and transmitted light microscopy to understand and determine texture, grain shape, mineralogy, and alteration of the Kiggavik deposit (Appendix D). A few samples were described in more detail because of their potential economic importance. One such example is a comparison between metagreywacke of the Pipedream assemblage, and rhyolite and epiclastic rocks of the Pukiq Lake Formation (Fig. 11). Such detailed follow-ups were determined based on closer inspection of hand specimens and outcrop photographs, and on parallel research supported by AREVA. Bedrock samples were chosen to represent all major rock types in and around the Kiggavik Camp in terms of their potential mineralogical contributions to bulk till samples down-ice. Samples were collected both in detailed drill core logging and at a regional scale (>10 km distant from KMZ) to observe the HMC of bedrock up-ice of Kiggavik.

Scanning electron microscope and electron probe micro-analyzer

Representative samples were analyzed using an environmental scanning electron microscope (ESEM - FEI MLA 650) and an electron probe micro-analyzer (EPMA, JEOL JXA-8230) at Queen's University. To target U-bearing samples, analyses were focused on samples that had a minimum of 300 total counts per second (cps) of total gamma-ray radiation, measured using an RS-230 portable spectrometer with Bi-Ge detector, made by Radiation Solutions Inc. This measures K (wt%), equivalent Th (eTh, ppm) and equivalent U (*e*U, ppm). The eTh and eU are measured indirectly from daughter products (Bi and Tl respectively) that are assumed to be in equilibrium with their parent isotopes, hence the prefix "e" (equivalent).

A total of 38 spot analyses were measured with the EMPA from 5 different samples (10-PTA-R045, -R046, -R051, and -R063) to determine the chemical compositions of U-ore minerals. Seven grains were targeted with multiple spot analyses: 6 compositions resolve as uraninite and 1 as coffinite. Another 38 spot analyses on Pb-apatite were measured in 2 samples. To reduce the time required for analyses, each spot analysis of a U-bearing mineral was limited to 10 elements reported as oxides (SiO_2, Al_2O_3, CaO, FeO, UO_2, ThO_2, Na_2O, Y_2O_3, PbO, P_2O_5), which constitute approximately 90% of the bulk chemical composition. Table 3 details the methods used to analyze the U-rich minerals and Pb-apatite crystals: standards, crystal selection, counting times, operating voltage and beam current. The mode for all analyses is wavelength dispersive X-ray spectroscopy. All EMPA results are listed in Appendix G.

Mineral liberation analysis

Mineral Liberation Analysis (MLA) was conducted using a MLA 650 FEG ESEM (MLA) at Queen's

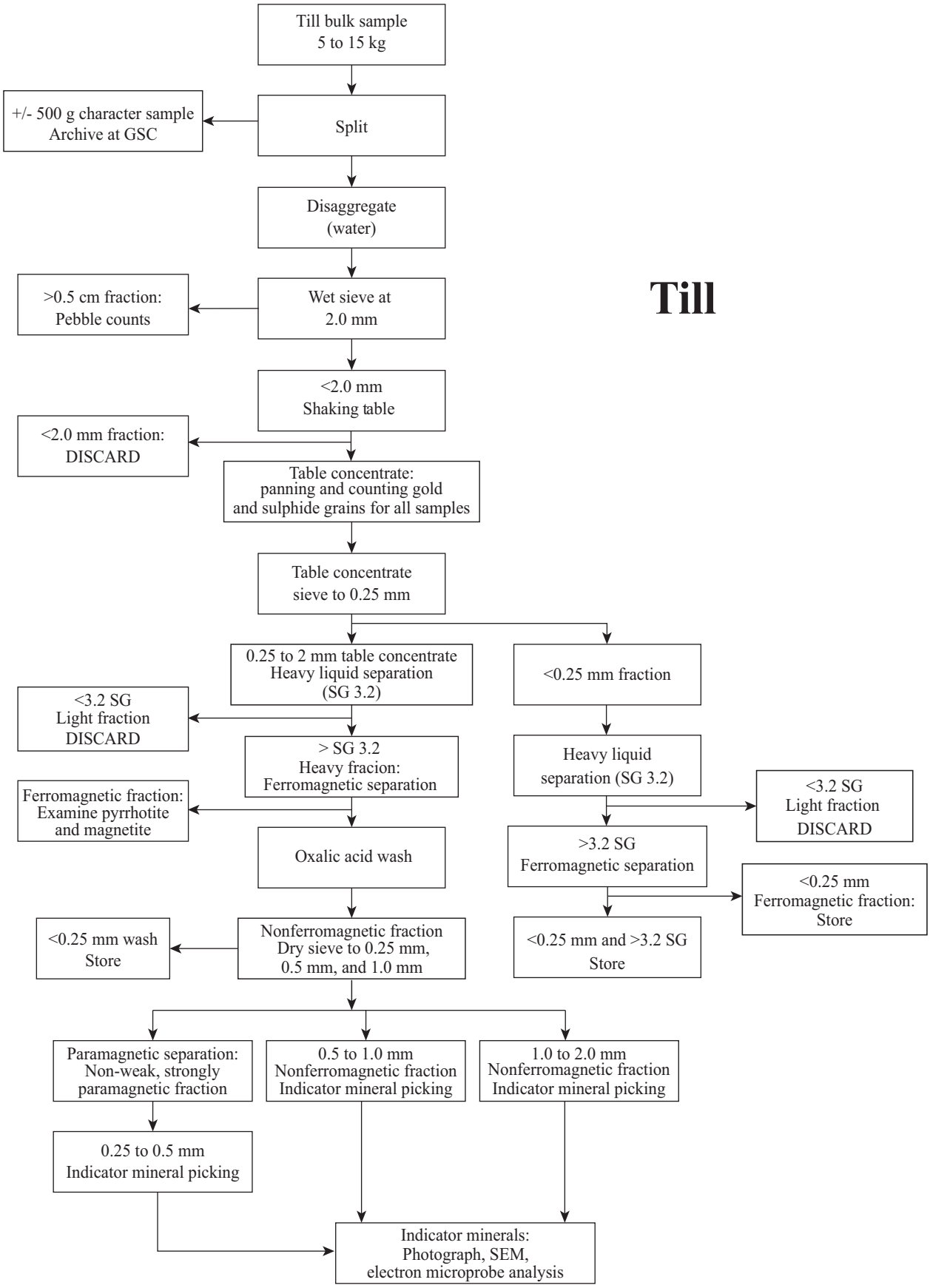

Figure 8. Flow chart from Overburden Drilling Management Ltd. for their processing of till samples and recovering indicator minerals from heavy mineral concentrates (HMCs).

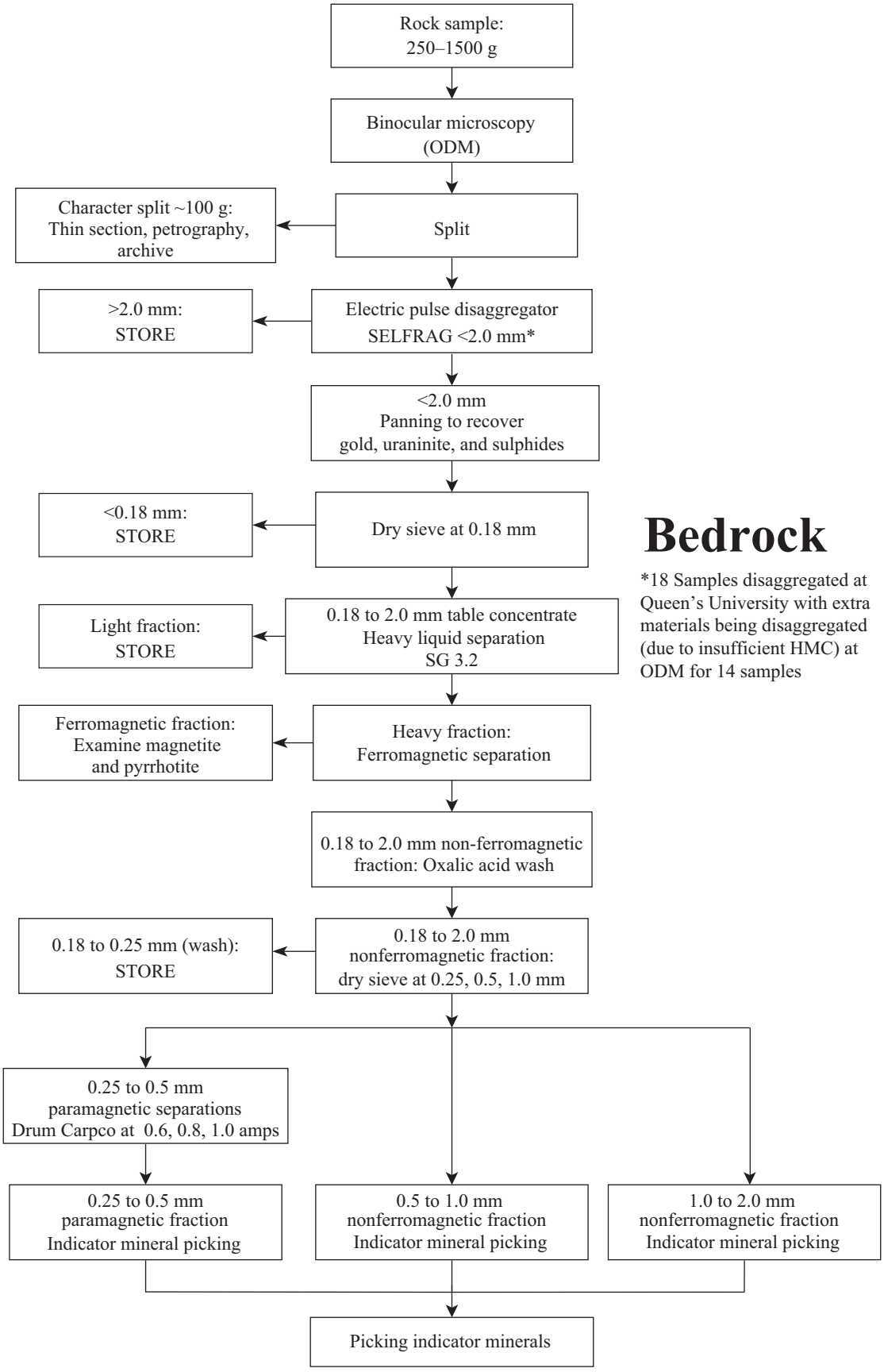

Figure 9. Flow chart from Overburden Drilling Management Ltd. (ODM) for processing of bedrock samples and recovery of potential indicator minerals from heavy mineral concentrates (HMCs).

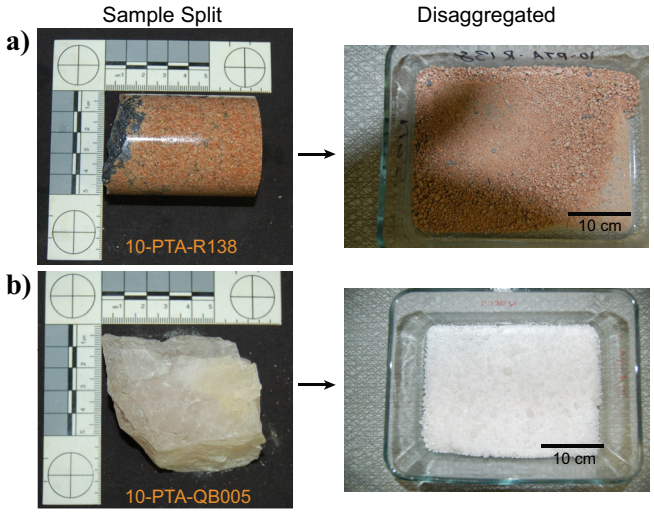

Figure 10. Example of an electronically pulse-disaggregated rock sample **(a)** and blank **(b)** using a SelFrag™ instrument at Queen's University, Kingston, Ontario.

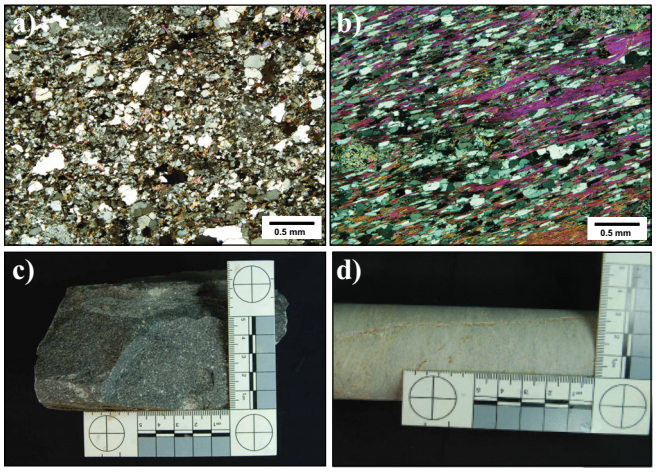

Figure 11. Contrast between seriate textured, moderately foliated metagreywacke of the Pipedream assemblage, Woodburn Lake group and the porphyritic, highly foliated rhyolite of the Pukiq Lake Formation, Snow Island Suite. **a)** Metagreywacke in transmitted light (XPL), non-altered, sample 10-PTA-R048. **b)** Foliated rhyolite in transmitted light (XPL), sample 10-PTA-R142. **c)** Surface sample of metagreywacke, sample 10-PTA-R048. **d)** Drill core sample of foliated porphyritic rhyolite, sample 10-PTA-R142.

University to verify the presence of very fine-grained Au-, Ag-, and Te-bearing minerals. The MLA, which is linked with the SEM, quantitatively evaluates the relationship between grain size, mineral associations, and mineral abundances in polished thin sections of U-mineralized samples. Mineral identification was aided by dual Bruker Energy Dispersive X-ray detectors with quantitative mineralogy software.

RESULTS

Bedrock petrology

Uraniferous and non-uraniferous, altered and unaltered samples were examined from a total of 54 specimens,

Table 3. Electron microprobe analyzer operating conditions for (a) uraninite and coffinite, and for (b) Pb-apatite at Queen's University using a JEOL JXA-8230 EMPA.

a) Uraninite / Coffinite EMPA Conditions and Standards

Element	X-Ray Line	Diffracting Crystal	Standard	Peak Count Time (seconds)	Gun (kV)	Beam (nA)
U	Mb	PET	synthetic UO_2	10	20	20
Th	Ma	PET	synthetic ThO_2	60	20	20
Pb	Ma	PETH	natural cerussite	30	20	20
Y	Ma	PETH	synthetic YPO_4	30	20	20
Si	La	TAP	natural diopside	30	20	20
Ca	Ka	LiFL	natural diopside	30	20	20
Fe	Ka	LiFL	synthetic fayalite	60	20	20
Na	Ka	TAP	Natural albite	30	20	20
Al	Ka	TAP	Natural albite	30	20	20

b) Pb-Apatite EMPA Conditions and Standards

Element	X-Ray Line	Diffracting Crystal	Standard	Peak Count Time (seconds)	Gun (kV)	Beam (nA)
Ca	Ka	PET	synthetic $Ca_2P_2O_7$	10	15	10
P	Ka	PET	synthetic $Ca_2P_2O_7$	10	15	10
Si	Ka	TAP	natural albite	20	15	10
Cl	Ka	PET	natural scapolite	20	15	10
F	Ka	TAP	durango apatite	10	15	10
Na	Ka	TAP	natural albite	10	15	10
U	Ka	PETH	synthethic UO_2	30	15	10
Th	Mb	PET	synthetic ThO_2	30	15	10
Pb	Ma	PETH	natural cerussite	30	15	10
Y	Ma	PETH	synthetic YPO_4	20	15	10
La	La	LiFL	synthetic $LaPO_4$	20	15	10
Ce	La	LiFH	synthetic $CePO_4$	20	15	10
Pr	La	LiFL	synthetic $PrPO_4$	20	15	10
Nd	Lb	LiFL	synthetic $NdPO_4$	20	15	10
Sm	Lb	LiFL	synthetic $SmPO_4$	20	15	10
Gd	Lb	LiFL	synthetic $GdPO_4$	20	15	10

which represent at least 24 different rock types (Table 2, Appendix A2); these specimens are described belows with spatial reference to Figure 2. Their modal mineralogical compositions are summarized in Table 4. Metagreywacke, altered epiclastic or metagreywacke, highly foliated rhyolite and epiclastic rocks, quartzite, and a variety of granitic rocks are the most abundant volumetrically in the study area. Linear magnetic units include dykes of bostonite, minette, and diabase, which form multiple arrays, and iron formation, which ranges from very thin layers near the U deposits (not analyzed here) to thick banded chert-magnetite-silicate facies at the south edge of the study area. The term "altered epiclastic or metagreywacke" is used herein to refer to fine-grained schistose rocks whose original textures and mineralogy are difficult to determine because of alteration. Some of the other rock types are also highly altered but their primary textures are distinct and well enough preserved to be recognizable. Mixed metasedimentary gneiss and orthogneiss, situated along the western margin of the Kiggavik Camp, were not analyzed in this study. Assignment of lithological and map units, and the frequency + ID-numbers of samples in each rock category are listed in Appendix A2, and data

Table 4. Summary of modal mineralogy of bedrock samples based on microscopic examinations. Note: * indicates that the mineral was only visible using the SEM. Abbreviation: tr = trace.

Sample Number	Rock Name	Quartz (%)	Alkaline Feldspar (%)	Plagioclase (%)	Biotite (%)	Muscovite (%)
10-PTA-R005	Hematitzed, arkosic metagreywacke	45	5			5
10-PTA-R009a	Arkostic metagreywacke / Bostonite Sill	25	30	15	20	2
10-PTA-R012	Quartz-feldspar porphyritic rhyolite	50	20		2	17
10-PTA-R018	Hematitzed clay-rich feldspathic quartz arenite	83	15			
10-PTA-R020	Hematitzed clay-rich feldspathic quartz arenite	90	7			
10-PTA-R026a	Mafic syenite	5	30	15	10	
10-PTA-R032	Weakly altered metagreywacke / epiclastic rock	30		60	15	5
10-PTA-R040	Quartzite	95				
10-PTA-R041	Nueltin Granite	30	45	20		7
10-PTA-R044	Altered metagreywacke	40				1
10-PTA-R045	Highly altered metagreywacke					
10-PTA-R046	Highly altered metagreywacke		5			
10-PTA-R048	Metagreywacke	35		20	25	5
10-PTA-R050	Altered metagreywacke	20				5
10-PTA-R051	Altered metagreywacke	45				10
10-PTA-R053	Highly altered metagreywacke					
10-PTA-R054	Hematite-bearing quartz vein	95				5
10-PTA-R055	Porphyriric, alkalite	15	33			
10-PTA-R056	Altered metagreywacke	40				3
10-PTA-R057	Minette (lamprophyre)	10		30	25	
10-PTA-R058	Arkosic metagreywacke	35	10			20
10-PTA-R060	Porphyritic leucogranite	40	45		5	2
10-PTA-R063	Heavily altered, mineralized metagreywacke					
10_PTA-R064	Heavily altered, mineralized metagreywacke					
10-PTA-R065	Diabase			50		
10-PTR-072a	Diorite with volcanosedimentary xenoliths	30		30		
10-PTA-R072b	Diorite	20		35	5	
10-PTA-R073	Sulphide-magnetite-silicate banded iron formation				2	
10-PTA-R138	Altered minette (lamprophyre)		50	5	10	
10-PTA-R139	Highly altered feldspathic wacke	35	10			20
10-PTA-R140	Altered metagreywacke	45	15			15
10-PTA-R141	Illitized / seritized arkosic metagreywacke	45	5			20
10-PTA-R142	Highly altered, recrystallized metagreywacke	60				5
10-PTA-R143	Heavily altered, weakly mineralized arkosic metagreywacke	45				
10_PTA-R144	Arkosic metagreywacke	35	5	30	20	
10-PTA-R145	Granitic pegmatite	20	55	15		5

Table 4 continued.

Sample Number	Chlorite (%)	Horneblende (%)	Clay Minerals (%)	Uraninite (%)	Coffinite(%)	Chalcopyrite (%)	Pyrite (%)	Hematite (%)
10-PTA-R005			28					17
10-PTA-R009a	7						1	1
10-PTA-R012			10				1	
10-PTA-R018								2
10-PTA-R020								3
10-PTA-R026a		20				tr	1	1
10-PTA-R032						tr	tr	tr
10-PTA-R040			2					1
10-PTA-R041	1						tr	
10-PTA-R044	15		40				4	
10-PTA-R045			98	tr			tr	1
10-PTA-R046							tr	tr
10-PTA-R048						1	3	1
10-PTA-R050	5		70	tr*			2	3
10-PTA-R051			44	tr*				1
10-PTA-R053			98	tr*			1	1
10-PTA-R054								
10-PTA-R055			50				tr	tr
10-PTA-R056	10		45			tr	2	
10-PTA-R057	30						3	
10-PTA-R058			10			tr	4	
10-PTA-R060							tr	tr
10-PTA-R063			29	50	15		tr	tr
10_PTA-R064			50	25	15			
10-PTA-R065						tr	tr	
10-PTR-072a	5	5				tr	tr	tr
10-PTA-R072b	5	25					1	tr
10-PTA-R073							10	tr
10-PTA-R138	5	8	10			tr	tr	
10-PTA-R139	5		25					2
10-PTA-R140			25					5
10-PTA-R141			28				2	
10-PTA-R142			35				tr	tr
10-PTA-R143			50	tr*			2	tr
10_PTA-R144	5					tr	3	
10-PTA-R145								

Table 4 continued.

Sample Number	Clinopyroxene (%)	Apatite (%)	Pb Apatite (%)	Fluorite (%)	Magnetite (%)	Molybdenite (%)	Galena (%)	Rutile (%)
10-PTA-R005								
10-PTA-R009a		1		tr				
10-PTA-R012								
10-PTA-R018								
10-PTA-R020								
10-PTA-R026a	15	1			1			
10-PTA-R032		tr						
10-PTA-R040								
10-PTA-R041					tr	tr		
10-PTA-R044								
10-PTA-R045		tr*	tr*					
10-PTA-R046		tr*	tr*				tr	tr
10-PTA-R048								
10-PTA-R050		tr	tr*					
10-PTA-R051		1*	tr*					1*
10-PTA-R053								
10-PTA-R054								
10-PTA-R055		1						
10-PTA-R056								
10-PTA-R057		2*						tr
10-PTA-R058					tr			
10-PTA-R060					tr			
10-PTA-R063								
10_PTA-R064							5	
10-PTA-R065	35				10			
10-PTR-072a								
10-PTA-R072b					3			
10-PTA-R073					tr			
10-PTA-R138								tr
10-PTA-R139								3
10-PTA-R140								
10-PTA-R141								
10-PTA-R142								
10-PTA-R143		tr*	tr*					1
10_PTA-R144								
10-PTA-R145								

Table 4 continued.

Sample Number	Calcite (%)	Olivine (%)	Ilmenite (%)	Actinolite (%)	Grunerite (%)	Almandine (%)	Tourmaline (%)
10-PTA-R005							
10-PTA-R009a							
10-PTA-R012							
10-PTA-R018							
10-PTA-R020							
10-PTA-R026a							
10-PTA-R032							
10-PTA-R040							
10-PTA-R041							
10-PTA-R044							
10-PTA-R045							
10-PTA-R046							
10-PTA-R048							
10-PTA-R050							
10-PTA-R051							
10-PTA-R053							
10-PTA-R054							
10-PTA-R055							
10-PTA-R056							
10-PTA-R057							
10-PTA-R058							
10-PTA-R060							
10-PTA-R063							
10_PTA-R064	5						
10-PTA-R065		5					
10-PTR-072a			2				
10-PTA-R072b				27			
10-PTA-R073					75	10	
10-PTA-R138							
10-PTA-R139							
10-PTA-R140							
10-PTA-R141							
10-PTA-R142							
10-PTA-R143							
10_PTA-R144							
10-PTA-R145							5

acquired are summarized in Table 2. Reported percentages of mineral phases represent modal abundances as determined by SEM; percentages of ore minerals are reported by weight, as determined by EMPA.

Metagreywacke of the ca 2.7 Ga Pipedream assemblage, Woodburn Lake group, is overwhelmingly the most abundant rock type volumetrically in the southern two-thirds of the study area. This assemblage includes subcategories such as fresh lithic to arkosic metagreywacke, altered and non-altered metagreywacke, and possibly mineralized metagreywacke. Original field sampling was intended to obtain more of this rock type for analysis than the others, but petrography showed that 9 of the highly altered samples collected to represent fine-grained metagreywacke are more likely to be felsic epiclastic facies of the 2.6 Ga Pukiq Lake Formation rhyolite (see below).

The metagreywacke includes fine-grained thin-bedded and medium- to coarse-grained thick-bedded facies. Depositional layering is transposed subparallel to strong S_1 foliation despite graded bedding being recognizable in places (Appendix B, sample 10-PTA-R043). In most cases bedding is sheared to the extent of being indistinct (e.g. Appendix B, sample (10-PTA-R044). The mineralogy of less altered metagreywacke samples is dominated by quartz, biotite, and altered feldspar with minor muscovite, and is typically enclosed in a fine matrix of clay and chlorite minerals. Quartz is seriate in grain size but typically less than 50 μm in diameter and polygonized. Samples that contain larger (>200 μm) pretectonic "quartz eyes", and that are wrapped by finer grained mica and quartz, are here assigned to the "epiclastic or metagreywacke" class (below). Feldspar typically constitutes about 20 to 30% of the metagreywacke mineralogy but due to metamorphic recrystallization, the original lithic clasts are identifiable only in hand specimen. Alkali feldspar is more prevalent than plagioclase and is in the same size range as quartz. Again, samples that preserve bimodal feldspar (phenocrysts ranging to >5 mm) are classified here as epiclastic. Muscovite is common, constitutes approximately 5 to 10% of the sample, and typically alters feldspar with a median grain size of 100 μm. Prior to ore-related alteration, the metagreywacke underwent regional upper greenschist- to lower amphibolite-grade metamorphism and multiple deformation events prior to regional retrograde chloritization. Localized, ore-related alteration (illitization, hematitization) took place during later hydrothermal events.

The content of highly altered samples is predominantly illite and hematite and their textures preserve little to no trace of the original coarse-grained (>200 μm) detrital quartz and feldspar or metamorphic muscovite, although muscovite was the last pre-alteration phase to be converted to clay minerals (Appendix G, Figs. G-10, -11, -12). Furthermore, with increasing alteration there is a greater likelihood the samples contain U-bearing minerals, Pb-apatite, pyrite, galena, and hematite. These minerals are commonly less than 50 μm and require an SEM to be identified.

Rhyolite and epiclastic rocks of the 2.6 Ga Pukiq Lake Formation are the extrusive equivalents of the Snow Island Suite of large domal granitoid intrusions and tectonic sheets (Peterson et al., 2015c; Fig. 3), and are characterized by flattened, polygonized, and variably comminuted phenocrysts of quartz and feldspar in a very fine-grained quartzofeldspathic matrix that has metamorphic lithons of muscovite and strung-out quartz defining the intense foliation. This class is represented by 8 samples, with some of the ***rhyolite*** examples being quite altered and uraniferous, yet retaining the above defining characteristics. Highly altered, fine-grained, foliated, and intensely clay-altered and mineralized supracrustal rocks without preserved phenocrysts are enigmatic, and thus assigned to the "Epiclastic or fine metagreywacke" class below. Nevertheless, abundant well preserved rhyolite outcrops and drill intersections, together with newly documented epiclastic rocks (this study; V. McNicoll, pers. comm., 2013; Johnstone, 2015) and the enigmatic highly altered schists are important along the south side of the Thelon Fault where they are structurally interleaved with contrasting quartzite of the Paleoproterozoic Ketyet River group. Outside the study area, especially around upper Meadowbank River and beneath the Amer Group, the rhyolite is extensively preserved between older Archean rocks and the unconformably overlying Paleoproterozoic conglomerate and quartzite, and is included as clasts within that conglomerate (Pehrsson et al., 2013; Jefferson et al., 2015). One of the best rhyolite examples studied here is sample 10-PTA-R012, which is light pink to white, strongly foliated, metamorphosed to upper greenschist facies, and displays mylonitic lamination that wraps around pretectonic phenocrysts of quartz and K-feldspar. The quartz and K-feldspar range in size from <50 μm to 2 mm. Larger quartz phenocrysts are polygonized and flattened by deformation. Larger phenocrysts of K-feldspar are fractured and variably altered to sericite and other clay minerals. Muscovite (median grain size of 200 μm) commonly forms metamorphic microlithons between quartz and K-feldspar microlithons and the muscovite wraps around phenocrysts. Lesser components include biotite, very fine-grained clay minerals, and fine-grained disseminated pyrite (1%) that is preferentially associated with the biotite (Appendix E). Epiclastic samples 10-PTA-R050, -R140, and -R141 were classified as such due to their clearly porphyritic texture despite intense alteration. These samples are composed of 45% quartz, 20% mus-

covite, and sericite, 5–15% K-feldspar, and 1% pyrite, with the remainder being finer clay and hematite alteration, mainly of the feldspar and matrix minerals. The non-rhyolite designation is based on several lines of evidence. Firstly, these samples are finely laminated to thinly bedded and have a sedimentary appearance. Secondly, they contain mafic impurities indicated by abundant hematite, which is interpreted as an alteration product of non-rhyolite material incorporated during sedimentary reworking of the dominantly extrusive volcanic detritus. Finally, to test for provenance, representative sample 12JP040 was taken from hole GG21, which was drilled in July 2012 in the Granite Grid area north of Bong, was analyzed for detrital zircons by V. McNicoll (pers. comm., 2013). The 50 analyses resulted in a nearly unimodal but clearly detrital zircon age distribution that ranged from ca. 2655 to 2595 and peaks at ca. 2607 Ma (V. McNicoll, unpubl. data).

Enigmatic ***epiclastic rock*** or fine-grained ***metagreywacke***, highly altered were originally classified in the field as altered fine-grained metagreywacke or metapelite, but after closer inspection the highly altered, strongly foliated, fine-grained rock samples appear more likely to be part of the Pukiq Lake Formation epiclastic facies. Some fine-grained rhythmically thin-bedded metasedimentary rocks, such as shown in the upper photograph of sample 10-PTA-R043 in Appendix B, have a porphyritic appearance and may be tectonic slices of Pukiq Lake Formation interleaved with metagreywacke of the Pipedream assemblage. Many such rocks in the study area may be reclassified as part of the Pipedream assemblage but in this study (stimulated by consistent camp-scale mapping of Urangeselleschaft in the 1980s, GEM-U from 2006 to 2012, and Dillon Johnstone, University of Regina and AREVA in 2015) the 9 samples listed in the enigmatic category are assigned to the Pukiq Lake Formation because of their context (structurally intercalated with quartzite of the Ketyet River group) and their greater resemblance in hand specimen to less altered epiclastic rocks than to coarse-grained greywacke (described above). Petrographically, what remains of the primary mineralogy in these highly altered samples is similar to the epiclastic rocks described above, although they lack preserved phenocrysts and their mineralogy is dominated by clay, hematite, and disseminated uraninite.

Granitoid rocks are represented in this study by several suites of pink, coarsely crystalline, mainly equigranular and undeformed, quartz – K-feldspar – plagioclase granite with minor muscovite and mafic minerals. The assignments made here to the various granitoid suites are based on Scott et al. (2015). The regional mid-crustal 1.83 Ga Hudson Granite is manifested as i) thin sheets structurally concordant within metagreywacke above the KMZ and CZ (sample 10PTA-R009B); ii) small plugs with local pyrite and molybdenite including the Lone Gull (samples 10PTA-R041,-R042,-R060, -R137) and a cluster in Granite Grid (sample 10PTA-R030); iii) aplite to pegmatite, such as patches within the Granite Grid plugs, and in solitary dykes, such as the northerly trending 2 m outcrop southwest of and above KMZ (sample 10PTA-R145); and iv) the Schultz Lake Intrusive Complex (samples 10PTA-R026B,-R028) that lies west of the Granite Grid, End and Andrew Lake prospects, and intrudes the Marjorie Hills assemblage. The Lone Gull plug underlies and is partly mineralized in the KMZ, and comprises predominantly medium crystalline equigranular Hudson Granite with a minor compositional and metasomatic component of hypabyssal porphyritic 1.75 Ga Nueltin Granite (Scott et al., 2015). The medium to coarsely crystalline mafic ***Martell Syenite*** (1.83 Ga, part of the Hudson Suite) is represented by sample 10PTA-R026A from the SLIC and sample 10PTA-R055 from below the KMZ. The latter strongly resembles the porphyritic Bong syenite plug as described by Scott et al. (2015).

From the Judge Sissons Lake pluton, sample 10PTA-R072A and –R027B, respectively, represent ***agmatite*** and ***quartz diorite*** to ***granodiorite*** and ***agmatite*** of the 2.6 Ga Snow Island Suite (Peterson et al., 2015c). The ***agmatite***, a diagnostic characteristic of the Snow Island Suite, looks like an intact-framework conglomerate, comprising abundant supracrustal xenoliths (greywacke, basalt, iron formation) in a diorite matrix. Mafic volcanic xenoliths are associated with abundant fibrous actinolite (<50–750 μm) at contacts with the granodiorite matrix. Minor 1–2 mm almandine porphyroblasts are present in hand samples of xenoliths. The ***quartz diorite*** to ***granodiorite*** is weakly foliated, medium to coarsely crystalline, with subhedral primary plagioclase, amphibole, and quartz that is partly altered mainly to chlorite. Plagioclase is dominant, ranging in size from 0.25 to 3 mm. Poikilitic hornblende constitutes up to 25% of the diorite: including biotite and chlorite within crystals and along fractures. Quartz (<50 μm – 3 mm) constitutes ≤30% of both samples, is localized in pockets, and appears to be one of the alteration products of some feldspars. Pyrite, ilmenite, and magnetite together make up ≤3% of the rock except locally where iron formation has been partly assimilated. Magnetite is generally 250 μm in size, commonly included within biotite grains, and partly altered to martite. Pyrite and ilmenite are finely disseminated throughout the rock and do not exceed 200 μm in size. No U-bearing minerals were detected.

Minor and trace minerals from the granitic samples were investigated as possible tracers in till. Biotite constitutes very little of the granite but ranges up to about

5% of the mafic syenite, whose main mafic mineral, hornblende, reaches 10% or more in the diorite. Biotite and hornblende typically range from 0.1 to 3 mm with a median diameter of 0.3 mm. Muscovite constitutes about 5% of the granite but is absent from syenite and diorite. Other granite-hosted minerals (pyrite, magnetite, fluorapatite, and molybdenite) are generally <1%, although locally abundant in patches. They rarely exceed 200 μm in size and are commonly interstitial to biotite grains and/or disseminated. Clay minerals in altered granite and syenite range in abundance from partial replacement of feldspar to 100%, and hematite ranges from coatings on pyrite to disseminated throughout. Some parts of the Lone Gull granite contain abundant disseminated uraninite (Fuchs et al., 1985; Weyer et al., 1989; Reyx, 1994), but were not examined in this study.

Magnetic dykes include multiple arrays and ages of ***bostonite***, ***minette***, and ***diabase***, all with distinct linear magnetic anomalies. The bostonite and minette dykes cut the Neoarchean and Paleoproterozoic units, are coeval with the 1.83 Ga Hudson Suite and Martell Syenite, and are texturally similar hypabyssal representatives of ultrapotassic felsic and mafic flows in the Christopher Island Suite (CIF). They are rarely exposed, but are commonly intersected by drill core. ***Bostonite*** (mafic syenite; sample 10PTA-R138) differs from the coeval Martell Syenite and Hudson Granite in that it has a red-brown aphanitic matrix with abundant phenocrysts of K-feldspar, biotite, and hornblende; and only relict, partly resorbed quartz (Appendices D, G). ***Minette*** (lamprophyre) dykes (samples 10PTA-R052, -R057) cut and are mingled with (sample 10PTA-R061) granite and syenite, and contain abundant biotite/hornblende phenocrysts generally altered to chlorite. The bostonite and minette samples are dominated by K-feldspar (35–50%), with grain size ranging from <50 to 350 μm. The cores of K-feldspar phenocrysts are typically altered to clay minerals. Biotite is abundant, ranging up to 25%. Platy to felted clusters of chlorite replace tabular mafic minerals interpreted to have been either hornblende or biotite. The tabular mafic phenocrysts and their pseudomorphs range from <50 to 500 μm in length. Primary hornblende, which constitutes 8% of sample 10-PTA-R138, ranges in length from 100 to 300 μm. Up to 3% disseminated pyrite ranges in size from <50 to 400 μm in most of these samples, with many minor inclusions of fine-grained trace chalcopyrite (<50 μm). Alteration ranges from minimal to extreme, in which the bostonite cannot be readily distinguished from minette. U minerals were not found. ***Diabase dykes*** include the moderately to strongly magnetic but very recessive (not sampled here) 1.75 Ga Thelon River (075°) and McRae Lake (015°) swarms of the 1.75 Ga KIS. A strongly magnetic Mackenzie Diabase (150°; sample 10PTA-R065) that cuts the Thelon Fault north of Siamese lake has ophitic texture with large interlocking plagioclase laths (50%) that range from 0.1 to 5mm in length. Equant augite (40%) ranges in diameter from 0.1 to 0.3 mm. Partly serpentinized fayalitic olivine (<5%) has a strong spatial association with magnetite. Trace disseminated chalcopyrite and pyrite range in size from 25 to 200 μm. No U minerals were observed.

Feldspathic litharenite: the alluvial Thelon Formation crops out northwest of the KMZ, north of the Thelon Fault. This heavily clay-altered litharenite to quartz pebble conglomerate with sparse to abundant quartz pebbles and abundant disseminated hematite is represented by samples 10PTA-R018, -R020, and -R024. The only framework mineral preserved is poorly sorted, moderately well rounded quartz (80%), although the outlines of altered lithic grains are well defined. The lithic and feldspar grains are 100% altered to clay minerals, which were not identified in this study (Appendices D, G). No U minerals were observed. Red mudstone with desiccation cracks (sample 10PTA-R033) is characteristically interbedded with the basal conglomerate facies of the Thelon Formation; its hematite is interpreted as diagenetic. Discontinuous lenses of silicified feldspathic quartzite (sample 10PTA-R016), which are found along the Thelon Fault, are interpreted as the older Amarook Formation of the Wharton Group.

Quartzite, which is represented by 3 samples, is locally hematitized and has yellowish patches believed to be sericite-altered interstitial clay minerals. The >95% quartz is highly polygonized and sutured. The only primary sedimentary structures preserved are stylolitized bedding planes, which have been transposed parallel to foliation and partially altered to earthy hematite. No U minerals were noted. Sample 10-PTA-R054 of the quartzite is dominated by extensional veins of white quartz with drusy terminations coated by abundant coarse-grained (0.5–2 mm) platy crystals of specular hematite. Specular hematite also fills crack-seal veins. No U minerals were observed.

Banded Iron Formation (BIF) is represented in the vicinity of the Kiggavik deposits by centimetre-scale laminated chert-magnetite interbeds within pelitic facies of the Pipedream metagreywacke; these BIF beds have no discernable aeromagnetic expression and were not noted within ore zones. The sample examined in this study is a magnetically lean portion of a silicate-magnetite-sulphide facies BIF within the Halfway Hills assemblage. Overall this BIF has a very strong linear aeromagnetic signature transecting Judge Sissons Lake with steep dips and considerable thickness. The studied sample consists mostly of acicular, medium-grained (0.3–0.5 mm) grunerite with ~10% coarse-grained (2–

5 mm) almandine porphyroblasts, minor coarse-grained biotite and magnetite, but 15 % recrystallized, fine- to medium-grained (0.1–0.5 mm) disseminated pyrite, which is also reconcentrated along fractures. No U minerals were observed.

Uranium ore minerals in the study area are developed in altered phases of three rock units: the 2.7 Ga Pipedream metagreywacke, the highly strained 2.6 Ga Pukiq Lake Formation epiclastic and rhyolite (this study), and the silicified brecciated products of the 1.75 Kivalliq Igneous Suite. The last includes Pitz Formation rhyolite, which is commonly silicified and brecciated, and Hudson granite plugs, which have been infiltrated and/or metasomatized by Nueltin granite (Scott et al., 2015). Cameco Corporation has defined uranium zones in altered metasedimentary gneiss (R. Hunter, oral presentation, Nunavut Mining Symposium, 5 April, 2011) that Jefferson et al. (2015) assigned to the Marjorie Hills assemblage. Hudson Granite, Martell Syenite, bostonite, minette, and diabase are not significant U hosts, even though all but the diabase have been altered to clay minerals (P. Wollenberg, pers. comm., 2009).

Uraninite and ***coffinite***, which are the dominant U minerals, rarely exceed 100 µm in size. Samples 10-PTA-R063 and -R064 are the only bedrock samples that contain a high abundance (>40%) of U minerals (Fig. 12c). Uraninite ranges from coarsely crystalline (>2 mm) and densely disseminated, to massive and transected by multiple intersecting veinlets of calcite and/or quartz. Uraninite and coffinite in samples 10-PTA-R063 and -R064 completely replace original detrital feldspar and mafic minerals, as well as forming an unresolvable matrix to felted replacement chlorite and illite along foliation planes. Uraninite intergrown with illite also partially replaces metamorphic muscovite. With the use of the SEM, uraninite was also identified in samples 10-PTA-R045, -R046, -R050, -R051, -R053, and R-139. Uraninite makes up less than 1% of any of the samples, does not exceed 50 µm in size and is commonly intermixed with alteration pyrite and hematite. Coffinite in samples 10-PTA-R063 and -R064 ranges in crystal size from <25 to 100 µm and has the same textural associations as uraninite.

Galena (<1%) is also present with uraninite and coffinite, within altered metagreywacke, and ranges in crystal size mostly from <25 to 75µm. Only one sample (10-PTA-R046) was observed to have a galena crystal greater than 150 µm in diameter (Appendix G).

Pyrite is present in both fresh and altered metagreywacke samples. In fresh samples, pyrite is subhedral to euhedral and ranges from <100 µm – 1.5 mm in diameter; sample 10-PTA-R058 contains up to 4%. In such samples, trace amounts of chalcopyrite are typi-

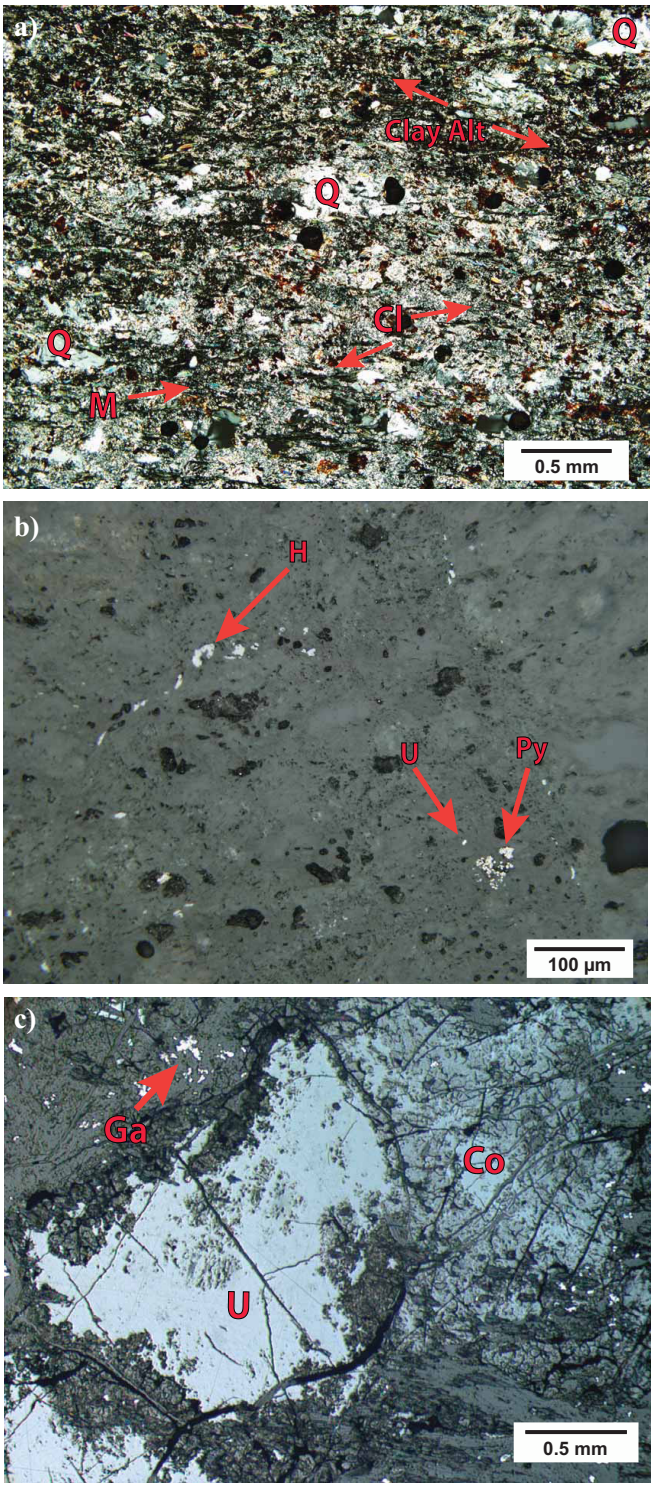

Figure 12. Samples with U oxide minerals. **a)** Original phyllosilicate mineralogy has been altered to chlorite and illite. Sample 10-PTA-R050, transmitted light (XPL), highly altered, weakly mineralized. **b)** Small grain size of uraninite is common in all samples with U oxide minerals with the exception of samples 10-PTA-R063 and -R064. Sample 10-PTA-045, reflected light. **c)** Coarse-grained uraninite and coffinite with fine-grained galena. Sample 10-PTA-R063, reflected light. Abbreviations: Cl = chlorite, Clay Alt = clay alteration, Co = coffinite, H = hematite, Ga, = galena, M = muscovite, Py = pyrite, Q = quartz, U = uraninite.

cally <50 μm in size (Appendix G). Within altered samples, pyrite ranges in texture from anhedral to subhedral to framboidal. It is commonly rimmed by hematite and is located proximal to uraninite, both along foliation planes and as a mica replacement. Chalcopyrite was not observed in altered metagreywacke.

Hematite occurs in most metagreywacke samples, altered and fresh. Hematite ranges from <25 to 200 μm with a median size of 50 μm and is more abundant in altered samples where hematite constitutes up to 3%. In altered samples, particularly U-rich zones, hematite is commonly in close association with pyrite and uraninite. Many hematite grains appear to be weathered, and exhibit alteration to limonite or goethite.

Multiple ***accessory and trace minerals***, in addition to those described above, are only identifiable in the metagreywacke generally with the aid of an SEM. Such minerals as apatite, rutile, titanite, and magnetite are present in non-altered greywacke, typically less than 100 μm in size and most less than 50 μm. Of particular interest is the presence of Pb-rimmed fluorapatite, which is found only in weakly mineralized (<2% U-minerals), altered metagreywacke. These disseminated fluorapatite grains are generally about 50 μm in diameter and some are also rimmed by uraninite. Further analyses of these Pb-apatite grains are discussed in the microprobe section of this report.

Summary of mineralogy

A significant amount of mineralogical variation is documented among the 10 different rock groupings detailed above. In order to assess what might possibly have contributed to the till HMCs, Table 5 highlights the respective grain-size ranges of light minerals (<3.2 g/cm^3) and heavy minerals (>3.2 g/cm^3) identified in this study.

Table 5. Summary of the mineralogy observed in bedrock samples and the range of grain sizes. Minerals are divided into light and heavy to illustrate potential application for recovery from bulk till samples.

Light Minerals (<3.2 g/cm^3)	
Mineral	**Grain Size Range**
Quartz	<25 μm – >5 mm
Alkali Feldspar	<0.1 mm – >5 mm
Plagioclase	0.1 mm – 5 mm
Muscovite	<25 μm – 3 mm
Biotite	<0.1 mm – 4 mm
Chlorite	50 μm – 2 mm
Hornblende	0.1 mm – 3.5 mm
Actinolite	<50 μm – 3 mm
Apatite	<25 μm –100 μm

Heavy Minerals (>3.2 g/cm^3)	
Mineral	**Grain Size Range**
Diopside	3 mm – 8 mm
Augite	0.1 mm – 0.3 mm
Pb -Apatite	15 μm – 100 μm
Hematite	<25 μm – 2 mm
Magnetite	0.1 mm – 2 mm
Pyrite	<25 μm – 1.5 mm
Chalcopyrite	<25 μm – 250 μm
Rutile	<25 μm – 150 μm
Coffinite	<25 μm – 100 μm
Uraninite	<25 μm – 700 μm
Titanite	<10 μm – 300 μm
Almandine	1 mm – 2 mm
Molybdenite	300 μm
Galena	<25 μm – 500 μm
Olivine	<0.2 mm – 1.5 mm
Ilmenite	<25 μm – 250 μm

Heavy mineral recovery techniques

Quality control of quartz blanks interspersed with bedrock samples is summarized in Table 6, with the results normalized to 500 g grain counts for the quartz blanks and disaggregated bedrock samples. Contamination was detected in 18 of the 19 blanks processed. Pyrite grains recovered from the pan concentrate of quartz blanks were the most common form of contamination: ranging from zero to 200 grains). In addition to low counts of pyrite grain contamination in the 0.25–0.5 mm fraction of the quartz blanks, other minerals and forms of contamination — such as metal turnings, hornblende, augite, molybdenite and diopside — were panned and picked. The source of contamination is typically the sample that had been processed just before the sample being reported. For instance, blanks with apparent high pyrite content (samples 10-PTA-QB507, -QB517, -QB518) had been processed immediately after samples containing >100 000 pyrite grains. Furthermore, 30 augite and 5 ilmenite grains were picked from sample 10-PTA-QB513 in the 0.25–0.5 mm fraction. This contamination can be attributed to the previous sample (10-PTA-R065), which is described as a fine- to medium-grained mafic intrusive rock (diabase) (Appendix E2). It is intriguing that sample 10-PTA-R065 was reported to yield no heavy minerals from the 0.25–0.5 mm fraction, whereas a diabase would be expected to produce at least a few heavy minerals, such as ilmenite and magnetite.

Processing quartz blanks after each bedrock sample allows for the carryover of pyrite grains from previous pyrite-rich samples, ultimately catching them and limiting the carryover of heavy minerals to the next bedrock sample of interest. Despite the limited carryover of heavy minerals among bedrock samples, there was some carryover into the quartz blanks. Despite

Table 6. Heavy minerals picked from pan concentrates and 0.25–0.5 mm heavy liquid HMCs of disaggregated bedrock samples and quartz blanks. Notes: * indicates that only the pan concentrate was picked; ** indicates that only the 0.25–0.5 mm HMC fraction was picked.

Sample Number	Pan Concentrate			0.25–0.5 mm	
	Gold	Pyrite	Additional Grains	Pyrite	Additional Grains
10-PTA-QB501	0	2	0	0	0
10-PTA-R072a	0	948	379 Arsenopyrite, 2 Galena	N/A	N/A
10-PTA-QB502	0	2	0	0	0
10-PTA-R048	0	5747	0	275	1 Apatite
10-PTA-QB503	0	0	0	0	0
10-PTA-R047	2	2	0	N/A	N/A
10-PTA-QB504	0	14		0	0
10-PTA-R072b	0	2576	86 Arsenopyrite, 2 Loellingite	1470	15 Apatite
10-PTA-QB505	0	15	0	0	0
10-PTA-R060	0	47438	474 Galena	~1800	36 Fluorite, 6 Hematite
10-PTA-QB506	0	50	0	0	0
10-PTA-R062	0	112918	0	~6750	0
10-PTA-QB507	0	100	0	2	2 metal turnings
10-PTA-R012	2	99	0	N/A	N/A
10-PTA-QB508	0	20	0	2	0
10-PTA-R026a	0	1779	0	60	~30000 Apatite
10-PTA-QB509	0	10	0	0	2 Augite, 2 metal turnings
10-PTA-R054	0	18	0	22	~2200 Hematite
10-PTA-QB510	0	3	0	0	5 Hornblende
10-PTA-R041	0	56883	38 Molybdenite	~1400	120 Barite, 81 Apatite
10-PTA-QB511	0	80	0	0	0
10-PTA-R041	0	96	4 Molybdenite	N/A	N/A
10-PTA-QB512	0	15	0	2	2 Molybdenite 2 Hornblende
10-PTA-R005	0	261	0	0	0
10-PTA-QB513	0	30	0	4	30 Augite, 5 Ilmenite
10-PTA-R065	0	39170	0	~12000	1 Hematite
10-PTA-QB514	0	0	0	7	2 metal turnings
10-PTA-R056	0	295	0	1	~16650 Hematite
10-PTA-QB515	0	40	0	0	1 Hornblende, 1 metal turnings
10-PTA-R020	0	2976	0	~1540	0
10-PTA-QB516	0	30	0	0	1 Augite
10-PTA-R032	0	40%	2 Galena	~29000	0
10-PTA-QB517	0	500	0	0	0
10-PTA-R057	0	182149	146 Molybdenite	~4200	1 Fluorite, 8 Molybdenite, 7 Apatite
10-PTA-QB514	0	200	0	7	2 Diopside
10-PTA-R056	0	104123	10412 Molybdenite	1	N/A
10-PTA-QB515	1	7217	0	0	180 Barite, 180 Molydenite
Quartz Blank	0	~200	0	N/A	N/A

pyrite carryover into many quartz blanks, the highest count of pyrite grains (200) recovered in a quartz blank (sample 10-PTA-QB518) represents 0.2% cross contamination because more than 180 000 grains were recovered from the preceding sample (10-PTA-R057). Ultimately, a cross-contamination rate of 0.2% should add very little to the next sampled being processed. Despite the minimal cross contamination, these results reinforce the due diligence of spending significant time on thoroughly cleaning equipment after each rock disaggregation, particularly after samples that have abundant sulphide minerals.

Quality control of till duplicates and background till samples is summarized in Table 7. The heavy minerals recovered are normalized to 10 kg from field duplicates. Gold grain recovery from the pan concentrate is highly variable for two of the three field duplicate pairs, wherein as an example, sample 10-PTA-118

Table 7. Heavy mineral recovery from **(a)** field till duplicate samples (normalized to 10 kg), and **(b)** standards (non-normalized).

a)

Till Duplicates	Pan Concentrate		0.25–0.5 mm			
	Gold grains	Miscellaneous	Fluorite	Barite	Pyrite	Chalcopyrite
10-PTA-095	11	0	0	154	0	0
10-PTA-113	29	0	0	244	2	0
10-PTA-128	5	0	43	259	0	0
10-PTA-138	7	0	134	223	0	0
10-PTA-118	24	0	2	56	15	6
10-PTA-119	5	0	15	35	0	8

b)

Standard	Pan Concentrate		0.25–0.5 mm
	Gold grains	Miscellaneous	Miscellaneous
10-PTA-095	0	0	0
10-PTA-113	0	0	1 chalcopyrite, 20 pyrite, 3 spinel, 50 chondrodite
10-PTA-128	1	0	0
10-PTA-138	0	0	20 chalchopyrite, 20 pyrite, 11 spinel, 40 chondrodite, 100 red rutile
10-PTA-118	0	1 galena	0

Bathurst standard (Weathered Granite)
Almonte standard (Canadian Shield Till)

has nearly 5 times more gold grains than sample 10-PTA-119. This discrepancy between duplicate pairs is not reciprocated in the larger 0.25–0.5 mm fraction, aside from the fluorite count in samples 10-PTA-128 and -133. Chalcopyrite is the sole heavy mineral of interest in the 0.25–0.5 mm fraction and there is little to no discrepancy between counts in samples 10-PTA-118 and -119.

The background samples (non-normalized) submitted with the bulk till samples were obtained from weathered Silurian-Devonian granite near Bathurst, New Brunswick (McClenaghan et al., 2012; Plouffe et al., 2013) and from till exposed in a borrow pit near Almonte, Ontario (Henderson, 1973; Plouffe et al., 2013). Only one grain of galena and one grain of gold were recovered from the pan concentrate in samples 10-PTA-148 and -150. The single gold grain found in sample 10-PTA-148 is possibly from carryover of the previously processed sample (10-PTA-098), which has a count of 17 gold grains in the pan concentrate. However, some Bathurst standards do contain very rare gold grains (Plouffe et al., 2013). The galena grain recovered in sample 10-PTA-150 is likely a result of contamination from an external source as opposed to carryover because that is the sole example of galena in all 71 till samples.

No heavy minerals were recovered from the 0.25–0.5 mm fraction of the Bathurst standards. Heavy minerals, such as chalcopyrite, pyrite, spinel, chondrodite and red rutile, were recovered from samples 10-PTA-147 and -149 (Table 7), but are not considered contamination because they are common in the Almonte standards (Plouffe et al., 2013).

Heavy minerals recovered from bedrock samples

Native gold grains less than 50 µm in diameter were recovered from the pan concentrates of two disaggregated samples (Table 6). Sample 10-PTA-R047 (1.75 Ga brecciated and silicified Pitz rhyolite that occupies a northerly trending fault zone southeast of Judge Sissons Lake) yielded 2 gold grains via selFrag™ disaggregation, and sample 10-PTA-R138 (1.83 Ga minette dyke cutting the Andrew Lake deposit) yielded 2 gold grains via EPD (Appendix E2b).

Pyrite grains were recovered from all of the pan concentrates and 13 of the 14 fine (0.25–0.5 mm) HMC fractions that were picked (Table 6). Pyrite from the pan concentrate ranges from 3 to >100 000 grains, with sample 10-PTA-R073 (silicate-facies iron formation) containing the most – more than 40% of the grains picked.

Molybdenite, ***galena***, and ***arsenopyrite*** recoveries are summarized in Table 6. Molybdenite grains were recovered from both the pan concentrate and the 0.25–0.5 mm HMC of five samples. Molybdenite grain counts normalized to 500 g range from 0 to 10,412 in the pan concentrate and 0 to 180 in the 0.25–0.5 mm fraction. Galena grains were recovered in three samples (10-PTA-R072a, -R060, -R032) solely in the pan concentrate, with counts ranging from 0 in most sample to 474 grains (normalized to 500 g) in sample 10-PTA-R060. Similarly to galena, arsenopyrite grains were recovered solely from the pan concentrate and were recovered in two samples (10-PTA-R072a, -R072b), with grain counts of 379 and 86 (normalized to 500 g), respectively.

Apatite grains were recovered from 5 samples (10-PTA-R048, R072b, -R026a, -R041, And -R057) in the 0.25–0.5 mm fraction. Grain counts range from 0 to ~30 000 in sample 10-PTA-R026. No fluorapatite was recovered from the pan concentrate.

Additional heavy minerals recovered, (in order of abundance: apatite, hematite, barite, fluorite, and loellingite) are normalized to 500 g in Table 6. Counts of common heavy minerals, such as hornblende, augite, and diopside, are reported in detail in Appendix E2.

Heavy minerals recovered from till samples (Appendix E)

Native gold grains in till are <100 µm in size, and all of these were recovered only from the pan concentrate (Table 8). Total gold grain content in the till samples ranges from 0 to 115 grains, with the average being 13 grains per sample. Samples containing abundant gold grains include 10-PTA-117 (115 grains), -120 (59 grains), -097 (48 grains), -125 (39 grains), and -047 (36 grains), which are located 5 m, 250 m, 3 km, 250 m, and 28 km from the KMZ, respectively (Fig. 13, Table 8). To help determine proximity to source, recovered gold grains were divided into three classes by ODM geologists: pristine being the most proximal to the source, modified, and reshaped, which is the most distal (Dilabio, 1990). The majority of grains (67%) were reported as reshaped, with 25% being classified as modified and 8% being pristine (Robinson, 2015). The distance between each till sampling location and the KMZ was compared to gold grain morphology. No correlation is apparent, which strongly suggests that the relative abundances of pristine grains (R = -0.04), modified grains (R = 0.15), and reshaped grains (R = -0.12) is independent of sampling distance. The total abundance of gold grains does however seem to relate to proximity to the source, given the high abundance in till right at Kiggavik and the local abundance at station 10PTA-R047 beside an outcrop of gold-bearing quartz-veins in rhyolite. More detailed data and testing of alternative possibilities would be required to verify this.

Pyrite grains were recovered from both the pan concentrate and the 0.25–0.5 mm fraction of the HMC (Table 8, Fig. 14), with the majority being recovered in the coarser fraction. Total pyrite content in the till samples ranged from 0 to 1000 grains, with most yielding 0 to 5 grains. Samples containing abundant pyrite in the 0.25–0.5mm fraction include 10-PTA-073 (800 grains), -117 (300 grains), -094 (1000 grains) and -116 (115 grains). Sample 10-PTA-098 with 20 pyrite grains and 10-PTA-134 with 10 pyrite grains were the only samples from which pyrite was recovered in the pan concentrate.

Chalcopyrite contents in till samples range from 0 to 21 grains, with an average of 3 grains per sample (Table 8, Fig. 15). Chalcopyrite grain counts are highest in samples 10-PTA-122 (21), -116 (17), -119 (8), and -10-PTA-129 (7) in the 0.25–0.50 mm size fraction normalized to 10 kg. Chalcopyrite was not observed in the pan concentrate.

Barite concentrations in till samples ranged from 0 to 2857 grains, with an average of 1164 grains per sample (Table 8, Fig. 16). As a result of the high number of barite grains, total counts by ODM (Appendix E2) are reported as a percentage of the total sulphide and arsenide minerals and are approximations. Barite is abundant in most samples, but is particularly elevated in samples 10-PTA-048 (2857), -071 (1031), -112 (562), -130 (463), and -085 (462) in the 0.25–0.50mm size fraction normalized to 10 kg. Barite grains were not observed in the pan concentrate.

Fluorite in till samples ranges from 0 to 216 grains, with an average of 22 grains per sample although most samples yielded none to few. Fluorite is abundant in samples 10-PTA-134 (216), 10-PTA-180 (139), -133 (134), -081 (123), -108 (115), and -135 (114) in the 0.25–0.50 mm size fraction normalized to 10 kg (Table 8, Fig. 17). Fluorite grains were not observed in the pan concentrate.

Apatite grains were recovered in all samples in the 0.25–0.5 mm fraction. The amount of fluorapatite grains recovered is reported as a percentage of the total amount of phosphate minerals present in the HMC. Fluorapatite percentages range from 5 to 80% of total phosphates, with sample 10-PTA-023 containing the highest amount.

Other heavy minerals in the till HMC (0.25–0.50 mm) are listed in Appendix F. The MMSIM spread sheet of Appendix F reports that all 71 samples contain abundant grey and specular, or red earthy hematite, ranging from 12 500 to 71 000 grains (samples normalized to 10 kg). Monazite grains were given counts for a total of 7 samples: 10-PTA-082 (1), -084 (1), -104 (0.5), -105 (1), -110 (4), -119 (5), and -120 (20). Trace (TR) monazite was noted for many samples, and a few were denoted as 0. Trace chromite was documented in 17 samples, with up to 4 grains in samples 10-PTA-092 and 10-PTA-073. Trace sapphire corundum is reported in 10-PTA-134, whereas 41% of samples contain trace red rutile. The "Selected KIMs" spreadsheet of Appendix F reports forsterite in the 0.25 to 0.5 mm fraction of 5 samples: 10-PTA-112 (2), 116 (7), 130 (3), 132 (1), and 149 (12). The pan concentrate for sample 10-PTA-090 (Table 8) yielded 1 thorianite, 1 galena, and 2 titanomagnetite grains.

Mineral liberation analysis

This analytical tool was utilized to confirm the presence of gold and other precious metals in the highly

Table 8. Heavy minerals picked from the pan concentrates compared to the 0.25–0.5 mm heavy liquid heavy mineral concentrate fractions (normalized to 10 kg) of 71 bulk till samples. The list is in three sections: proximal, medium and regional distances from the KMZ deposit. Samples with the same distances from the KMZ are listed in numerical order.

			Pan Concentrate		0.25–0.5 mm			
Sample Number	**Interpretation**	**Distance from Deposit** (m)	Gold grains	Miscellaneous	Fluorite	Barite	Pyrite	Chalcopyrite
10-PTA-117	overlying mineralization	10	115	~1000 Anatase	16	81	300	4
10-PTA-115	down ice	50	4	0	1	58	0	4
10-PTA-116	down ice	50	4	0	5	238	115	17
10-PTA-114	down ice	100	8	0	0	54	0	0
10-PTA-118	down ice	100	24	0	2	56	15	6
10-PTA-119	down ice	100	5	0	15	35	0	8
10-PTA-121	down ice	150	5	0	0	198	0	0
10-PTA-120	down ice	250	59	0	0	39	0	0
10-PTA-122	down ice	250	6	0	46	138	50	21
10-PTA-123	down ice	250	6	0	6	270	8	1
10-PTA-124	down ice	250	3	0	0	326	15	5
10-PTA-125	down ice	250	39	0	3	89	0	0
10-PTA-130	down ice	250	2	0	0	463	7	0
10-PTA-131	down ice	250	4	0	0	110	2	1
10-PTA-110	down ice	500	4	0	67	167	4	2
10-PTA-112	down ice	500	9	0	112	562	6	1
10-PTA-126	down ice	500	5	0	35	442	0	0
10-PTA-127	down ice	500	3	0	92	367	0	3
10-PTA-128	down ice	500	5	0	43	259	0	0
10-PTA-129	down ice	500	6	0	13	62	10	7
10-PTA-132	down ice	500	6	0	1	281	10	6
10-PTA-133	down ice	500	7	0	134	223	0	0
10-PTA-093	down ice	1000	8	0	0	200	0	1
10-PTA-099	down ice	1000	12	0	0	82	0	2
10-PTA-101	down ice	1000	9	0	25	267	3	0
10-PTA-104	down ice	1000	9	0	33	233	20	5
10-PTA-105	down ice	1000	13	0	12	149	0	1
10-PTA-106	down ice	1000	3	0	0	206	0	0
10-PTA-108	down ice	1000	5	0	115	308	5	3
10-PTA-092	down ice	2000	16	0	0	194	0	0
10-PTA-094	down ice	2000	10	0	0	42	1000	0
10-PTA-096	down ice	2000	8	0	21	202	15	1
10-PTA-098	down ice	2000	17	20 Pyrite	27	303	60	3
10-PTA-100	down ice	2000	10	0	0	143	0	2
10-PTA-102	down ice	2000	23	0	0	198	0	0
10-PTA-090	down ice	2200	17	1 Thorianite, 1 Galena, 2 Titanomagnetite	0	41	0	1
10-PTA-091	down ice	3000	9	0	0	69	0	0
10-PTA-095	down ice	3000	11	0	0	154	0	0
10-PTA-097	down ice	3000	48	0	0	20	2	0
10-PTA-107	down ice	3000	26	0	0	0	0	0
10-PTA-109	down ice	3000	11	0	0	8	0	0
10-PTA-111	down ice	3000	3	0	1	65	1	3
10-PTA-113	down ice	3000	29	0	0	244	2	0
10-PTA-136	up ice	3100	5	0	0	101	0	2
10-PTA-134	down ice	4300	17	10 Pyrite	216	216	0	1
10-PTA-066	up ice	4800	19	0	0	93	1	0
10-PTA-135	up ice	5000	9	0	114	114	0	0
10-PTA-083	down ice	5000	26	0	6	190	0	0
10-PTA-084	down ice	5000	19	0	0	50	0	3
10-PTA-085	down ice	5000	2	0	46	462	2	3
10-PTA-086	down ice	5000	20	0	0	40	4	2
10-PTA-087	down ice	5000	4	0	0	0	1	0
10-PTA-088	down ice	5000	4	0	2	81	1	2
10-PTA-089	down ice	5000	6	0	0	0	2	9
10-PTA-103	down ice	5500	22	0	5	64	0	0
10-PTA-035	down ice	6300	11	0	0	0	0	0
10-PTA-036	down ice	6400	2	0	0	68	2	3
10-PTA-037	down ice	6500	11	0	0	123	1	0
10-PTA-071	down ice	7100	7	0	0	1031	0	0
10-PTA-074	down ice	10 (km)	0	0	44	46	4	0
10-PTA-075	down ice	10 (km)	1	0	0	0	2	2
10-PTA-076	down ice	10 (km)	5	0	0	1		0
10-PTA-077	down ice	10 (km)	2	0	22	0	3	0
10-PTA-078	down ice	10 (km)	7	0	0	82	1	0
10-PTA-079	down ice	10 (km)	1	0	1	35	5	0
10-PTA-080	down ice	10 (km)	3	0	139	6	15	0
10-PTA-081	down ice	10 (km)	4	0	123	2	0	0
10-PTA-082	down ice	10 (km)	5	0	3	11	0	1
10-PTA-048	background up ice	14 (km)	7	0	36	2857	0	0
10-PTA-073	down ice	18 (km)	10	0	0	20	800	0
10-PTA-047	background up ice	28 (km)	36	0	0	170	0	0

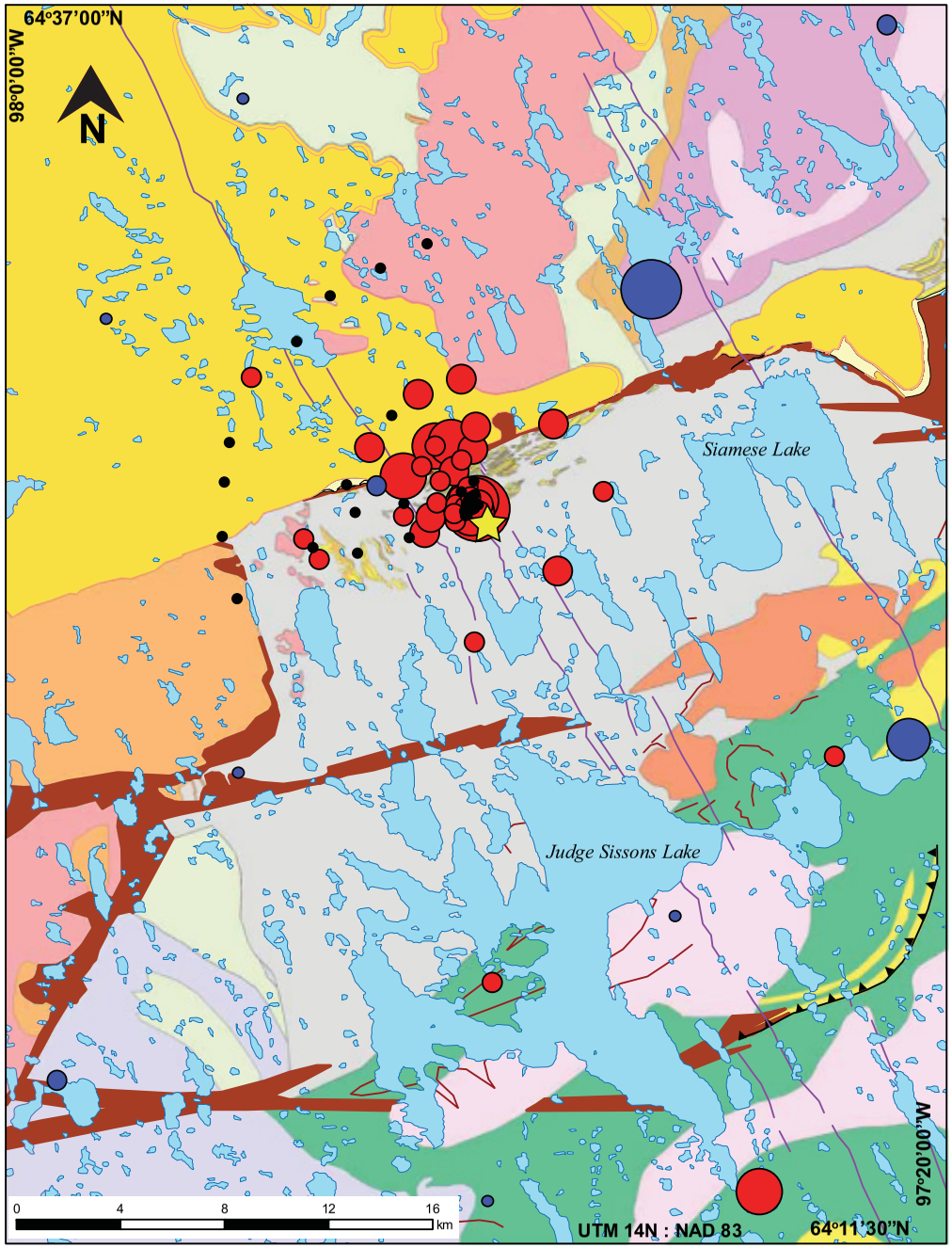

Total Gold Grains / 10 kg

No. Samples	No. Grains
32	0 - 6
21	7 - 13
12	14 - 26
5	27 - 59
1	60 - 116

McMartin et al., 2006

Kiggavik Main Zone

Bedrock Geology Legend

Mackenzie Igneous Event (1.27 Ga, 150°)

Diabase dyke

Barrensland Group (<1.75 to > 1.54 Ga)

Thelon Formation
sandstone, conglomerate, and mudstone

Hematite-altered rocks
Thelon and basement

Wharton Group

Amarook Formation
sandstone and conglomerate

Pitz Formation
rhyolite, basalt, and epiclastic rocks

Hudson Intrusive Suite

Hudson granodiorite

Martell syenite

Lower Ketyet River Group (inferred >2.153 Ga)

Grey schist

White quartzite and conglomerate

Snow Island Suite (SIS; 2.6 Ga)

Gabbro to granite
including Judge Sissons Pluton

Pukiq Lake Formation
rhyolite and epiclastic rocks

Marjorie Hills Assemblage (MHA; <2.63 Ga)

Metasedimentary and metavolcanic gneiss

Banded iron formation

Woodburn Lake Group (WLG; Neoarchean)

Amarulik assemblage (<2.68 Ga)
Greywacke, intra-formational breccia

Pipedream assemblage (2.71 Ga)
Feldspathic greywacke, local graphitic schist

Halfway Hills assemblage (2.73 Ga)
Ultramafic to felsic volcanic and sedimentary rocks

Archean Basement Gneiss

Undifferentiated granitoid gneiss and amphibolite
possible basement to WLG

Regional Fault

Figure 13. Total gold grain abundances in bulk till samples (normalized to 10 kg) from the entire project area. For local- and deposit-scale representation, see Appendix H. Gold grain counts reported by McMartin et al. (2006) are also shown for comparison. Bedrock geology map is simplified from unpublished ArcGIS files of Jefferson et al. (in prep) and was prepared prior to analysis of sample 10PTA-R047 (3 gold grains), which was collected from the southeast corner of the area (an updated map is shown in Fig. 3).

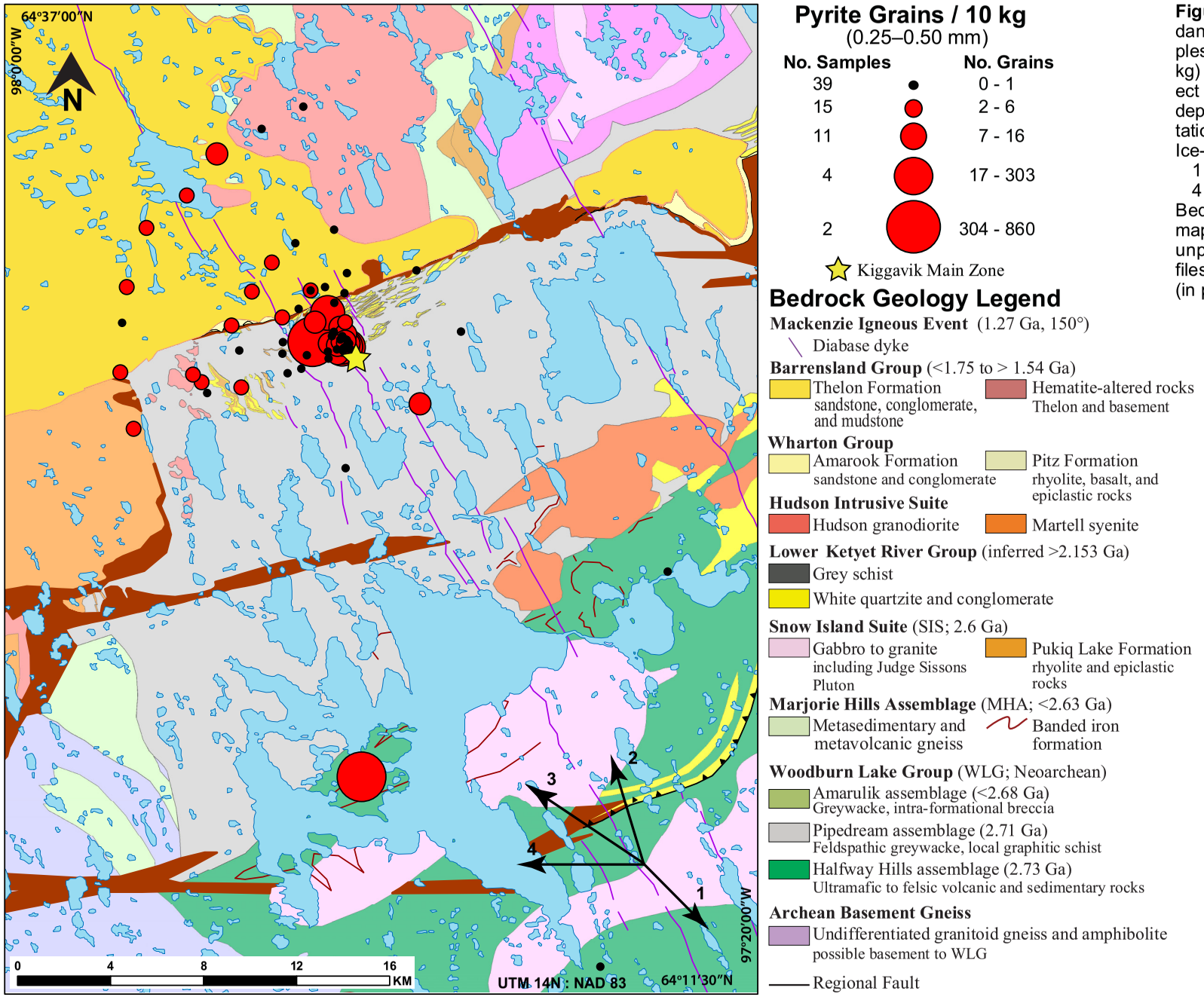

Figure 14. Pyrite abundances in bulk till samples (normalized to 10 kg) from the entire project area. For local- and deposit-scale representation, see Appendix H. Ice-flow sequence:
1 = oldest, ‘
4 = youngest.
Bedrock geological map is simplified from unpublished ArcGIS files of Jefferson et al. (in prep.).

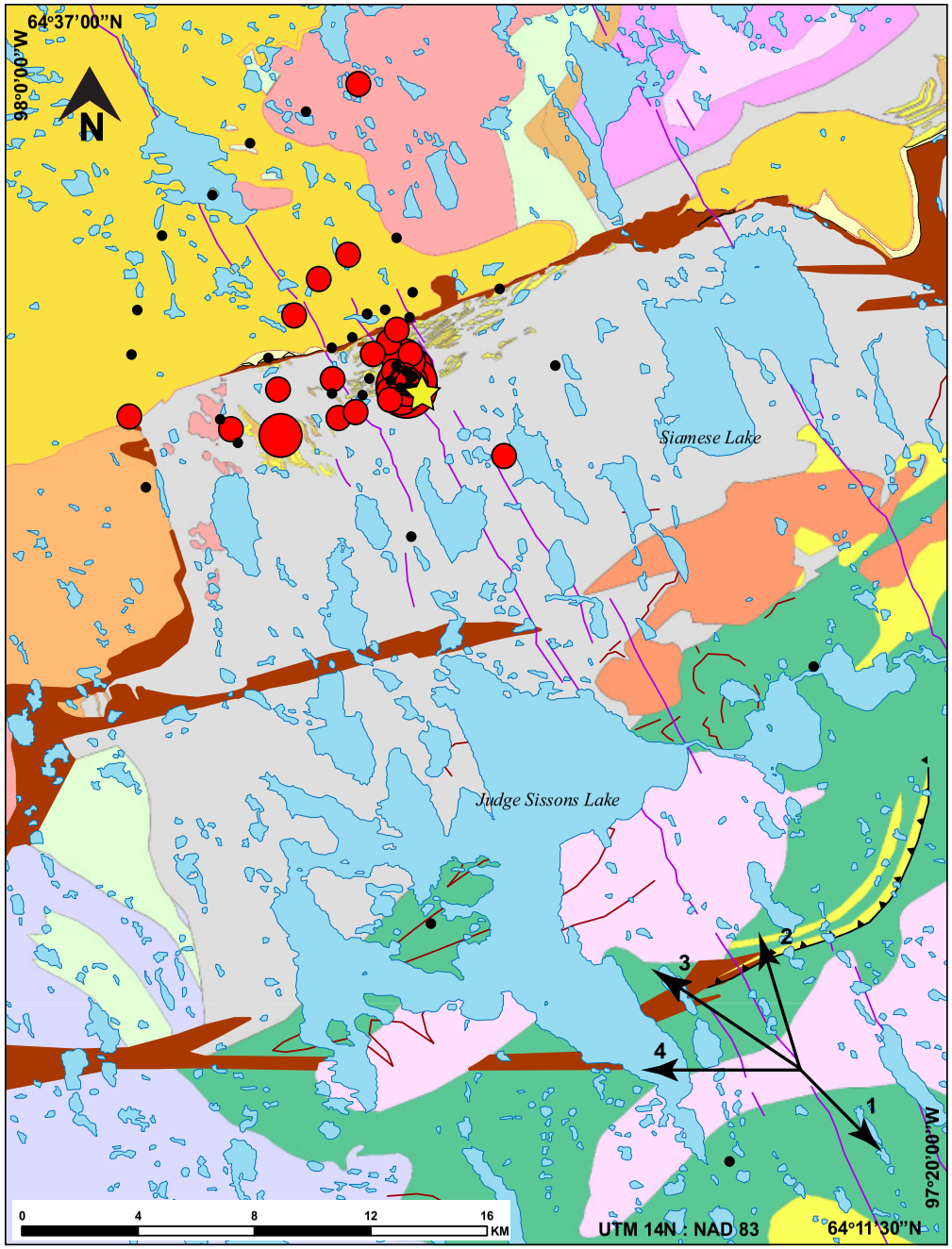

Chalcopyrite Grains / 10 kg

(0.25 - 0.5 mm)

No. Samples	No. Grains
37	0
27	1 - 5
6	6 - 17
1	18 - 21

Kiggavik Main Zone

Bedrock Geology Legend

Mackenzie Igneous Event (1.27 Ga, 150°)
- Diabase dyke

Barrensland Group (<1.75 to > 1.54 Ga)
- Thelon Formation: sandstone, conglomerate, and mudstone
- Hematite-altered rocks: Thelon and basement

Wharton Group
- Amarook Formation: sandstone and conglomerate
- Pitz Formation: rhyolite, basalt, and epiclastic rocks

Hudson Intrusive Suite
- Hudson granodiorite
- Martell syenite

Lower Ketyet River Group (inferred >2.153 Ga)
- Grey schist
- White quartzite and conglomerate

Snow Island Suite (SIS; 2.6 Ga)
- Gabbro to granite including Judge Sissons Pluton
- Pukiq Lake Formation: rhyolite and epiclastic rocks

Marjorie Hills Assemblage (MHA; <2.63 Ga)
- Metasedimentary and metavolcanic gneiss
- Banded iron formation

Woodburn Lake Group (WLG; Neoarchean)
- Amarulik assemblage (<2.68 Ga): Greywacke, intra-formational breccia
- Pipedream assemblage (2.71 Ga): Feldspathic greywacke, local graphitic schist
- Halfway Hills assemblage (2.73 Ga): Ultramafic to felsic volcanic and sedimentary rocks

Archean Basement Gneiss
- Undifferentiated granitoid gneiss and amphibolite: Possible basement to WLG

Regional Fault

Figure 15. Chalcopyrite grain counts in bulk till samples (normalized to 10 kg) from the entire project area. For local and deposit scale representation see Appendix H. Ice-flow sequence:
1 = oldest,
4 = youngest.
Bedrock geology map is simplified from unpublished ArcGIS files of Jefferson et al. (in prep).

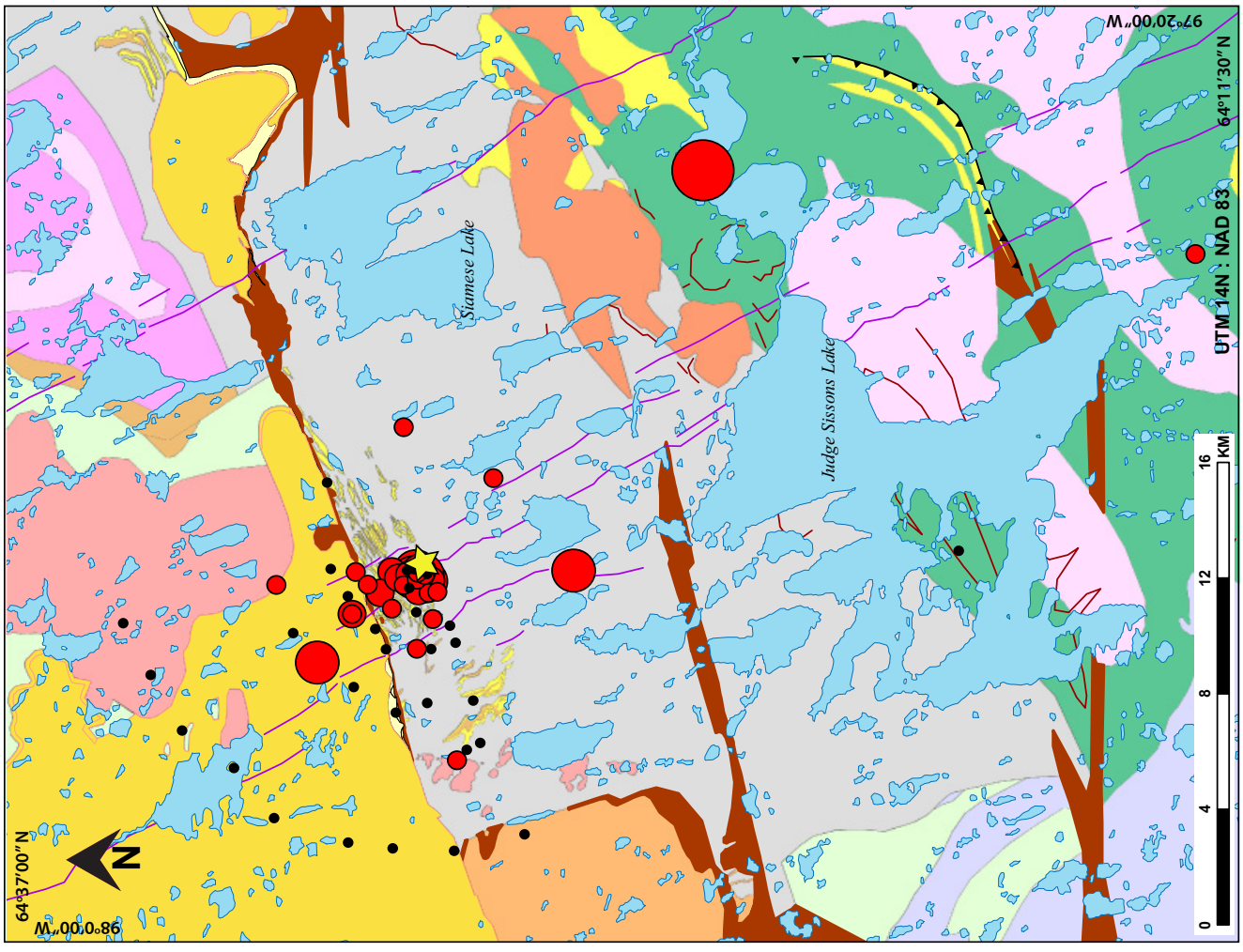

Figure 16. Barite grain abundances in bulk till samples (normalized to 10 kg) from the entire project area. For local- and deposit-scale representation, see Appendix H. Ice-flow sequence:
1 = oldest,
4 = youngest.
Bedrock geology map is simplified from unpublished ArcGIS files of Jefferson et al. (in prep.).

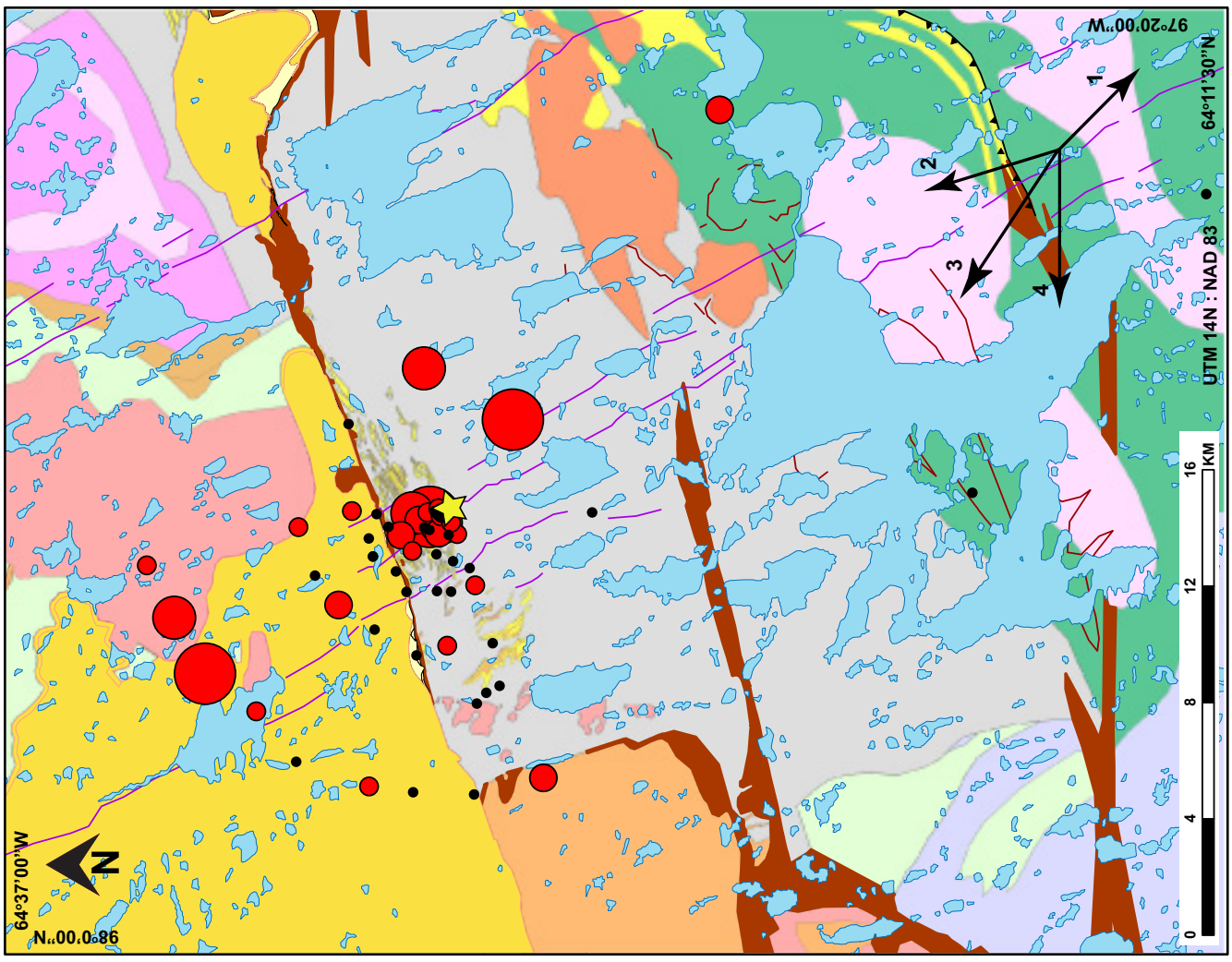

Fluorite Grains / 10 kg
(0.25–0.50 mm)

No. Samples	No. Grains
35	0
19	1 - 25
10	26 - 92
6	93 - 123
1	124 - 216

Kiggavik Main Zone

Bedrock Geology Legend

Mackenzie Igneous Event (1.27 Ga, 150°)
- Diabase dyke

Barrensland Group (<1.75 to > 1.54 Ga)
- Thelon Formation sandstone, conglomerate, and mudstone
- Hematite-altered rocks Thelon and basement

Wharton Group
- Amarook Formation sandstone and conglomerate
- Pitz Formation rhyolite, basalt, and epiclastic rocks

Hudson Intrusive Suite
- Hudson granodiorite
- Martell syenite

Lower Ketyet River Group (inferred >2.153 Ga)
- Grey schist
- White quartzite and conglomerate

Snow Island Suite (SIS; 2.6 Ga)
- Gabbro to granite including Judge Sissons Pluton
- Pukiq Lake Formation rhyolite and epiclastic rocks

Marjorie Hills Assemblage (MHA; <2.63 Ga)
- Metasedimentary and metavolcanic gneiss
- Banded iron formation

Woodburn Lake Group (WLG; Neoarchean)
- Amarulik assemblage (<2.68 Ga) Greywacke, intra-formational breccia
- Pipedream assemblage (2.71 Ga) Feldspathic greywacke, local graphitic schist
- Halfway Hills assemblage (2.73 Ga) Ultramafic to felsic volcanic and sedimentary rocks

Archean Basement Gneiss
- Undifferentiated granitoid gneiss and amphibolite
  Possible basement to WLG

Regional Fault

Figure 17. Fluorite grain abundances in bulk till samples (normalized to 10 kg) from the entire project area. For local- and deposit-scale representation, see Appendix H Ice-flow sequence:
1 = oldest,
4 = youngest.
Bedrock geology map is simplified from unpublished ArcGIS files of Jefferson et al. (in prep.).

Table 9. Spot analyses of U-oxide minerals by EMPA, arranged in order by figure number and numbered spots on those. Ten selected elements are reported as weight % oxide. Note samples with lesser UO_2 are interpreted as including coffinite and/or coffinite films or inclusions in uraninite, based on work by Fuchs and Hilger (1989) and Riegler (2014). Detailed photomicrographs showing the locations of spot analyses are in Appendix G.

Figure - Spot	Samples 10-PTA-R	SiO_2	Al_2O_3	CaO	FeO	UO_2	ThO_2	Na_2O	Y_2O_3	PbO	P_2O_5	Total (%)
1-1	045-MP1	7.34	na	0.92	na	80.67	na	0.00	0.01	0.20	na	89.15
2-1	046-MP1	5.22	na	3.51	na	80.29	na	0.00	0.01	0.22	na	89.25
2-2	046-MP1	5.34	na	3.86	na	81.02	na	0.01	0.00	0.02	na	90.25
3-1	051-MP-1	1.03	0.49	2.11	1.14	79.81	0.01	0.26	0.08	0.18	3.24	88.36
4-2	053-MP-1	4.31	0.80	3.32	0.53	63.49	0	0.07	0.56	0.11	1.33	74.51
5-1	053-MP-2	1.51	na	4.94	na	74.57	na	0.01	0.07	0.02	na	81.12
6-1	063-MP-1	1.81	0.13	5.58	0.47	82.50	0	0.75	0.11	4.16	0.08	95.60
6-2	063-MP-1	1.98	0.15	5.40	0.51	82.90	0	0.73	0.12	4.40	0.09	96.27
6-3	063-MP-1	1.96	0.18	5.43	0.51	83.00	0	0.66	0.08	4.49	0.08	96.40
6-4	063-MP-1	2.03	0.18	5.31	0.51	83.63	0	0.81	0.08	4.16	0.09	96.81
6-5	063-MP-1	1.90	0.16	5.77	0.49	82.57	0	0.67	0.05	4.12	0.08	95.81
6-6	063-MP-1	2.04	0.14	5.55	0.56	82.34	0.01	0.69	0.12	4.21	0.09	95.75
6-7	063-MP-1	2.08	0.28	5.06	0.51	82.45	0	0.89	0.11	5.13	0.09	96.60
6-9	063-MP-1	1.58	0.11	6.08	0.39	83.01	0	0.65	0.08	4.44	0.08	96.42
7-1	063-MP-2	1.69	0.12	5.75	0.41	82.55	0	0.64	0.08	3.98	0.04	95.27
7-2	063-MP-2	1.86	0.14	5.83	0.46	82.61	0	0.71	0.07	3.92	0.07	95.65
7-3	063-MP-2	2.14	0.19	5.30	0.50	82.12	0	0.94	0.12	3.95	0.08	95.32
7-4	063-MP-2	1.98	0.22	5.21	0.47	82.30	0	0.79	0.08	4.16	0.09	95.31
7-5	063-MP-2	2.24	0.19	5.78	0.52	82.46	0	0.74	0.09	4.28	0.08	96.37
7-6	063-MP-2	1.92	0.15	5.46	0.51	83.39	0	0.65	0.10	3.90	0.10	96.18
7-7	063-MP-2	1.87	0.21	5.43	0.49	82.55	0	0.53	0.11	4.03	0.11	95.33
7-8	063-MP-2	2.02	0.17	5.51	0.44	82.87	0.01	0.63	0.07	4.21	0.10	96.03
8-1	063-MP-3	14.97	0.36	3.43	0.55	60.68	0	0.03	0.25	4.97	0.16	85.41
8-2	063-MP-3	14.24	0.16	3.51	0.59	60.85	0	0.02	0.17	3.80	0.18	83.51
8-3	063-MP-3	15.08	0.23	3.25	1.32	54.50	0	0.01	0.23	6.08	0.15	80.85
8-4	063-MP-3	15.36	0.24	3.57	1.39	57.93	0	0.01	0.25	5.82	0.15	84.73
8-5	063-MP-3	13.94	0.92	2.74	0.50	53.47	0	0.01	0.14	14.30	0.13	86.14
8-6	063-MP-3	15.26	0.23	3.18	0.11	59.21	0	0.02	0.16	5.48	0.13	83.78
8-7	063-MP-3	15.62	0.20	3.74	2.39	57.16	0	0.05	0.18	3.79	0.12	83.25
8-8	063-MP-3	15.56	0.21	3.76	1.84	59.25	0	0.06	0.14	3.74	0.16	84.71
9-1	063-MP-4	2.29	0.25	4.83	0.44	82.46	0	0.82	0.09	4.53	0.09	95.79
9-2	063-MP-4	2.45	0.28	5.31	0.51	81.59	0	0.78	0.06	4.60	0.09	95.68
9-3	063-MP-4	2.15	0.19	5.32	0.58	82.79	0	0.80	0.08	3.91	0.06	95.89
9-4	063-MP-4	2.27	0.27	5.06	0.56	82.08	0	0.95	0.09	4.02	0.06	95.35
9-5	063-MP-4	2.43	0.29	4.40	0.40	82.15	0	0.74	0.08	4.77	0.11	95.38
9-6	063-MP-4	4.88	0.96	5.39	1.29	63.87	0	0.32	0.32	8.47	0.15	85.66
9-7	063-MP-4	2.07	0.25	5.40	0.48	83.18	0	0.71	0.08	4.18	0.10	96.46
9-9	063-MP-4	2.65	0.36	4.40	0.43	81.11	0	0.87	0.09	4.61	0.15	94.67

U-mineralized sample 10-PTA-R063. A single, <5 μm grain of electrum was found amongst distorted and strongly altered phyllosilicate minerals adjacent to fine-grained uraninite. Detailed methods, samples tested, and results are not captured in any appendix.

Electron microprobe and scanning electron microscope analyses

EMPA and SEM analyses (Appendix G) focused on samples that have a minimum of 300 counts per second (cps) of gamma radiation. SEM was used in reconnaissance mode to map polished thin sections and in spot mode to provide preliminary analyses of radioactive minerals. Three minerals were then quantitatively analyzed by EMPA: uraninite (UO_2), coffinite ($U(SiO_4)_{1-x}(OH)_{4x}$), and fluorapatite ($Ca_5(PO_4)_3(F,Cl,OH)$. Based on SEM and thin section petrography, these three minerals were selected for mineral chemistry to confirm mineralogy and examine the minor element chemistries. Table 9 shows the results of 38 spot analyses from 9 different mineral grains in 5 samples (10-PTA-R045, -R046, -R051, -R053, and -R063) containing uraninite and coffinite. Another 38 spot analyses of 5 fluorapatite crystals containing Pb (Table 10) were obtained for 2

Table 10. Spot EMPA analyses of fluorapatite. Values are expressed as weight % of selected elements as oxides. Detailed descriptions and illustrations of samples 10-PTA-R050 and 10-PTA-R053 are in Appendix G and Figures 10 to 19 inclusive. Analytical spots labelled on the photomicrographs are linked to this table by "figure – spot" numbers. The designations a1, a2, and a3 under the "Sample" column refer to different fluorapatite crystals in the same sample, which are shown in successive figures. Grey-shading: analyses of the apparently least-altered portions of the fluorapatite crystals, based on colour and texture variations in the photomicrographs.

Spot Point Analysis	Sample 10-PTA-R	F	SiO_2	Gd_2O_3	Sm_2O_3	Nd_2O_3	Pr_2O_3	La_2O_3	P_2O_5	CaO	Cl	ThO_2	Na_2O_3	UO_2	PbO	Y_2O_3	Ce_2O_3	Total	O=F	Total
1	050 a1	3.64	0.06	0.17	0.14	0.41	0.09	0.03	38.30	48.07	0.00	0.45	0.15	**0.91**	**8.06**	0.27	0.02	100.76	1.53	99.23
2	050 a1	4.49	0.08	0.00	0.34	0.00	0.00	0.00	38.87	49.41	0.00	0.00	0.12	**1.43**	**5.37**	0.28	0.15	100.55	1.89	98.66
3	050 a1	3.91	0.07	0.00	0.00	0.19	0.00	0.13	38.41	50.95	0.00	0.06	0.03	**1.20**	**3.45**	0.13	0.01	98.53	1.65	96.89
4	050 a1	4.79	0.04	0.00	0.04	0.05	0.17	0.00	39.49	55.10	0.00	0.05	0.03	**0.02**	**0.43**	0.12	0.01	100.33	2.02	98.31
5	050 a1	4.60	0.05	0.00	0.07	0.17	0.01	0.00	39.76	55.08	0.01	0.02	0.05	**0.07**	**0.47**	0.21	0.04	100.62	1.94	98.68
6	050 a1	4.10	0.08	0.06	0.20	0.34	0.00	0.00	38.23	54.54	0.01	0.17	0.02	**0.08**	**0.33**	0.07	0.06	98.30	1.73	96.57
7	050 a1	4.22	0.07	0.11	0.00	0.12	0.00	0.00	42.53	55.89	0.00	0.00	0.00	**0.01**	**0.00**	0.03	0.00	102.98	1.78	101.20
8	050 a1	3.94	0.09	0.02	0.04	0.02	0.14	0.00	38.68	48.72	0.00	0.33	0.13	**1.33**	**5.96**	0.24	0.02	99.66	1.66	98.00
9	050 a1	5.63	0.27	0.06	0.05	0.11	0.07	0.06	39.00	54.90	0.00	0.08	0.05	**0.12**	**0.55**	0.23	0.02	101.20	2.37	98.83
10	050 a1	3.86	0.09	0.03	0.13	0.00	0.03	0.00	42.42	55.59	0.01	0.00	0.01	**0.00**	**0.00**	0.00	0.00	102.16	1.63	100.53
1	050 a2	4.00	0.00	0.11	0.03	0.00	0.09	0.00	43.09	53.58	0.02	0.00	0.06	**0.03**	**0.01**	0.06	0.13	101.20	1.68	99.52
2	050 a2	3.80	0.03	0.01	0.00	0.10	0.00	0.17	39.18	50.22	0.00	0.57	0.13	**1.06**	**3.86**	0.20	0.11	99.45	1.60	97.85
3	050 a2	3.87	0.94	0.00	0.06	0.13	0.04	0.15	37.86	49.70	0.00	1.03	0.23	**1.71**	**2.23**	0.16	0.03	98.13	1.63	96.50
4	050 a2	3.71	0.04	0.00	0.00	0.00	0.00	0.00	40.11	52.70	0.00	0.02	0.04	**0.42**	**2.17**	0.00	0.10	99.31	1.56	97.74
5	050 a2	4.92	0.07	0.26	0.09	0.00	0.06	0.02	39.95	52.79	0.00	0.26	0.06	**0.16**	**0.85**	0.14	0.00	99.63	2.07	97.56
1	050 a3	2.84	0.17	0.06	0.00	0.10	0.12	0.09	42.17	53.56	0.02	0.00	0.14	**0.03**	**0.04**	0.18	0.02	99.55	1.20	98.35
2	050 a3	2.94	0.22	0.03	0.00	0.00	0.10	0.10	38.36	48.54	0.01	0.06	0.17	**1.63**	**5.60**	0.31	0.00	98.07	1.24	96.83
3	050 a3	3.23	1.35	0.13	0.09	0.03	0.11	0.05	38.03	48.84	0.00	0.00	0.16	**1.36**	**4.54**	0.24	0.08	98.25	1.36	96.89
4	050 a3	3.53	0.20	0.26	0.00	0.00	0.00	0.05	39.23	51.18	0.00	0.01	0.14	**1.25**	**4.34**	0.17	0.13	100.49	1.49	99.01
5	050 a3	4.16	0.44	0.02	0.15	0.23	0.08	0.00	39.11	53.72	0.01	0.08	0.06	**0.32**	**0.89**	0.14	0.01	99.42	1.75	97.67
6	050 a3	3.59	0.35	0.12	0.15	0.00	0.00	0.03	38.45	48.97	0.00	0.15	0.14	**1.44**	**5.62**	0.20	0.12	99.32	1.51	97.81
7	050 a3	3.51	0.43	0.07	0.03	0.05	0.06	0.00	39.65	49.20	0.00	0.26	0.18	**1.22**	**5.13**	0.23	0.09	100.09	1.48	98.61
8	050 a3	4.34	0.06	0.00	0.00	0.11	0.00	0.00	41.46	54.10	0.01	0.08	0.02	**0.00**	**0.91**	0.03	0.00	101.12	1.83	99.29
9	050 a3	3.08	0.04	0.00	0.24	0.02	0.04	0.00	42.15	53.62	0.10	0.03	0.05	**0.00**	**0.01**	0.08	0.05	99.52	1.30	98.23
1	053 a1	4.65	0.02	0.34	0.34	1.19	0.19	0.09	37.51	49.34	0.00	0.00	0.21	**1.20**	**2.38**	0.30	0.11	97.89	1.96	95.93
2	053 a1	5.04	0.03	0.30	0.30	0.88	0.25	0.22	36.92	50.28	0.01	0.04	0.12	**0.95**	**1.90**	0.32	0.15	97.71	2.12	95.59
3	053 a1	3.67	0.04	0.01	0.04	0.00	0.04	0.11	41.88	54.09	0.01	0.04	0.08	**0.00**	**0.02**	0.11	0.05	100.19	1.55	98.64
4	053 a1	3.24	0.04	0.09	0.04	0.14	0.05	0.03	42.78	54.45	0.01	0.02	0.07	**0.00**	**0.00**	0.21	0.00	101.16	1.36	99.80
5	053 a1	4.27	0.03	0.13	0.25	0.72	0.25	0.11	36.62	51.88	0.03	0.04	0.17	**0.78**	**1.67**	0.24	0.14	97.34	1.80	95.54
6	053 a1	3.96	0.02	0.37	0.30	1.36	0.24	0.00	36.95	49.58	0.01	0.00	0.16	**1.29**	**2.45**	0.27	0.13	97.10	1.67	95.43
7	053 a1	3.35	0.06	0.27	0.38	1.27	0.22	0.07	37.29	49.11	0.00	0.00	0.26	**1.11**	**2.35**	0.24	0.14	96.10	1.41	94.69
8	053 a1	4.90	0.08	0.43	0.17	0.90	0.00	0.07	36.41	50.51	0.01	0.05	0.21	**0.90**	**1.76**	0.25	0.06	96.69	2.06	94.63
1	053 a2	3.75	0.04	0.00	0.00	0.17	0.00	0.12	42.24	54.26	0.00	0.00	0.09	**0.00**	**0.00**	0.14	0.03	100.86	1.58	99.28
2	053 a2	3.93	0.03	0.23	0.14	1.11	0.23	0.29	36.07	49.20	0.00	0.01	0.21	**1.39**	**2.60**	0.27	0.07	95.79	1.65	94.14
3	053 a2	4.17	0.02	0.11	0.33	0.88	0.02	0.12	36.22	50.35	0.00	0.00	0.12	**0.91**	**2.17**	0.30	0.02	95.75	1.76	94.00
4	053 a2	4.04	0.02	0.14	0.00	0.00	0.22	0.00	42.17	54.29	0.00	0.01	0.10	**0.00**	**0.07**	0.09	0.08	101.24	1.70	99.54
5	053 a2	4.55	0.03	0.64	0.65	1.42	0.07	0.11	37.07	49.43	0.00	0.00	0.26	**1.13**	**2.30**	0.30	0.20	98.16	1.92	96.24
6	053 a2	5.26	0.02	0.27	0.17	0.93	0.17	0.07	36.17	50.76	0.00	0.00	0.14	**0.83**	**1.90**	0.31	0.06	97.06	2.21	94.84

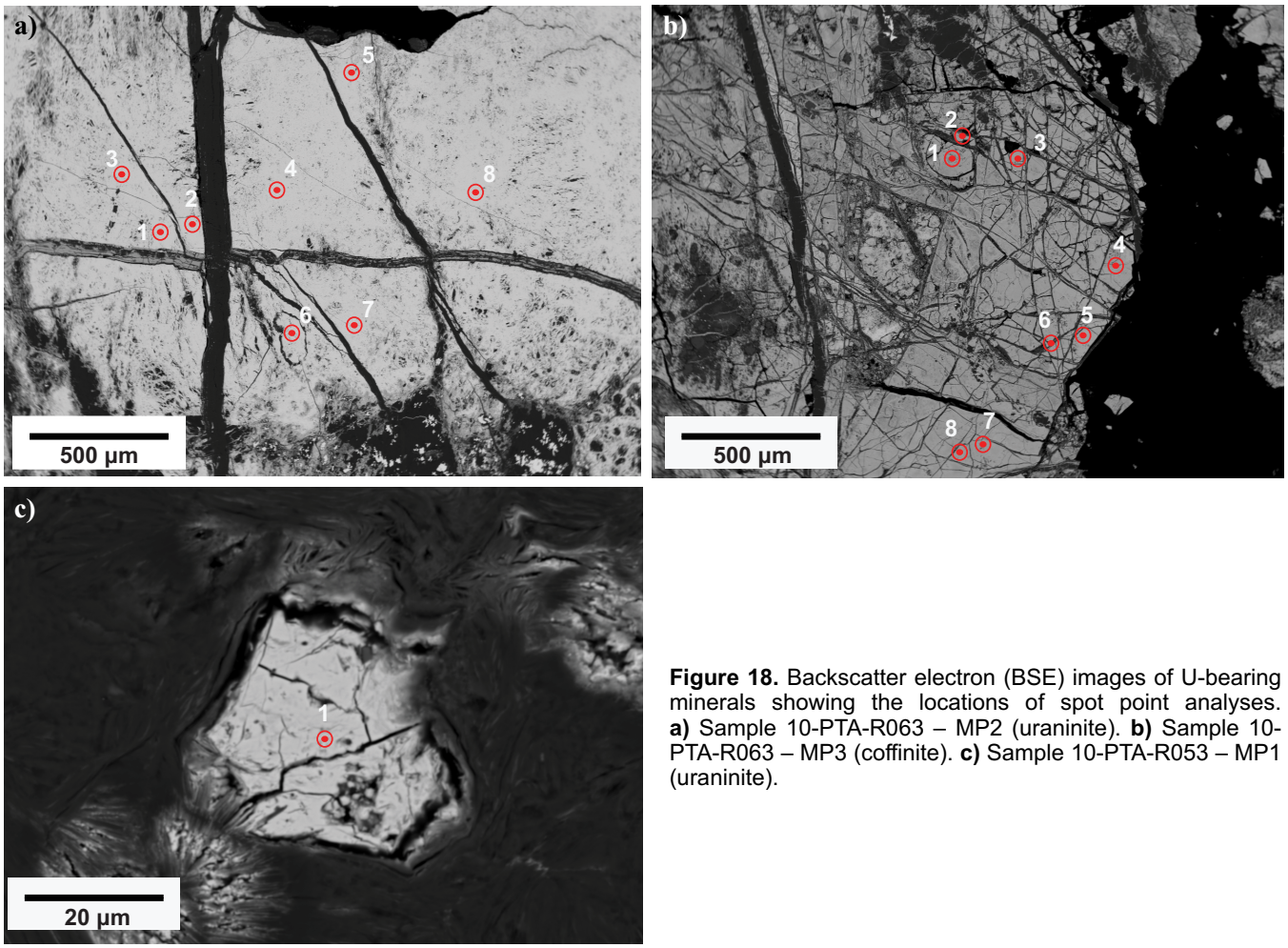

Figure 18. Backscatter electron (BSE) images of U-bearing minerals showing the locations of spot point analyses. **a)** Sample 10-PTA-R063 – MP2 (uraninite). **b)** Sample 10-PTA-R063 – MP3 (coffinite). **c)** Sample 10-PTA-R053 – MP1 (uraninite).

samples (10-PTA-R050 and -R053) to document the variability in composition compared to typical fluorapatite $Ca_5(PO_4)_3(OH,F,Cl)$.

U oxide minerals from the nine U-bearing samples were analyzed with the following results highlighted, all from Table 9. UO_2 ranges from 53 to 84%. Most the analyses are >80% UO_2, suggesting uraninite (Fig. 18a,c). One crystal (063-MP-3) averages 58% UO_2 over 8 spot analyses and is likely coffinite (Fig. 18b). SiO_2 ranges from 1 to 16%; the lower values are associated with higher U, further supporting the uraninite diagnosis. Mineral grain 063-MP-3 is the only one with SiO_2 >7% (8 spot analyses average 15% SiO_2), and has a lower reflectance in microphotographs (Fig. 18b), reinforcing the coffinite determination. Fine crystals (20–50 µm) of relatively pure uraninite in samples 10-PTA-R045, -R046, and -053 are disseminated but clustered near the centres of the uraninite-silicate intergrowth patches, and thus have higher SiO_2 (5.0–7.5%) (Fig. 18c).

Lead content ranges from 0–14% PbO, with all samples (10-PTA-R045, -R046, -R051, and -R053), with the exception of 10-PTA-R063, having less than 1% PbO. The average PbO content for all uraninite and coffinite grains in sample 10-PTA-R063 is 4.8%, with the high spot analysis 8-5 (14.3% PbO) being of a coffinite grain (Table 9, Fig. 18b). Aluminum (Al_2O_3) ranges from 0 to 0.96% and CaO from 0.92 to 6.08%. Higher CaO values are associated with uraninite crystals with higher UO_2 content. Iron (FeO) varies from 0 to 2.39%, with the coffinite grain having higher FeO content. Sodium (Na_2O) ranges from 0 to 0.95%, the higher values being associated with uraninite crystals and not the coffinite crystal. Yttrium (Y_2O_3) and phosphorous (P_2O_5) content ranges from 0 to 0.56% and 0 to 3.24%, respectively, with no discernible trends.

Fluorapatite compositions from samples 10-PTA-R050 and 10-PTA-R053 are highlighted as follows with reference to Table 10 and Appendix G. These samples are of interest because they both have strongly elevated Pb and U abundances. The crystals exhibit systematic chemical variations from core to rim, particularly for Pb, U, and Ca (Figs. 19, 20). Calcium (CaO) and phosphorous (P_2O_5) contents vary from core to rim, from approximately 56 to 48% and 43 to 36%, respectively. The Pb content averages 2.2% and varies irregularly from 0 to 8.1% PbO. UO_2 concentrations vary from 0 to 1.7%. The F content within the 5 fluo-

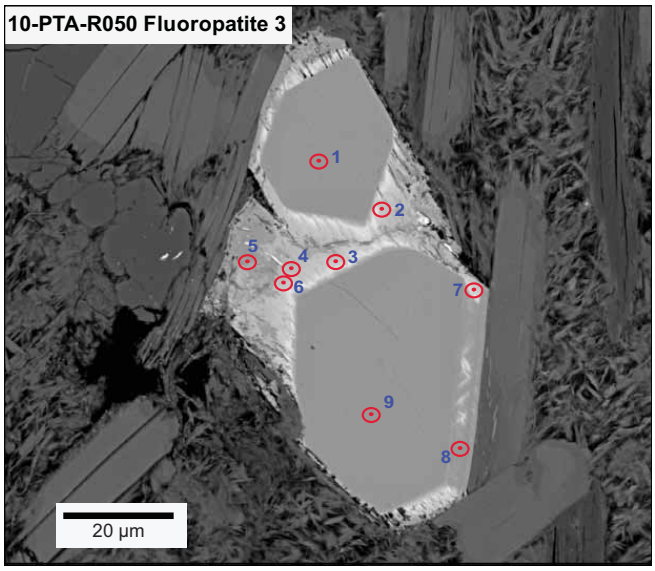

Figure 19. Backscatter electron image of coalesced fluorapatite euhedra displaying chemical partitions from low Pb+U in the core (spots 1, 9) to high Pb+U in the surrounding overgrowths and/or alteration zones of the primary fluorapatite (Table 10). The fluorapatite is bracketed by and partly replaces aligned muscovite books that are partly replaced by felted randomly oriented illite. A cluster of irregular quartz grains is visible at the middle left. Figure 20 shows X-ray images of the same crystals, highlighting counts for Pb, U, and Ca.

rapatite crystals varies from 2.8 to 5.6%, hence the term fluorapatite. The fluorapatite crystals were also analyzed for the trace elements: Sm, Nd, Pr, La, Cl, Th, Na, Y, and Ce. Only Nd_2O_3 and ThO_2 exceed 1% in spot analyses.

Both U and Pb contents are greatest and Ca least in the fibrous, outer overgrowths or altered portions of the fluorapatite crystals (Fig. 20). High concentrations of U and Pb coincide with higher overall reflectance and fibrous texture (Fig. 19; Appendix G). Spot analyses 1 and 9 of fluorapatite 3 of sample 10-PTA-R050 (Fig. 19) were focused in the fresh fluorapatite cores. These have PbO contents of 0.04 and 0.01%, respectively, with UO_2 contents of 0.03% and not detected, respectively (Table 10). In contrast, spot analyses 2, 3, and 7 of the fibrous outer altered or overgrowth zones (Fig. 19) have PbO contents of 5.6, 4.5, and 5.1%, respectively, and UO_2 contents of 1.63, 1.36, and 1.22%, respectively (Table 10).

DISCUSSION

Gold grains recovered from bedrock samples

Five gold grains, ranging in size from 25 to 75 µm, were recovered from only 2 of 18 disaggregated bedrock samples:2 grains from sample 10-PTA-R047 (silicified brecciated rhyolite marked "P" southeast of Judge Sissons Lake, Fig. 1) and 2 from sample 10-PTA-R138 (altered minette dyke from the Andrew Lake prospect, Fig. 1). These are located 28 km to the south and 16 km southwest of the KMZ, respectively. The following descriptions are summarized from Appendices C and D. Auriferous sample 10-PTA-R047 is cherty, brecciated, and silicified porphyritic rhyolite collected from southeast of Judge Sissons Lake where the Judge Sissons pluton has been dated as 2606 +4/-3 Ma (C. Roddick, unpubl. data, in Hadlari et al., 2004).

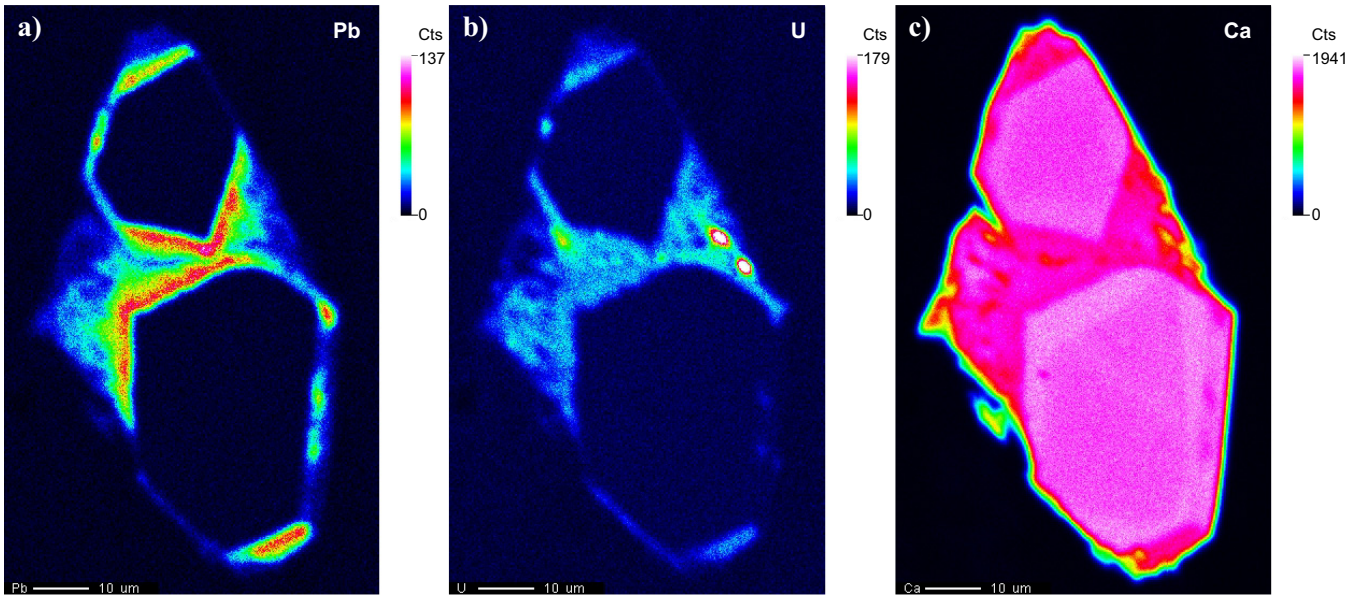

Figure 20. X-ray map of a single composite fluorapatite grain shown in Figure 19, illustrating two euhedral cores that are connected by overgrowths into a single larger euhedral crystal with compositional zonation of **(a)** Pb, **(b)** U, and **(c)** Ca. The sharply defined outer portions of the euhedral core that correspond to the fibrous textured brighter zones visible in BSE images of these fluorapatite crystals, are rich in Pb and U, and are depleted in Ca. The two fresh cores show subtle Ca zonation and an absence of Pb and U. Sample 10-PTA-R050, Fluorapatite 3.

Based purely on its geographic location and prior to understanding the distinctions between the 2.6 Ga Snow Island Suite (Peterson et al., 2015c) and the 1.75 Ga Kivalliq Igneous Suite (KIS, Peterson et al., 2014), this sample was originally assigned to the Snow Island Suite and was not described in thin section. The precise sample location is however within previously unmapped metavolcanic rocks, not granite, and the rhyolite occupies a northerly trending steep fault that truncates moderately west-dipping quartzite, also previously unmapped (Appendix B, sample 10-PTA-R047). Therefore the silicified rhyolite is now understood to be a small body unrelated to the massive Judge Sissons Pluton. In particular, the hand sample photograph of sample 10-PTA-R047 (Appendix B) illustrates a non-foliated, finely crystalline granitoid lithology, extensively cut by cherty quartz veins and reticulate chert alteration, with the pseudo-granitic porphyritic texture being mainly preserved in relict ovoid patches surrounded by chert. The largest cherty quartz vein includes some white drusy quartz as well as dark brownish hematite-coated open-space vugs. All of these textures and compositions are characteristic of the KIS as described in the Bedrock Geology section above (see also following section), not the SIS. This sample thus represents a new occurrence of anomalous native gold in a fault zone occupied by hydrothermally altered and silicified rhyolite related to the 1.75 Ga KIS. This new knowledge has led to significant improvements in the geological map of the area around sample 10PTA-R047 (compare southeast portions of Fig. 3, new, to Fig. 13).

Sample 10-PTA-R138 (Appendix B) is an altered bostonite or minette (lamprophyre) dyke from drill core of the Andrew Lake deposit that is part of the Kiggavik U Camp. The Andrew Lake deposit, like the Kiggavik deposits, was developed in highly foliated and complexly faulted metasedimentary and epiclastic strata intruded by multiple elements of magmatism at both 1.83 Ga and 1.75 Ga. The 1.83 Ga event is represented here by Hudson Granite and dykes of the Christopher Island Formation (e.g. this ultrapotassic dyke sample). This dyke is so altered that its protolith could have been bostonite or minette, however its dark hematitized appearance is more suggestive of minette. The 1.75 Ga magmatic event within the study area represented by both rhyolite and cherty drusy quartz veining, especially developed along the Judge Sissons Fault and splays from it. As documented by Scott et al. (2015) for the Lone Gull composite granite and by P. Wollenberg (pers. comm.., 2011), the Andrew Lake deposit is developed mainly in metagreywacke but also in 1.75 Ga rhyolite and granite of the KIS, but not in the 1.83 Ga Hudson Suite. The presence of gold in this minette sample could be related to both the KIS alteration and the later alteration responsible for the U deposition.

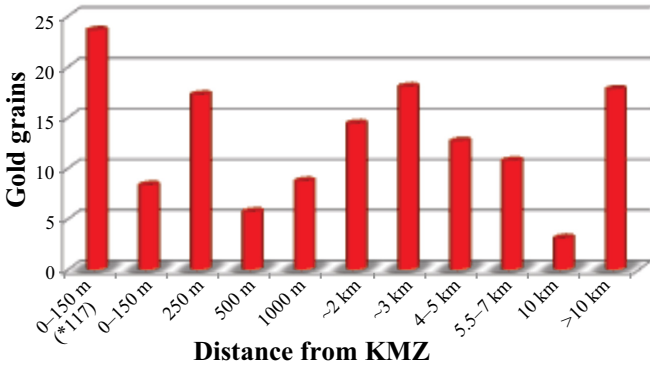

Figure 21. Average gold grain count per till sample at variable distances from the Kiggavik mineralized zone (KMZ). Note: * denotes that sample 10-PTA-117 was included in the average gold grain calculation.

Although ore-grade U samples were not disaggregated for this study due to health and safety issues, a thorough search for gold grains was conducted by SEM. Whereas microscopy did not reveal any gold grains in these samples, brief analysis using an automated mineral identification system (mineral liberation analysis) did detect a single, 2 µm native gold grain in sample 10-PTA-R063. This discovery, although minor, supports the geochemistry of till samples and an unpublished Urangesellschaft petrographic study by Reyx (1994), who reported Au-Ag alloys associated with Bi-telluride in uraninite clusters at Kiggavik. The petrographic documentation conducted during this study is consistent with his geochemical analysis of up to 2020 ppb Au.

Gold grains recovered from till samples

Seventy of the 71 bulk till samples yielded gold grains in HMCs, with an average of 13 grains per sample (Fig. 13, Appendix E). Distance from the KMZ is not a factor in the abundance of gold grains in till (Fig. 21), given the sample spacing achieved in this study. Sample 10-PTA-117, located directly over the KMZ, has the highest gold grain count of 115. However, the gold grain counts of other samples located just 50 or more metres farther away from the KMZ are significantly lower. For example samples 10-PTA-115 and -116, each located within 50 m of the KMZ, yielded only 4 gold grains each. Furthermore, excluding sample 10-PTA-117, the average gold grain content of samples collected less than 150 m from the KMZ (n=6) is 8 (Fig. 22). No trend spatially related to U deposits was discernable (Fig. 22). Samples collected 10 km northwest of the KMZ, overlying the Thelon Formation sandstone (Fig. 13), yielded low gold grain counts that are considered equivalent to background. Overall, not including sample 10-PTA-117, the average gold grain

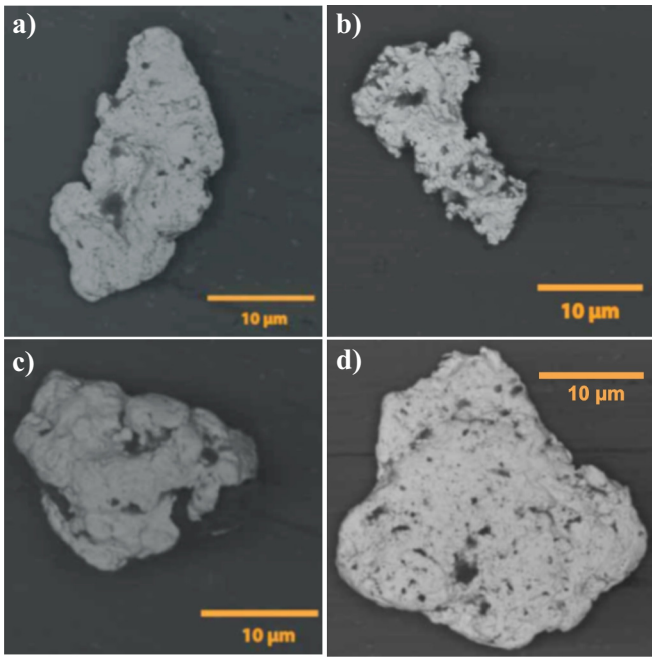

Figure 22. Microphotographs of gold grains recovered from bulk till samples. **a)** Sample 10-PTA-047 (reshaped), **b)** Sample 10-PTA-117 (reshaped) with soluble intergrown leached-out tellurides, **c)** Sample 10-PTA-125 (modified), and **d)** Sample 10-PTA-090 (reshaped).

count in this study is 11, similar to the regional average of the Schultz Lake map area, which is 9 gold grains (not normalized) as reported by McMartin et al. (2006).

Other till samples with high gold grain contents are 10-PTA-120 (61 grains), -097 (40 grains), -125 (35 grains) and -113 (24 grains), located 250 m, 3 km, 250 m and 3 km, respectively, to the west-northwest of the Kiggavik deposit. These overlie Woodburn Lake group metagreywacke, Pukiq Lake Formation epiclastic rocks and Ketyet River group quartzite. Furthermore, high gold grain counts were reported by McMartin et al. (2006) immediately down-ice of similar bedrock types within 3 km of the KMZ (Fig. 13). As reported by McMartin et al. (2006), potential gold grain sources in the Schultz Lake map area include gossanous iron-formation in Woodburn Lake group rocks and pyritic quartz-pebble conglomerate within quartzite of the Woodburn Lake or Ketyet River groups (Zaleski et al., 2000; Zaleski and Pehrsson, 2005).

Gold grain morphologies described by ODM (Appendix F) indicate that the majority of recovered grains in this study are reshaped or modified, and thus qualitatively record some physical transport (Averill, 1988; Dilabio, 1990). Interestingly, although sample 10-PTA-117 directly overlies the KMZ and has the highest count of gold grains at 114, fully 74% of these grains are described as reshaped (Fig. 22b, Appendix F). The Kiggavik deposits do contain gold (Reyx, 1994; D. Quirt, pers. comm., 2012) and therefore may be the source of the high gold grain count observed in sample 10-PTA-117, despite the majority of grains being described as "reshaped". Alternatively, the 1.77–1.74 Ga intrusion of Nueltin granite and abundant mafic dykes of the KIS spanning the Kiggavik exploration camp, (Scott, 2012; Peterson et al., 2015a,b; Scott et al., 2015) could have generated hydrothermal fluid flow that in turn introduced silicification and gold to the pre-ore setting of the Kiggavik deposits. A nearby analogy is the epithermal gold at Mallery Lake, which was studied by Turner et al. (2001, 2003) and placed into context of the 1.77–1.74 Ga KIS by Peterson et al. (2014, 2015a,b). Figure 22b displays a "reshaped" gold grain with soluble intergrown leached-out telluride minerals (confirmed by SEM-EDS) from sample 10-PTA-117. These observations are very similar to those of Reyx (1994), who reported the association of gold in the Lone Gull U oxide ores with Bi and Ag telluride minerals, reinforcing the hypothesis that the gold in sample 10-PTA-117 was likely derived from the exposed KMZ deposit. Moreover, Henderson and Roy (1995) questioned the validity of using gold grain morphology in weathered tills, such as those in the Kiggavik area, as an indication for glacial transport. Ultimately, gold grain count abundance is likely the best indicator for proximal U occurrences (Henderson and Roy, 1995), supporting our interpretation that the higher gold grain content within 3 km of the Kiggavik deposit was derived from the KMZ, with minor additions from other potential gold sources in proximal but unmineralized rock units.

Uraninite and Pb+U-rich fluorapatite as indicator minerals

Uraninite is the main ore mineral at Kiggavik, (Fuchs et al., 1985; Weyer et al., 1989; Reyx, 1994). Less abundant U minerals, such as coffinite and uranophane (Pacquet, 1993; Reyx, 1994), would have made only a minor contribution to till. Despite the presence of U minerals in bedrock at the KMZ, no U minerals were recovered from bulk till samples in this study. There are numerous explanations for this. Firstly, uraninite forms under reducing conditions, and when exposed to oxidizing conditions, U^{4+} oxidizes to U^{6+} and the mineral dissolves (Bradshaw and Lett, 1980; Finch and Ewing, 1992). Secondly, U^{6+} species are highly mobile in oxidizing environments and thus readily leached (Grandstaff, 1976; Romberger, 1984). Thirdly, despite the coarsely crystalline massive uraninite that is here documented for sample 10-PTA-R063 (Fig. 12b), most of the U minerals at Kiggavik are very finely crystalline (<50 microns), which increases oxidation reaction rates (Grandstaff, 1976; Fuchs et al., 1985; Pacquet, 1993; Reyx, 1994; this study) (Fig. 11b). Unfortunately, it is likely that many of the samples

collected in this study were weathered, reducing the chance of uraninite ever being recovered in the HMC. In summary, uraninite is poorly suited to be an indicator mineral for the Kiggavik style of unconformity U deposits because it is too easily weathered and too fine grained to be separated by traditional HMC methods (>250 μm grain sizes).

The discovery of Pb+U-rich fluorapatite in thin section is, however, intriguing because it has not previously been reported as a component of basement-hosted unconformity-related U deposits. Such fluorapatite has significant potential for improving geochronological constraints on the timing of U mineralization, it may be unique to such deposits, and as a stable, durable, moderately heavy mineral it could be used as an indicator mineral in till derived from the highly altered, weakly mineralized bedrock halo around basement-hosted unconformity-associated U deposits.

Challenges for using the Pb+U-rich fluorapatite as a till marker include its silt grain size and its marginal density. ODM geologists did recover thousands of coarse fluorapatite grains from the Kiggavik bulk till samples as a common mineralogical phase (Appendix E) despite their specific gravity of 3.2 g/cm^3, which is the threshold density commonly employed using heavy liquids such as methylene iodide (McClenaghan, 2007). With enriched Pb and U, and concomitant depleted Ca, the altered fluorapatite grains are sufficiently denser than unaltered specimens to be separated by precise heavy liquid methodology. However at the time the till samples were processed using industry-standard technology at the ODM, our focus was on coarse silt- to sand-size HMC of a more traditional nature and the thousands of separated apatite grains were not screened for such Pb+U-rich fluorapatite species. Furthermore the SEM and EMPA study here suggests that only fine-grained Pb+U-rich fluorapatite is likely to be related to the U deposits. More work is required to characterize apatite species and develop standard criteria to efficiently and effectively pick and/or use precise heavy liquid densities to separate the fine Pb+U-rich fluorapatite from other types of apatite in the <100 μm HMC fraction.

Other heavy minerals recovered from bedrock and till heavy metal concentrates

A wide variety of heavy minerals were recovered from both the pan concentrate and the 0.25 mm fraction of disaggregated bedrock samples. Pyrite was the most abundant mineral, found in almost every lithology sampled (Table 6). High counts of molybdenite were recovered for two samples (10-PTA-R057, 10-PTA-R137). The former is a lamprophyre that is quartz veined and has patchy disseminated pyrite, both of which appear to be alteration related and may possibly represent a specific compositional response to U-related alteration because of its ultrapotassic and mafic character. The rationale for this possible is link is from the drilled Jane prospect south of the Andrew Lake deposit, both of which are part of the Kiggavik exploration camp. U in the Jane occurrence is concentrated in a highly altered mafic phase of the basement metamorphic assemblage along the Andrew Lake Fault system (A.R. Miller, 1997, Petrography and Mineral Chemistry of the Jane Prospect: A Platinum Group Element-bearing Basement-hosted Unconformity-Related Uranium Deposit Type, Schultz Lake Uranium District, Western Churchill Province; unpubl. report to COGEMA Resources Inc., 87 p.).

Arsenopyrite and galena were also recovered from the pan concentrate of bedrock samples, whereas high counts of hematite, barite, and fluorapatite and moderate molybdenite were recovered from the 0.25–0.5 mm fraction. Although not disaggregated, detailed microscopy of weakly to strongly U-mineralized rock samples identified potential indicator minerals such as pyrite, galena, uraninite, coffinite, chalcopyrite, and Pb+U fluorapatite. Additionally, Table 1 lists the Kiggavik U deposit ore, accessory, and associated gangue minerals from previous studies that could possibly be recovered in till samples and utilized as indicator minerals.

Markedly few heavy minerals were recovered from the pan concentrates of till samples, aside from gold and the approximately 1000 anatase grains recovered solely from sample 10-PTA-117. Altogether, only fluorite, barite, pyrite, and chalcopyrite were continuously recovered in the 0.25–0.5 mm fraction, neither geographic nor bedrock geological trend is evident (Appendix H). Furthermore, fluorite and barite were rarely found in strongly mineralized samples (Table 1). Chalcopyrite (rare) and pyrite seldom exceed 100 μm in diameter. The likely source of fluorite and barite proximal to the Kiggavik deposit is the composite Lone Gull intrusion (Scott, 2012).

CONCLUSIONS

Uraninite and coffinite are the primary ore minerals at the Kiggavik U deposit, associated with minor galena, pyrite, and gold. The U-bearing minerals are predominantly fine-grained, and rarely exceed 100 μm in diameter, even though coarsely crystalline uraninite is locally present. Nevertheless no uraninite, coffinite, or galena were recovered from the till pan concentrates or heavy liquid HMCs and therefore those phases are unlikely to be useful as indicator minerals in till. This is a result of these minerals not being resistant to oxidizing conditions in weathered till, and being too fine grained for effective recovery. Minor pyrite was recovered mainly in the 0.25–0.5mm fraction, but exhibits

no association with the Kiggavik deposit, also limiting its potential as an indicator mineral.

Gold grains did provide some intriguing results, being recovered from till via both pan concentrates and HMCs, in many cases above regional background levels. A dramatic count of 115 gold grains was obtained for sample 10PTA-117 that was collected directly above the Kiggavik Main Zone deposit. That anomaly is mitigated by an immediate drop in gold grain counts for samples collected within 50 metres. Nevertheless, several highly elevated gold grain counts were also noted in till collected up to 3 km west and northwest (down-ice) of the KMZ and the CZ, suggesting further study is required to assess gold as an indicator mineral for unconformity associated U deposits. Textural analysis of gold from the till sample at the Main Zone trench suggests that gold grain morphology does not reflect glacial transport distance. Some particular examples of these hot spots include samples 10-PTA-120 (61 grains, due west of the CZ), -097 (40 grains, along the Thelon Fault), and -125 (35 grains, 125 m west-southwest of KMZ) and -047 (32 grains). These are located 250 m N, 3 km west-northwest, and 290 m west-southwest of the KMZ, respectively, and may well not be derived from the KMZ.

A particularly intriguing gold anomaly is that of till sample 10-PTA-047 (32 grains) collected southeast of Judge Sissons Lake – some 28 km south-southwest of the KMZ (Fig. 6; Appendix F). This anomaly is coincident with a linear outcrop of Pitz Formation rhyolite that has been brecciated and quartz-veined, localized along a northerly trending, steep fault zone that cuts moderately west-dipping quartzite, all previously unmapped. A single gold grain was also recovered by the selFrag™ method from the rhyolite rock sample (10PTA-R047) collected at that locality (Appendix E2a). These samples were collected as part of the regional field documentation of the study area, and the first author was drawn to this particular site by a shapely roche moutonnée that developed on the rhyolite and quartzite. This new geological knowledge has been incorporated by the GEM-U project as major revisions to the geological map. Further field and laboratory follow-ups are recommended.

More intriguing for method development on till indicator minerals is the SEM and EMPA diagnosis of numerous Pb+U-enriched fluorapatite crystals in highly altered, weakly U-mineralized samples. This micro-analytical discovery has the potential to benefit till pathfinder studies for unconformity-associated U deposits like Kiggavik. The utility of finely crystalline Pb+U fluorapatite as a pathfinder is dependent upon developing a method that can efficiently and effectively separate it from the <100 μm size HMC fraction.

ACKNOWLEDGEMENTS

This report is part of an M.Sc. thesis by the first author at Queen's University, supported by the Tri-Territorial Indicator Mineral Project, co-funded by NSERC, AREVA Resources Canada Inc. (AREVA), and the Geo-mapping for Energy and Minerals (GEM) Program (2008–2013) through the NSERC-University-Industry-GEM cooperative research and development (CRD) grant process, led by G. Beaudoin, D. Layton-Matthews, S.-J. Barnes, S. Gleeson, and K. Kyser. The U part of the CRD was closely coordinated with the GEM Northern Uranium for Canada (NUC) Project. AREVA provided access to the Kiggavik Camp as a natural laboratory, cash funding, logistical support, confidential geological information, and rock samples from the Kiggavik deposits to both GEM projects. As part of AREVA's field collaboration, Mario Blain and Peter Wooenberg provided guidance to both type and intriguing rock units in the field, and Dillon Johnstone (M.Sc. in progress at University of Regina) later shared his new 2015 knowledge about the characteristics and great extent of epiclastic rocks hosting the Kiggavik deposits. Dillon's insights led to major revisions of the map and sample descriptions herein. In the field, Beth McClenaghan (GSC) mentored and provided supervision for till and rock sampling methods and Matthew Pyne (GSC) assisted with rock collection. Also from the GSC, Isabelle McMartin gave professional guidance, shared her deep knowledge of surficial geology in the Schultz Lake area, and pointed out relevant literature. Igor Bilot professionally photographed many polished rock specimens, especially gold-bearing rhyolite sample 10PTA-R047 that suggests lode precious metal potential southeast of Judge Sissons Lake. At Overburden Drilling Management, Stu Averill provided oversight and thorough, accurate descriptions of bedrock samples, while Remy Huneault answered many questions on procedures. At Queen's University, Jersey tirelessly cut rocks and prepared thin sections of exceptionally high quality while Anna Hicken generously mentored on ARCMAP© GIS and shared her knowledge of heavy minerals. An early version of this manuscript was thoroughly peer reviewed by Eric Potter. Elizabeth Ambrose technically edited and laid out the entire Open File, correcting many errors in the process.

REFERENCES

Averill, S.A., 1988. Regional variations in the gold content of till in Canada, *In:* Prospecting in Areas of Glaciated Terrain – 1988, (ed.) D.R. MacDonald and K.A. Mills; Canadian Institute of Mining and Metallurgy, p. 271–284.

Averill, S.A., 2001. The application of heavy indicator mineralogy in mineral exploration with emphasis on base metal indicators; in glaciated metamorphic and plutonic terrains, *In:* Drift Exploration in Glaciated Terrain, (ed.) M.B. McClenaghan, P.T.

Borowsky, G.E.M. Hall, and S.J. Cook; Geological Society, London, Special Publications, v. 185, p. 69–81.

Averill, S.A., 2013. Discovery and delineation of the Rainy River gold deposit using glacially dispersed gold grains sampled by deep overburden drilling: A 20 year odyssey, *In:* New frontiers for exploration in glaciated terrain, (ed.) R.C. Paulen and M.B. McClenaghan; Geological Survey of Canada, Open File 7374, p. 37–46.

Aylsworth, J.M. and Shilts, W.W., 1989. Glacial features around the Keewatin Ice Divide: Districts of Mackenzie and Keewatin; Geological Survey of Canada, Paper 88-24, 21 p.

Aylsworth, J.M., Cunningham, C.M., Shilts, W.W., 1990. Surficial geology, Schultz Lake, District of Keewatin, Northwest Territories; Geological Survey of Canada, Map 43-1989, 1:125 000 scale.

Beak Consultants Limited, 1988. Project concept description of the Kiggavik (Lone Gull) Uranium mine, Summary Report; Urangesellschaft Canada Limited, Beak Reference, 2305.3, 43 p.

Berthet, L., 2011. Technical Report on resource estimation Andrew Lake Deposit Kiggavik Area, Nunavut; AREVA report number BGM/DS/SER RT 11/015, 78 p. plus appendix.

Berthet, L. and Osorio, J-C., 2011a. Technical Report on resources Main Zone Deposit Kiggavik area, Nunavut; AREVA report number BGM/DS/SER RT 11/016, 73 p.

Berthet, L. and Osorio, J-C., 2011b. Technical Report on resources Centre Zone Deposit Kiggavik area, Nunavut; AREVA report number BGM/DS/SER RT 11/017, 63 p.

Bostock, H.S., 1970. Physiographic regions of Canada; Geological Survey of Canada, Map 1254A, scale 1:5,000,000.

Bradshaw, P.M.D. and Lett, R.E.W., 1980. Geochemical Exploration for uranium using soils, *In:* Geochemical Exploration for Uranium, (ed.) R.H Carpenter; Journal of Geochemical Exploration, v.13, p. 305–319.

Cabri, L.J., Rudashevsky, N.S., Rudashevsky, V.N., and Oberthur, T., 2008. Electric-pulse disaggregation (EPD), Hydroseparation (HS) and their use in combination for mineral and advanced characterization of ores; Proceedings of the 40th Annual Canadian Mineral Processors Conference, Ottawa 2008, p. 221–235.

Campbell, J.E., 2009. Drift prospecting for uranium in the Athabasca Basin, Saskatchewan, *In:* Application of Till and Stream Sediment Heavy Mineral and Geochemical Methods to Mineral Exploration in Western and Northern Canada, (ed.) R.C. Paulen and I. McMartin; Geological Association of Canada, Short Course Notes 18, p. 207–214.

Campbell, R. and Clark, M., 2009. Kiggavik-Sissons Updated Technical Report 2007/2008; SRK Consulting Canada Incorporated, SRK Project Number 1CA015.003, prepared for AREVA Resources Canada.

Carlson, J.A., Kirkley, M.B., Thomas, E.M., and Hillier, W.D., 1999. Recent Canadian kimberlite discoveries, *In:* The J.B. Dawson Volume, Proceedings of the VIIth International Kimberlite Conference, (ed.) J.J. Gurney, J.L. Gurney, M.D. Pascoe, M.D., and S.H. Richardson, Cape Town, p. 81–89.

Corriveau, L., Ootes, L., Mumin, H., Jackson, V., Bennett, V., Cremer, J.F., Rivard, B., McMartin, I., and Beaudoin, G., 2007. Alteration vectoring to IOCG/U deposits in frontier volcano-plutonic terrains, Canada, *In:* Proceedings of Exploration 07, Fifth Decennial International Conference on Mineral Exploration, (ed.) B. Milkereit; Mine Site Exploration and Ore Delineation & Ore Deposits and Exploration Technology, p. 1171–1177.

Cunningham, C.M. and Shilts, W.W., 1977. Surficial geology of the Baker Lake area, District of Keewatin, *In:* Report of Activities, Part B, (eds.) R.G. Blackadar, P.J. Griffin, H. Dumych, and E.J.W. Irish; Geological Survey of Canada, Paper 77-1B, p. 311–314.

Dilabio, R.N.W., 1979. Drift prospecting in uranium and base-metal mineralization sites, District of Keewatin, Northwest Territories, Canada, *In:* Prospecting in Areas of Glaciated Terrain – 1979, (ed.) M.J. Jones; The Institution of Mining and Metallurgy, Dublin, Ireland, p. 91–100.

Dilabio, R.N.W., 1990. Classification and interpretation of the shapes and surface textures of gold grains from till on the Canadian Shield; *In:* Current Research, Part C: Geological Survey of Canada, Paper 90-1C, p. 323–329.

Donaldson, J.A., 1965. The Dubawnt Group, districts of Keewatin and Mackenzie; Geological Survey of Canada, Paper 64-20, p. 11.

Dyke, A.S., 2004. An outline of North American deglaciation with emphasis on central and northern Canada; *In:* Quaternary Glaciations; Extent and Chronology Part II – 2004, (ed.) K. Ehlers and P.L. Gibbard; Elsevier, Amsterdam, p. 373–424.

Dyke, A.S., Andrews, J.T., Clark, P.U., England, J.H., Miller, G.H., Shaw, J., and Veillette, J.J., 2002. The Laurentide and Innuitian ice sheets during the Last Glacial Maximum; Quaternary Science Reviews, v. 21, p. 9–31.

Earle, S., 2001. Application of composite glacial boulder geochemistry to exploration for unconformity-type uranium deposits in the Athabasca Basin, Saskatchewan, Canada, *In:* Drift Exploration in Glaciated Terrain (ed.) M.B. McClenaghan, P.T. Bobrowsky, G.E.M. Hall and S.J. Cook; Geological Society, London, Special Publication 185, p. 225–235.

Finch, R.J. and Ewing, R.C., 1992. The corrosion of uraninite under oxidizing conditions; Journal of Nuclear Materials, v. 190, p. 133–156.

Fuchs, H.D. and Hilger, W., 1989. Kiggavik (Lone Gull): An unconformity related uranium deposit in the Thelon Basin, Northwest Territories, Canada, *In:* Uranium Resources and Geology of North America, (ed.) E. Muller-Kahle; International Atomic Energy Agency-TECDOC-500, p. 429–454.

Fuchs, H.D., Hilger, W., and Prosser, E., 1985. Geology and exploration history of the Lone Gull property, *In:* Uranium Deposits of Canada, (ed.) E.L. Evans; Canadian Institute of Mining and Metallurgy, v. 33, p. 286–292.

Gall, Q., Peterson, T.D., and Donaldson, J.A., 1992. A proposed revision of early Proterozoic stratigraphy of the Thelon and Baker Lake basins, Northwest Territories, *In:* Current Research, Part C, Canadian Shield; Geological Survey of Canada; Paper no. 92-1C, p. 129–137.

Geddes, R.S., 1982. The Vixen Lake indicator train, northern Saskatchewan, *In:* Prospecting in Glaciated Terrain, (ed.) P.H. Davenport; Canadian Institute Mining Metallurgy, Proceedings, p. 264–283.

Grandstaff, D.E., 1976. A kinetic study of the dissolution of uraninite; Economic Geology, v.71, p. 1493–1506.

Griep J., 1978. Final Report on Diamond Drilling Programme, Lone Gull Lake, NTS Area 66-A-5; Urangesellschaft Assessment Report.

Griep, J., Hesse, B.P., Hilger, W., and Prosser, E., 1980. Annual Report on Exploration and Drilling, Baker Lake Area, Lone Gull Project; Urangesellschaft Canada Limited, 127 p.

Grunsky, E., Harris, J.R., and McMartin, I., 2006. Predictive mapping of surficial materials, Schultz Lake area (NTS 66A), Nunavut, Canada; Geological Survey of Canada, Open File 5153. doi:10.4095/221968

Grunsky, E; Harris, J; McMartin, I., 2009. Predictive mapping of surficial materials, Schultz Lake area (NTS 66A), Nunavut, Canada, *In:* Remote Sensing and Spectral Geology, (ed.) R. Bedell, A.P. Crosta, and E. Grunsky; Reviews in Economic Geology, v. 16, p. 177–198 (ESS Cont.# 20080009).

Hadlari, T., Rainbird, R.H., and Pehrsson, S.J., 2004. Geology, Schultz Lake, Nunavut; Geological Survey of Canada, Open File 1839, 1 sheet, scale 1:250 000.

Hiatt, E. E., Kyser, K., and Dalrymple, R. W., 2003. Relationships among sedimentology, stratigraphy, and diagenesis in the Proterozoic Thelon Basin, Nunavut, Canada: Implications for paleoaquifers and sedimentary-hosted mineral deposits; Journal of Geochemical Exploration, v. 80, no. 2-3, p. 221–240.

Hicken, A.K., McClenaghan, M.B., Paulen, R.C., and Layton-Matthews., D., 2012. Till geochemical signatures of the Izok Lake Zn-Cu-Pb-Ag volcanogenic massive sulphide deposit, Nunavut; Geological Survey of Canada, Open File 7046.

Henderson, E.P., 1973. Surficial geology of Kingston (north half) map-area, Ontario; Geological Survey of Canada, Paper 74–28.

Henderson, P.J. and Roy, M., 1995. Distribution and character of gold in surface till in the Flin Flon greenstone belt, Saskatchewan, *In:* Current Research 1995-E; Geological Survey of Canada, p. 175–186.

Jefferson, C.W., Thomas, D.J., Gandhi, S.S., Ramaekers, P., Delaney, G., Brisbin, D., Cutts, C., Quirt, D., Portella, P., and Olson, R.A. 2007. Unconformity-associated uranium deposits of the Athabasca Basin, Saskatchewan and Alberta, *In:* Mineral Deposits of Canada: A Synthesis of Major Deposit Types, District Metallogeny, the Evolution of Geological Provinces, and Exploration Methods, (ed) W.D. Goodfellow; Geological Association of Canada, Mineral Deposits Division, Special Publication No. 5, p. 273–305.

Jefferson, C.W., Chorlton, L.B., Pehrsson, S.J., Peterson, T., Wollenberg, P., Scott, J., Tschirhart, V., McEwan, B., Bethune, K., Calhoun, L., White, J.C., Leblon, B., LaRocque, A., Shelat, Y., Lentz, D., Patterson, J., Riegler, T., Skulski, T., Robinson, S., Paulen, R., McClenaghan, B., Layton-Matthews, D., MacIsaac, D., Riemer, W., Stieber, C., and Tschirhart, P., 2011a. Northeast Thelon Region: Geomapping for Uranium in Nunavut; Geological Survey of Canada, Open File 6862, Power Point Presentation, 38 slides. doi:10.4095/289037

Jefferson, C.W., Hunter, R., McLaren, M., Peterson, T., Skulski, T., Rainbird, R., Young, G.M., Gandhi, S.S., and Costello, K., 2011b. Northeastern Thelon Basin uranium region: geological compilation for geophysical consortium planning; Geological Survey of Canada, Open File 6950, 1 sheet. doi:10.4095/288801

Jefferson, C.W., Pehrsson, S., Peterson, T., Chorlton, L., Davis, W., Keating, P., Gandhi, S., Fortin, R., Buckle, J., Miles, W., Rainbird, R., LeCheminant, A., Tschirhart, V., Tschirhart, P., Morris, W., Scott, J., Cousens, B., McEwan, B., Bethune, K., Riemer, W., Calhoun, L., White, J., MacIsaac, D., Leblon, B., Lentz, D., LaRocque, A., Shelat, Y., Patterson, J., Enright, A., Stieber, C., Riegler, T., 2011c. Northeast Thelon region geoscience framework - new maps and data for uranium in Nunavut; Geological Survey of Canada, Open File 6949, 1 sheet. doi:10.4095/288791

Jefferson, C.W., Peterson, T., Tschirhart, V., Davis, W., Scott, J.M.J., Reid, K., Ramaekers, P., Gandhi, S.S., Bleeker, W., Pehrsson, S., Morris, W.A., Fayek, M., Potter, E., Bridge, N., Grunsky, E., Keating, P., Ansdell, K., and Banerjee, N., 2013. LIPs and Proterozoic uranium (U) deposits of the Canadian Shield; Geological Survey of Canada, Open File 7352, 56 pages + spread sheet. doi:10.4095/292377

Jefferson, C.W., White, J.C., Young, G.M., Patterson, J., Tschirhart, V.L., Pehrsson, S.J., Calhoun, L., Rainbird, R.H., Peterson, T.D., Davis, W.J., Tella, S., Chorlton, L.B., Scott, J.M.J., Percival, J.A., Morris, W.A., Keating, P., Anand, A., Shelat, Y., and MacIsaac, D., 2015. Outcrop and remote predictive geology of the Amer Belt and basement beside and beneath the northeast Thelon Basin, in parts of NTS 66-A, B, C, F, G and H, Kivalliq Region, Nunavut; Geological Survey of Canada, Open File 7242, 1 sheet. doi:10.4095/296825

Jefferson, C.W., Pehrsson, S.J., Peterson, T.D., Tschirhart, V.L., Anand, A., Wollenberg, P., LeCheminant, A.N., Riegler, T., Davis, W.J., McEwan, B.J., Bethune, K.M., Chorlton, L.B., Tschirhart, P.A., Scott, J.M.J., McNicoll, V.J., Robinson, S.V.J., Riemer, W.C., Patterson, J.D., Morris, W.A., Keating, P. and Stieber, C.M., in prep. Outcrop and remote predictive geology of the western Marjorie–Tehek supracrustal belt and Northeast Thelon Basin margin in parts of NTS 66A and 66B, Nunavut – context of the Kiggavik uranium camp; Geological Survey of Canada, Open File 7241.

Johnstone, D., Bethune, K., Quirt, D., and Benedicto, A. 2015. Summary and compilation of work for Dillon Johnstone's M.Sc. thesis, May 2015 to November 2015: Structural controls of uranium mineralization in the Kiggavik East Zone, Central Zone, and Main Zone deposits and their potential extensions to the northeast; AREVA Resources Canada Inc., internal report, number 15-CND-92-04, 18 p. plus appendices.

Kaszycki, C.A., Nielsen, E., and Gobert, G. 1996. Surficial geochemistry and response to volcanic-hosted massive sulphide mineralization in the Snow Lake region, *In:* EXTECH I: A Multidisciplinary Approach to Massive Sulphide Research in the Rusty Lake-Snow Lake Greenstone Belts, Manitoba, (ed.) G.F. Bonham-Carter, A.G. Galley, and G.E.M. Hall; Geological Survey of Canada, Bulletin 426, p. 139–154.

Klassen, R.A. and Shilts, W.W., 1977a. Uranium exploration using till, District of Keewatin; Geological Survey of Canada, Report of Activities, Paper 77-1A, p. 471–477.

Klassen, R.A. and Shilts, W.W., 1977b. Glacial dispersal of uranium in the District of Keewatin, Canada, *In:* Prospecting in Areas of Glaciated Terrain, (ed.) M.J. Jones; The Institution of Mining and Metallurgy, Espoo, Finland, p. 80–88.

Lundqvist, J., 1990. Glacial morphology as an indicator of the direction of glacial transport, *In:* Glacial Indicator Tracing, (eds.) R. Kujansuu and M. Saarnisto; A.A. Balkema, Rotterdam, p. 61–70.

McClenaghan, M.B., 2001. Regional and local-scale gold grain and till geochemical signatures of lode Au deposits in the western Abitibi Greenstone Belt, central Canada, *In:* Drift Exploration in Glaciated Terrain, (eds.) M.B. McClenaghan, P.T. Borowsky, G.E.M. Hall, and S.J. Cook; Geological Society, London, Special Publications 185, p. 201–224.

McClenaghan, M.B., 2005. Indicator mineral methods in mineral exploration. Geochemistry: Exploration, Environment, Analysis, v. 5, p. 233–245.

McClenaghan, M.B., 2007. Till geochemical and heavy mineral exploration methods in glaciated terrain, *In:* Exploration Geochemistry, Basic Principles and Concepts, Workshop 2; Exploration 07, International Conference on Mineral Exploration, p. 23–31.

McClenaghan, M.B., 2013. Volcanogenic massive sulphide exploration in glaciated terrain using till geochemistry and indicator minerals, *In:* New Frontiers for Exploration in Glaciated Terrain, (eds.) R.C. Paulen and M.B. McClenaghan; Geological Survey of Canada, Open File 7374, p. 53–64.

McClenaghan, M.B. and Kjarsgaard, B.A., 2007. Indicator mineral and surficial geochemical exploration methods for kimberlite in glaciated terrain; Examples from Canada, *In:* Mineral Deposits of Canada: A Synthesis of Major Deposit Types, District Metallogeny, the Evolution of Geological Provinces, and Exploration Methods, (ed.) W.D. Goodfellow; Geological Association of Canada, Mineral Deposits Division, Special Publication No. 5, p. 983–1006.

McClenaghan, M.B., Budulan, G., Averill, S.A., Layton-Matthews, D., and Parkhill, M.A., 2012. Indicator mineral abundance data

for bedrock and till samples from the Halfmile Lake Zn-Pb-Cu volcanogenic massive sulphide deposit, Bathurst Mining Camp, New Brunswick; Geological Survey of Canada, Open File 7076.

McClenaghan, M.B., Parkhill, M.A., Seaman, A.A., Pronk, A.G., Averill, S.A., Rice, J.M., and Pyne, M., 2014. Indicator mineral signatures of the Sisson W-Mo deposit, New Brunswick: Part 2 Till; Geological Survey of Canada, Open File 7467.

McConnel, J.Q. and Batterson, M.J., 1987. The strange Lake Zr-Y-Nb-Be-REE deposit, Labrador: A geochemical profile in till, lake and stream sediment and water; Journal of Geochemical Exploration, v. 29, p. 105–127.

McEwan, B., Bethune, K.M., Riemer, W., and Jefferson, C.W., 2011. Structural style and regional correlation of the Ketyet River and Woodburn Lake groups in the Baker Lake area, Nunavut: New insights into the age and stratigraphic / structural relationships between complexly interfolded Archean and Paleoproterozoic supracrustal sequences of the central Rae Province; NE Thelon Consortium Workshop, McMaster University, Hamilton, ON, March 10, 2011 (extended abstract).

McMartin, I. and Campbell, J.E., 2009. Near-surface till sampling protocols in Shield terrain, with examples from western and northern Canada, *In:* Application of Till and Stream Sediment Heavy Mineral and Geochemical Methods to Mineral Exploration in Western and Northern Canada, (eds.) R.C. Paulen and I. McMartin; Geological Association of Canada, Short Course Notes 18, p. 75–95.

McMartin, I. and Dredge, L.A., 2005. History of ice flow in the Schultz Lake (NTS 66a) and Wager Bay (NTS 56G) areas, Kivalliq Region, Nunavut; Geological Survey of Canada, Current Research, 2005-B-2, 10 p.

McMartin, I. and Henderson, P.J., 2004. Evidence from Keewatin (central Nunavut) for paleo-ice divide migration; Géographie physique et Quaternaire, v. 58, p. 163–186.

McMartin, I. and McClenaghan, M.B., 2001. Till geochemistry and sampling techniques in glaciated terrain: a review, *In:* Drift Exploration in Glaciated Terrain, (eds.) M.B. McClenaghan, P.T. Bobrowsky, G.E.M. Hall, and S. Cook; Geological Society of London, Special Publication 185, p. 83–123.

McMartin, I. and Paulen, R.C., 2009. Ice-flow indicators and the importance of ice-flow mapping for drift prospecting, *In:* Application of Till and Stream Sediment Heavy Mineral and Geochemical Methods to Mineral Exploration in Western and Northern Canada, (eds.) R.C. Paulen and I. McMartin; Geological Association of Canada, Short Course Notes 18, p. 15–34.

McMartin I., Dredge L.A., Ford K.L., and Kjarsgaard, I.M., 2006. Till composition, provenance and stratigraphy beneath the Keewatin Ice Divide, Schultz Lake area (NTS 66A), mainland Nunavut; Geological Survey of Canada, Open File 5312, 81 p.

McMartin, I., Dredge, L.A., and Aylsworth, J.M., 2008. Surficial geology, Schultz Lake South, Nunavut; Geological Survey of Canada, "A" Series Map 2120A, 1 sheet, 1 CD-ROM. doi:10.4095/224825

Miller, A.R. and LeCheminant, A.N., 1985. Geology and uranium metallogeny of Proterozoic supracrustal successions, central district of Keewatin, N.W.T with comparisons to northern Saskatchewan, *In:* Geology of Uranium Deposits, (eds.) T.I.I. Sibbald and W. Petruk; Canadian Institute of Mining and Metallurgy, Special Volume 32, p. 167–185.

Morrison, D., 2009. Kiggavik-Sissons Project; AREVA Annual Report 2008, v. I. Report 08-CND-92-02.

Osorio, J-C., 2011. Technical Report on resources End Grid (North Pod) Deposit Kiggavik area, Nunavut; AREVA report number BGM/DS/SER RT 11/018, 62 p.

Pacquet, A., 1993. Kiggavik Main Zone; Urangesellschaft Canada Limited, Report 8493, 38 p.

Parkhill, M. and Doiron, A., 2003. Quaternary geology of the Bathurst Mining Camp and implications for base metal exploration using drift exploration, *In:* Massive Sulfide Deposits of the Bathurst Mining Camp, New Brunswick, and Northern Maine, (ed.) W.D. Goodfellow, S.R. McCutcheon, and J.M. Peter; Society of Economic Geologists, Monograph 11, p. 631–660.

Pehrsson, S., Jefferson, C.W., Peterson, T., Scott, J., Chorlton, L., and Hillary, B., 2010. Basement to the Thelon Basin, Nunavut – revisited; GeoCanada 2010, Calgary, AB, May 10–14, 4 p. (extended abstract).

Pehrsson, S.J., Berman, R., and Davis, W.J., 2013. Paleoproterozoic orogenesis during Nuna aggregation: a case study of reworking of the Archean Rae craton, Woodburn Lake, Nunavut. Precambrian Research, 232, 167-188. http://dx.doi.org/10.1016/j.precamres.2013.02.010

Peterson, T.D., van Breemen, O., Sandeman, H., and Cousens, B., 2002. Proterozoic (1.85–1.75 Ga) igneous suites of the Western Churchill Province: granitoid and ultrapotassic magmatism in a reworked Archean hinterland; Precambrian Research, v. 119, p. 73–100.

Peterson, T.D., Scott, J.M.J., LeCheminant, A.N., Chorlton, L.B., and D'Aoust, B.M.A., 2014. Geology, Tebesjuak Lake, Nunavut; Geological Survey of Canada, Canadian Geoscience Map 158 (preliminary), scale 1:250 000. doi:10.4095/293892

Peterson, T.D., Scott, J.M.J., LeCheminant, A.N., Jefferson, C., and Pehrsson, S.J., 2015a. The Kivalliq Igneous Suite: Anorogenic bimodal magmatism at 1.75 Ga in the western Churchill Province, Canada; Precambrian Research, v. 262, p. 101–119. doi.org/10.1016/j.precamres.2015.02.019

Peterson, T.D., Scott, J.M.J., LeCheminant, A.N., Tschirhart, V., Chorlton, L.B., Davis, W.J., and Hamilton, M., 2015b. Nueltin granites and mafic rocks in the Tebesjuak Lake map area, Nunavut: new geochronological, petrological, and geophysical data; Geological Survey of Canada, Current Research (Online) 2015-5, 23 p. doi:10.4095/296163

Peterson, T.D., Jefferson, C.W., and Anand, A., 2015c. Geological setting and geochemistry of the ca. 2.6 Ga Snow Island Suite in the central Rae Domain of the Western Churchill Province, Nunavut; Geological Survey of Canada, Open File 7841, 29 p. doi:10.4095/296599

Plouffe, A., McClenaghan, M.B., Paulen, R.C., McMartin, I., Campbell, J.E., and Spirito, W.A., 2013. Processing of glacial sediments for the recovery of indicator minerals: protocols used at the Geological Survey of Canada; Geochemistry: Exploration, Environment, Analysis, v. 13, p. 303–316.

Rainbird, R.H., Hadlari, T., Aspler, L.B., Donaldson, J.A., LeCheminant, A.N., and Peterson, T.D., 2003. Sequence stratigraphy and evolution of the Paleoproterozoic intracontinental Baker Lake and Thelon basins, western Churchill Province, Nunavut, Canada; Precambrian Research, v. 125, p. 21–53.

Riegler, T., 2014. Système d'altération et minéralisation en uranium le long du faisceau structural Kiggavik - Andrew Lake (Nunavut, Canada). modèle génétique et guides d'exploration; Ph.D. thesis, Université Poitiers, Poitiers, France, 244 p.

Reilly, B., 1997. Assessment Report for Uranium exploration Activities: 1996 Field Season Diamond Drilling, COGEMA Resources Incorporated; Nunavut Assessment Report 083829, 26 p.

Reyx, J., 1994. Petrographic report 8634, Canada, Kiggavik Project; COGEMA, unpublished internal report, No. 94-UGC-92-01, 33 p.

Romberger, S.B., 1984. Transport and deposition of uranium in hydrothermal systems of temperatures up to 300°C: geological implications, *In:* Uranium Geochemistry, Resources, (eds.) B. de Vivo, F. Ippolito, G. Capaldi, and P.R. Simpson; The Institution of Mining and Metallurgy, London, UK, p. 12–17.

Robinson, S.V.J., 2015 Till geochemical and heavy mineral signatures of the Kiggavik uranium deposit, Nunavut, Canada; M.Sc. thesis, Queen's University, Kingston, Ontario, 549 p.

Robinson, S.V.J., Paulen, R.C., Jefferson, C.W., McClenaghan, M.B., Layton-Matthews, D., Quirt, D., and Wollenberg, P., 2014. Till geochemical signatures of the Kiggavik Uranium Deposit, Nunavut; Geological Survey of Canada, Open File 7550; 168 p. doi:10.4095/293857

Scott, J.M.J., 2012. Paleoproterozoic (1.75 Ga) Granitoid Rocks and Uranium Mineralization in the Baker Lake—Thelon Basin region, Nunavut. M.Sc. thesis, Carleton University, Ottawa, Ontario,136 p.

Scott, J.M.J., Peterson, T.D., Davis, W.J., Jefferson, C.W., and Cousens, B.L., 2015. Petrology and geochronology of Paleoproterozoic intrusive rocks, Kiggavik uranium camp, Nunavut; Canadian Journal of Earth Sciences; doi:10.1139/cjes-2014-0153

Sharpe, R., Fayek, M., Quirt, D., and Jefferson, C.W., 2015. Geochronology and genesis of the Bong uranium deposit, Thelon Basin, Nunavut, Canada; Economic Geology, v. 110, p. 1759–1777.

Shi, F., Manlapig, E., and Zuo, W., 2014. Progress and challenges in electrical comminution by high-voltage pulses; Chemical Engineering and Technology, v. 37, no. 5, p. 765–769.

Shilts, W.W., 1973. Drift Prospecting: Geochemistry of Eskers and Till in Permanently Frozen Terrain, District of Keewatin, Northwest Territories; Geological Survey of Canada, Paper 72-45.

Shilts, W.W., 1978. Nature and genesis of mudboils, central Keewatin, Canada; Canadian Journal of Earth Sciences, v. 15, p. 1053–1068.

Shilts, W.W. and Cunningham, C.M., 1977. Anomalous uranium concentrations in till north of Baker Lake, District of Keewatin, *In:* Report of Activities; Geological Survey of Canada, Paper 77-1B, p. 291–292.

Shilts, W.W. and Klassen, R.A., 1976. Drift prospecting in the District of Keewatin – uranium and base metals, *In:* Report of Activities; Geological Survey of Canada, Paper 76-1A, p. 255–257.

Shilts, W.W., Cunningham, C.M. and Kaszycki, C.A., 1979. Keewatin Ice Sheet – Re-evaluation of the traditional concepts of the Laurentide Ice Sheet; Geology, v. 7, p. 537–541.

Stea, R.R., Johnson, M., and Hanchar, D., 2009. The geometry of kimberlite indicator mineral dispersal fans in Nunavut, Canada, *In:* Application of Till and Stream Sediment Heavy Mineral and Geochemical Methods to Mineral Exploration in Western and Northern Canada, (ed.) R.C. Paulen and I. McMartin; Geological Association of Canada, Short Course Notes 18, p. 1–13.

Tschirhart, V., Morris, W.A., Ugalde, H., and Jefferson, C.W., 2011. Preliminary 3D geophysical modelling of the Aberdeen subbasin, northeast Thelon Basin region, Nunavut; Geological Survey of Canada, Current Research 2011-4, 12 p. doi:10.4095/287165

Turner, W.A., Richards, J.P., Nesbitt, B.E., Muehlenbachs, K., and Biczok, J.L., 2001. Proterozoic low-sulfidation epithermal Au-Ag mineralization in the Mallery Lake area, Nunavut, Canada; Mineralium Deposita, v. 36, p. 442–457.

Turner, W.A., Heaman, L.M., and Creaser, R.A., 2003. Sm–Nd fluorite dating of Proterozoic low-sulfidation epithermal Au–Ag deposits and U–Pb zircon dating of host rocks at Mallery Lake, Nunavut, Canada; Canadian Journal of Earth Sciences, v. 40, p. 1789–1804.

Tyrrell, J.B., 1897. Report on the Dubawnt, Kazan and Ferguson Rivers, and the northwest coast of Hudson Bay; and on two overland routes from Hudson Bay to Lake Winnipeg; Geological Survey of Canada, Annual Report, v. 9, p. 1–218.

Tyrrell, J.B., 1898. The glaciation of north-central Canada; Journal of Geology, v. 6, p. 147–160.

Weyer, H.J., 1992. The Kiggavik uranium deposit, Northwest Territories, Canada; Ph.D. thesis, Rheinish-Westfaelishe Technishe Hochschule Aachen, Germany.

Weyer, H.J., Friedrich, G., Bechtel, A., and Ballhorn, R.K., 1989. The Lone Gull uranium deposit – new geochemical and petrological data as evidence for the nature of the ore bearing solutions; International Atomic Energy Agency, Vienna (Austria); Panel proceedings series, TC-542/19, p. 293–305.

Wright, G.M., 1955. Geological notes on central District of Keewatin, Northwest Territories; Geological Survey of Canada, Paper 55-17, 17 p.

Zalesky, E. and Pehrsson, S., 2005. Geology, Half Way Hills and Whitehills Lake area, Nunavut; Geological Survey of Canada, "A" Series Map, 2069A, 1 sheet, 1:150 000.

Zaleski, E., Pehrsson, S., Duke, N., Davis, W.J., L'Heureux, R., Greiner, E., and Kerswill, J.A., 2000. Quartzite sequences and their relationships, Woodburn Lake group, western Churchill Province, Nunavut; Geological Survey of Canada, Current Research, no. 2000-C7, 10 p.

APPENDIX H. Distribution maps of select heavy minerals from till samples

Appendix H1. Reconnaissance-scale maps

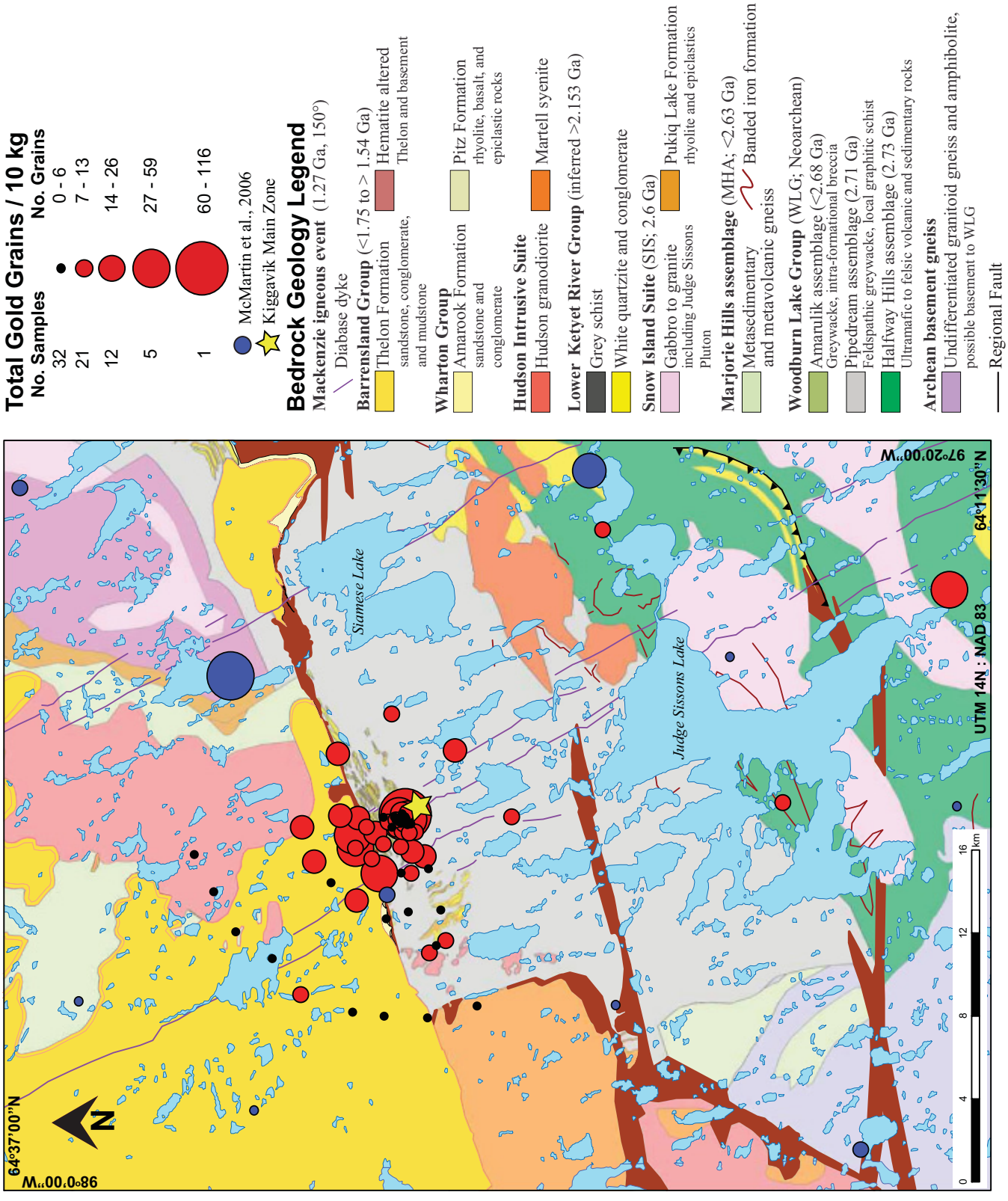

Appendix H1 continued.

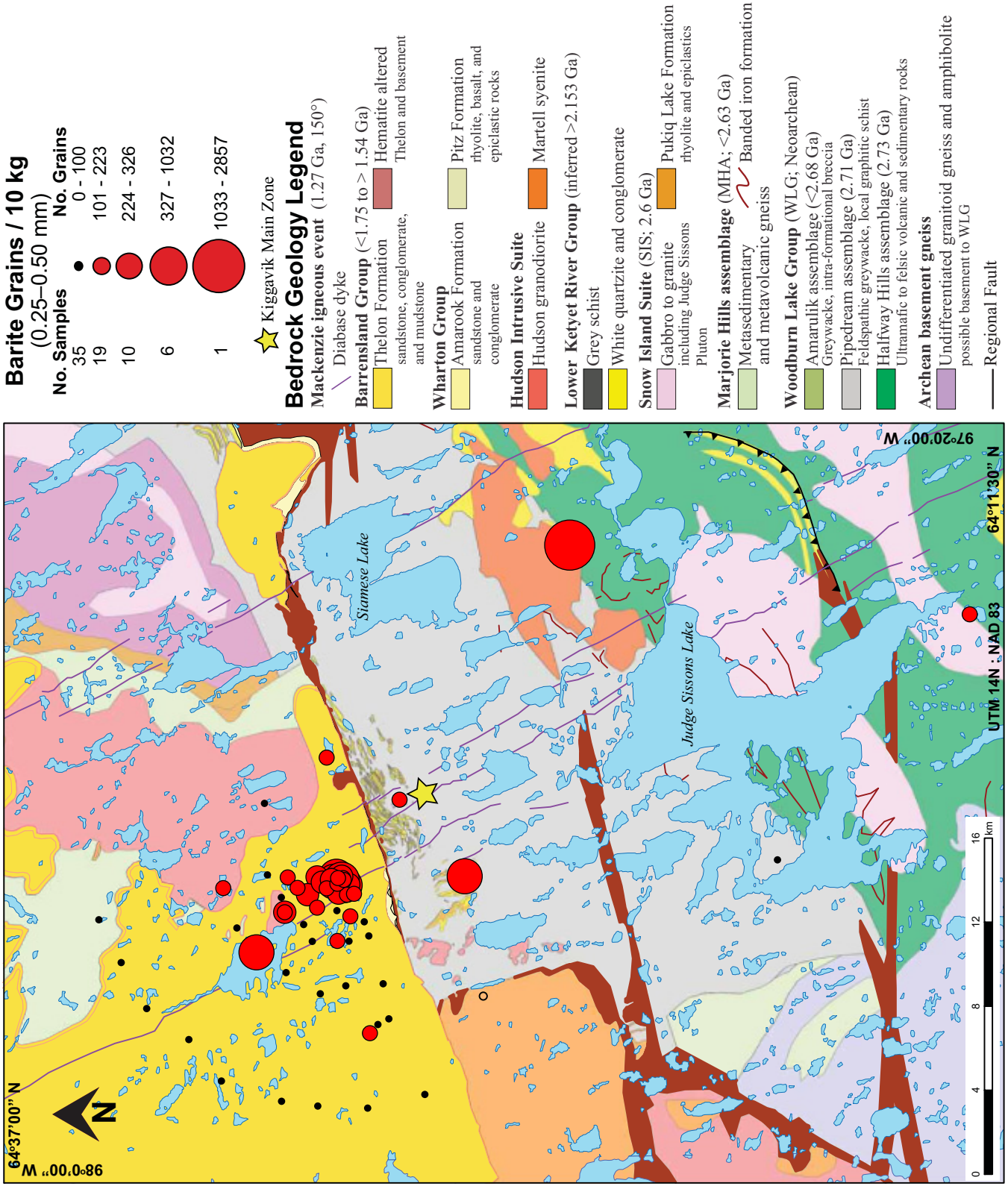

Appendix H1 continued.

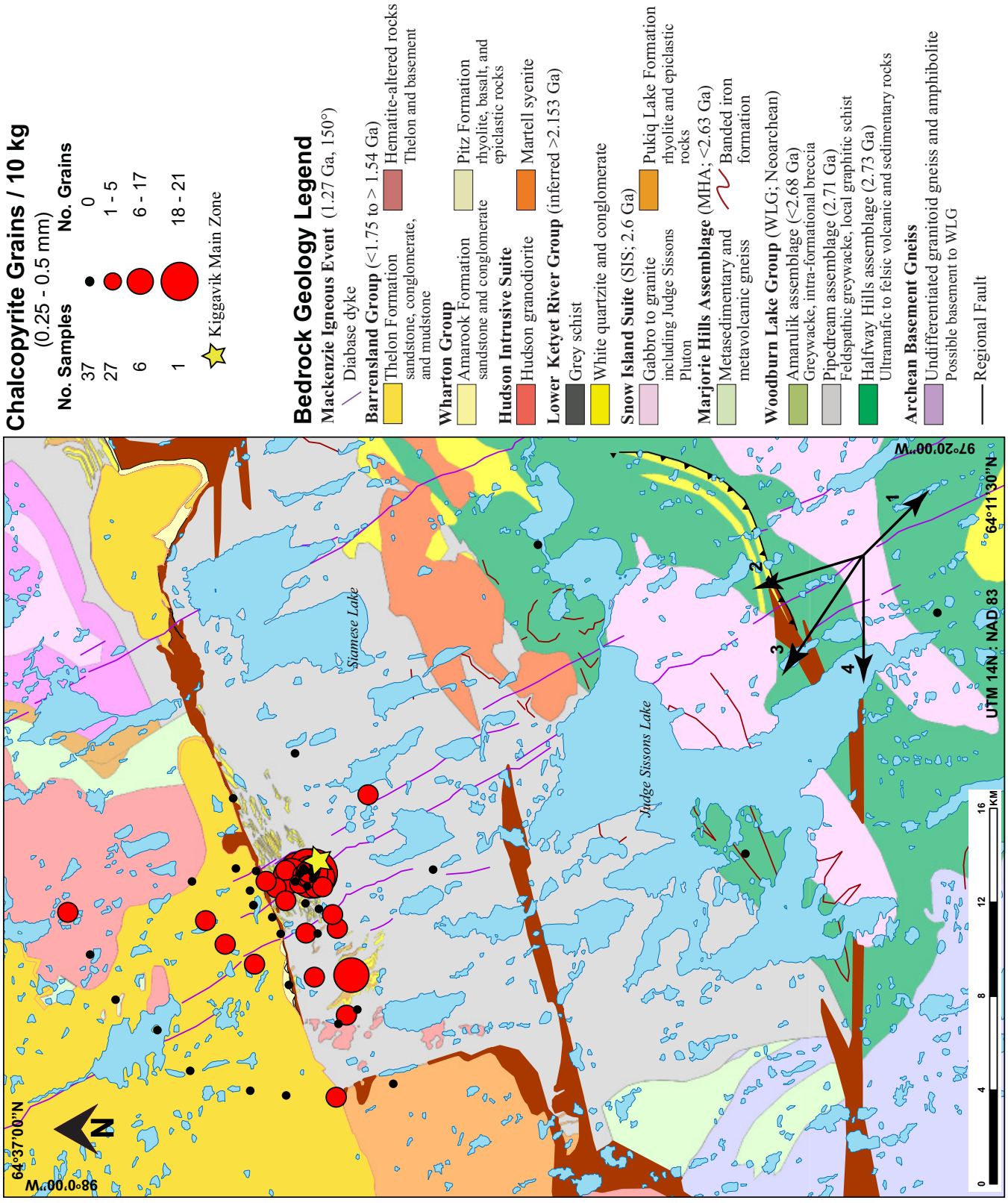

Appendix H1 continued.

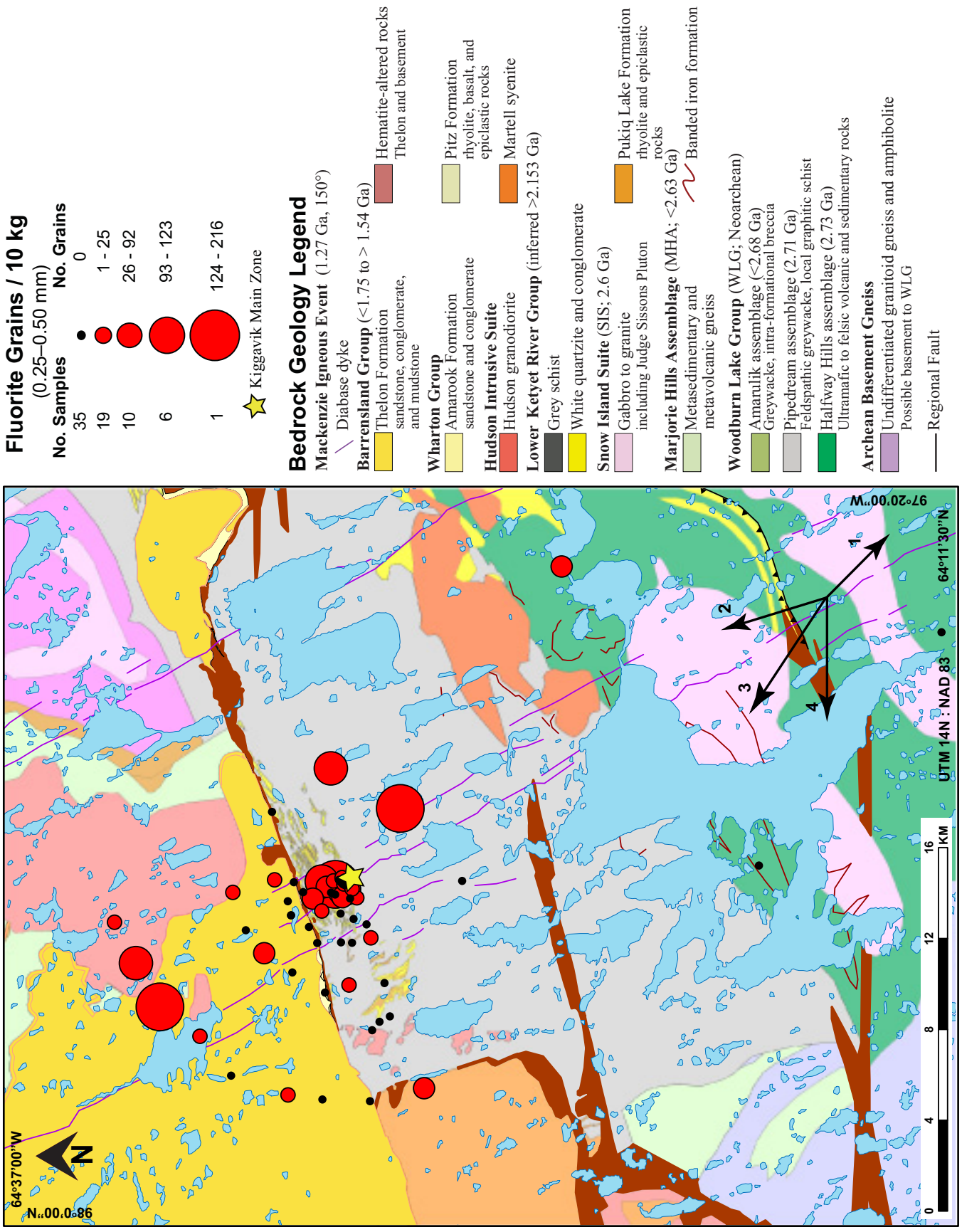

Appendix H1 continued.

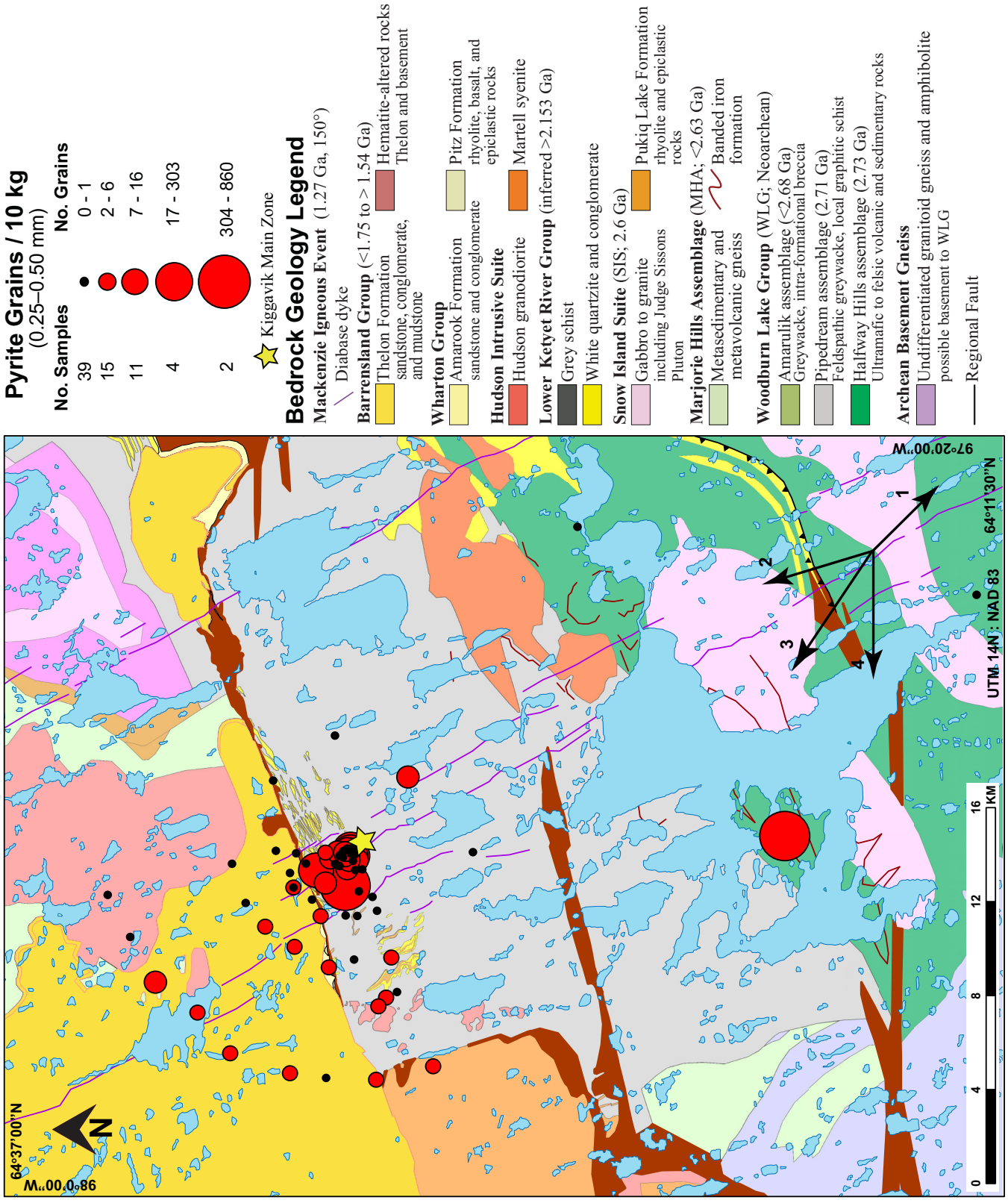

Appendix H2. Regional-scale maps

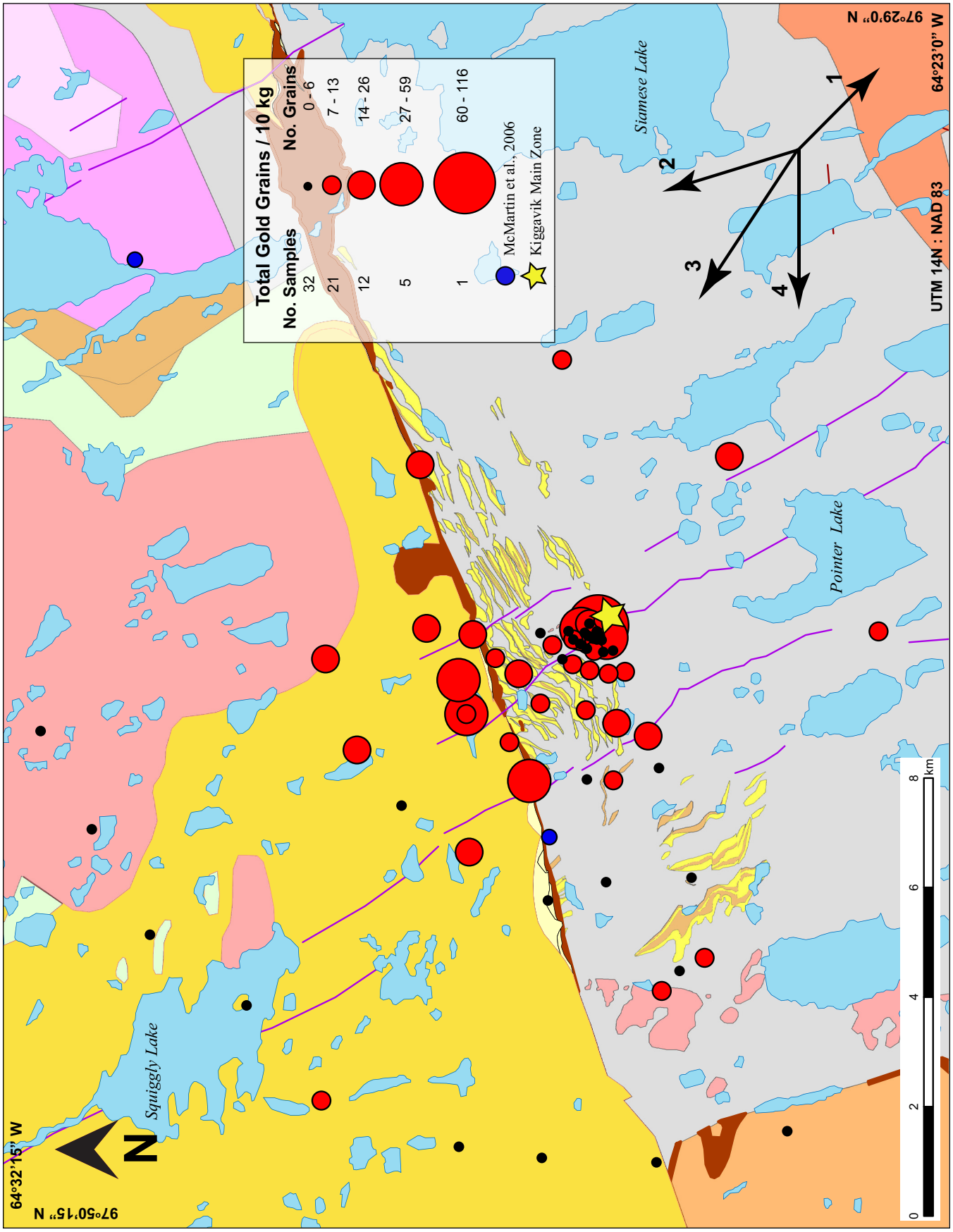

Appendix H2 continued.

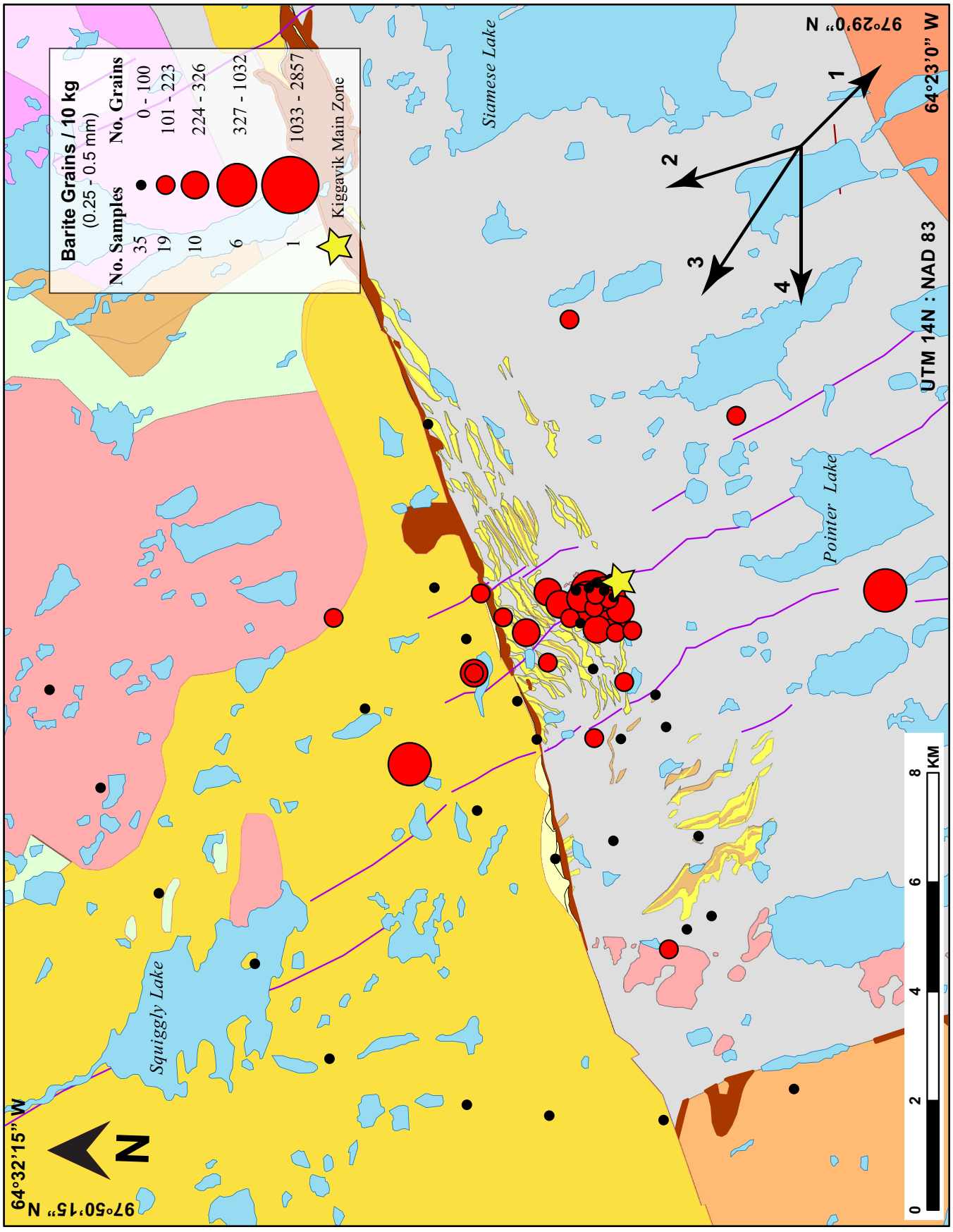

Appendix H2 continued.

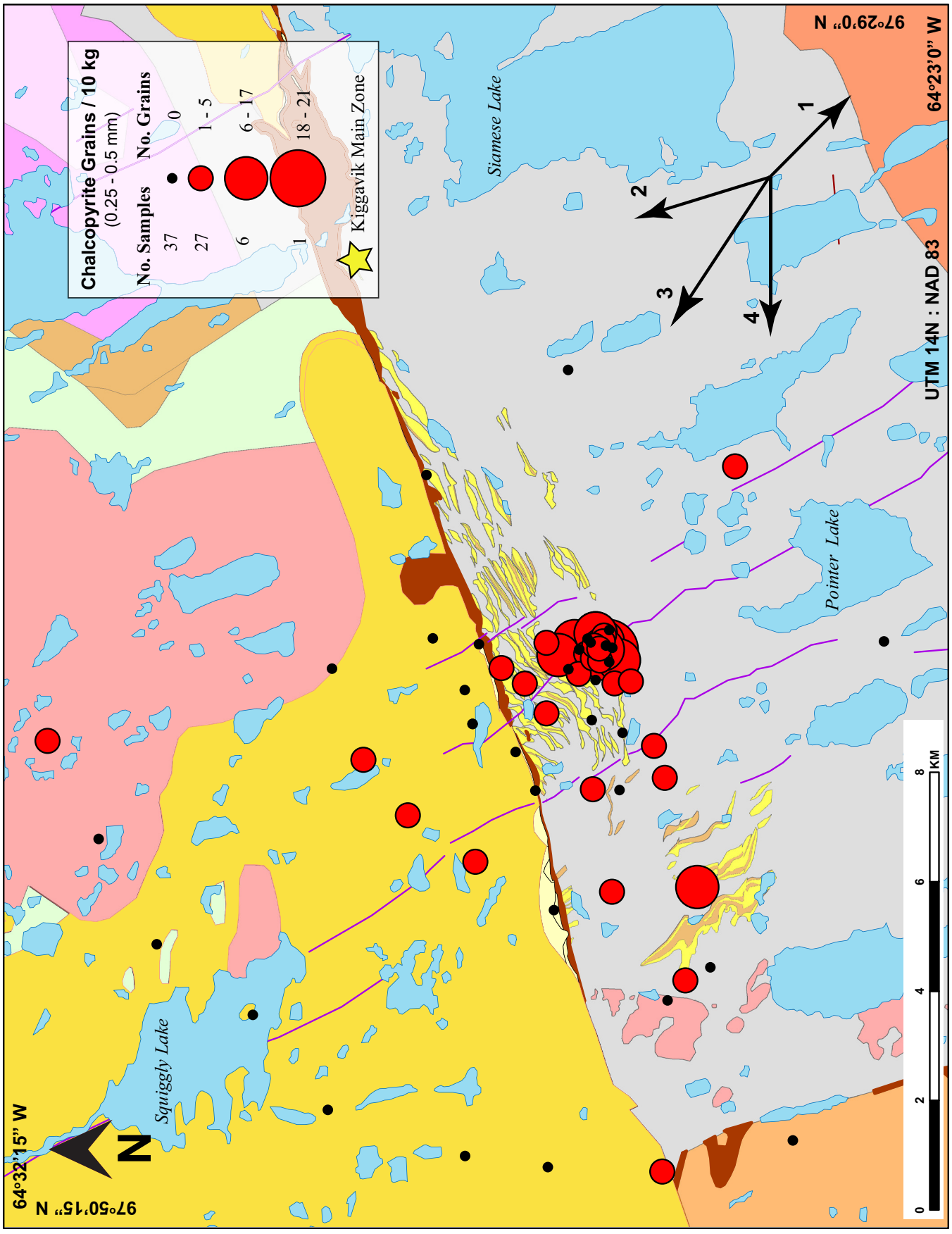

Appendix H2 continued.

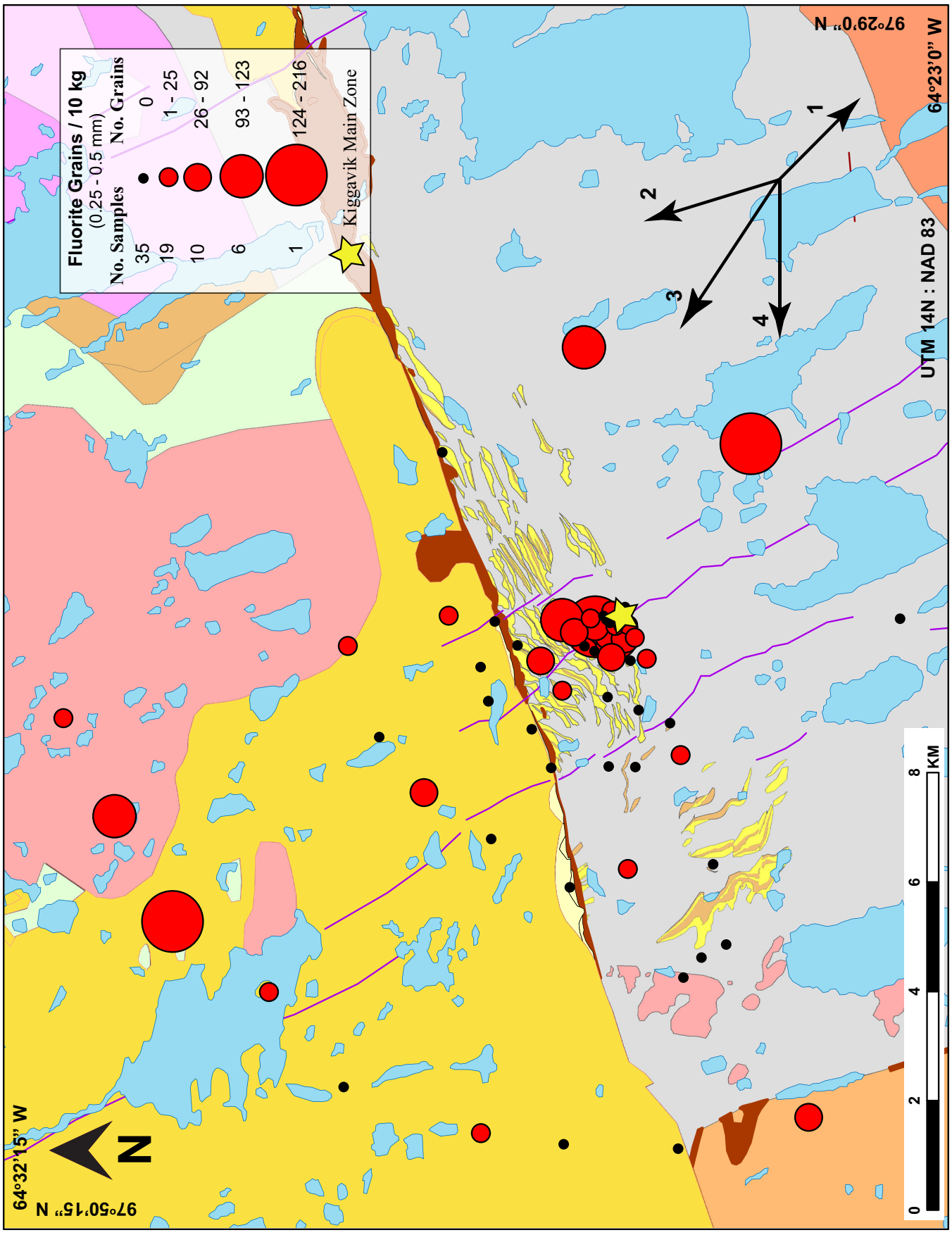

Appendix H2 continued.

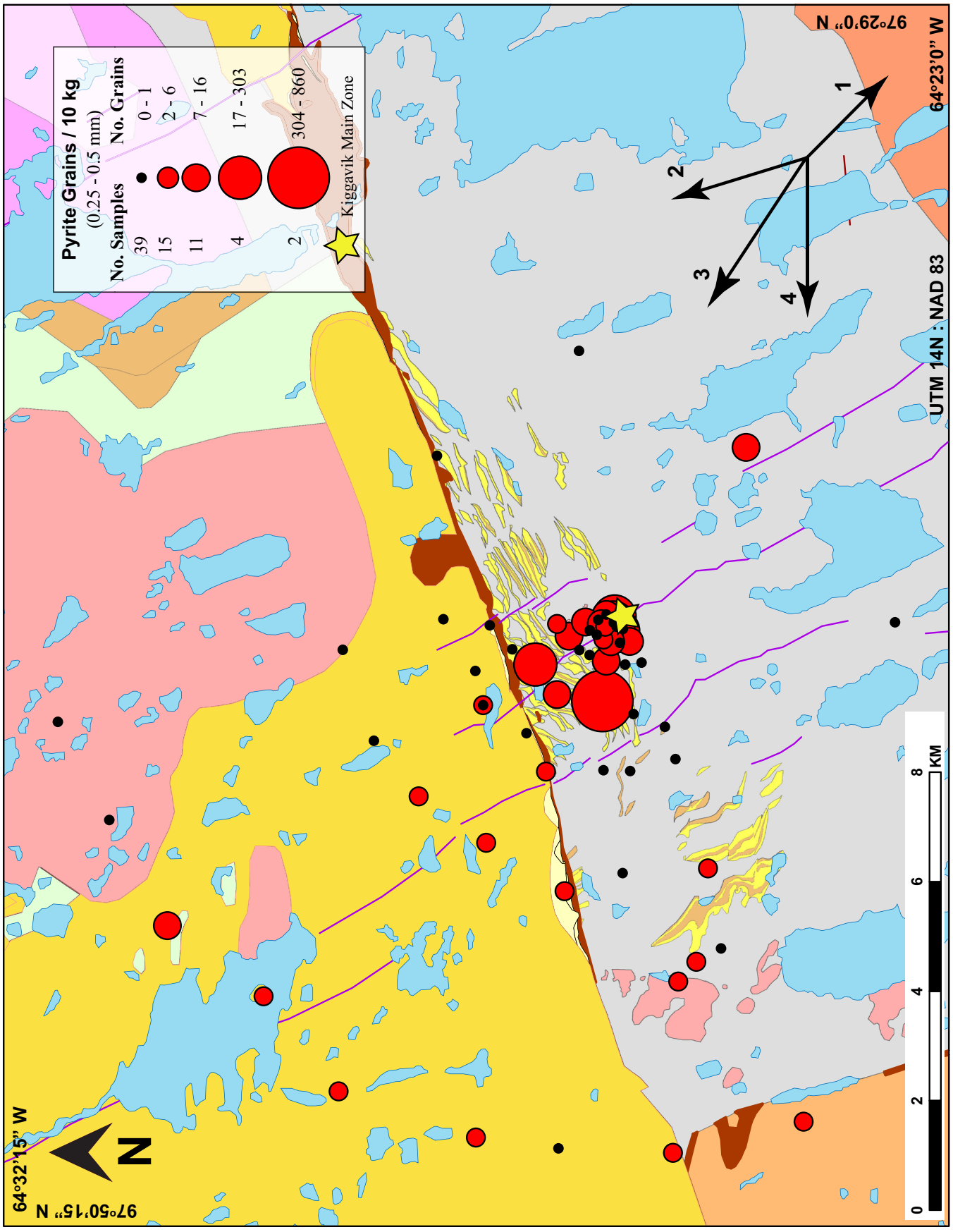

Appendix H3. Deposit-scale maps

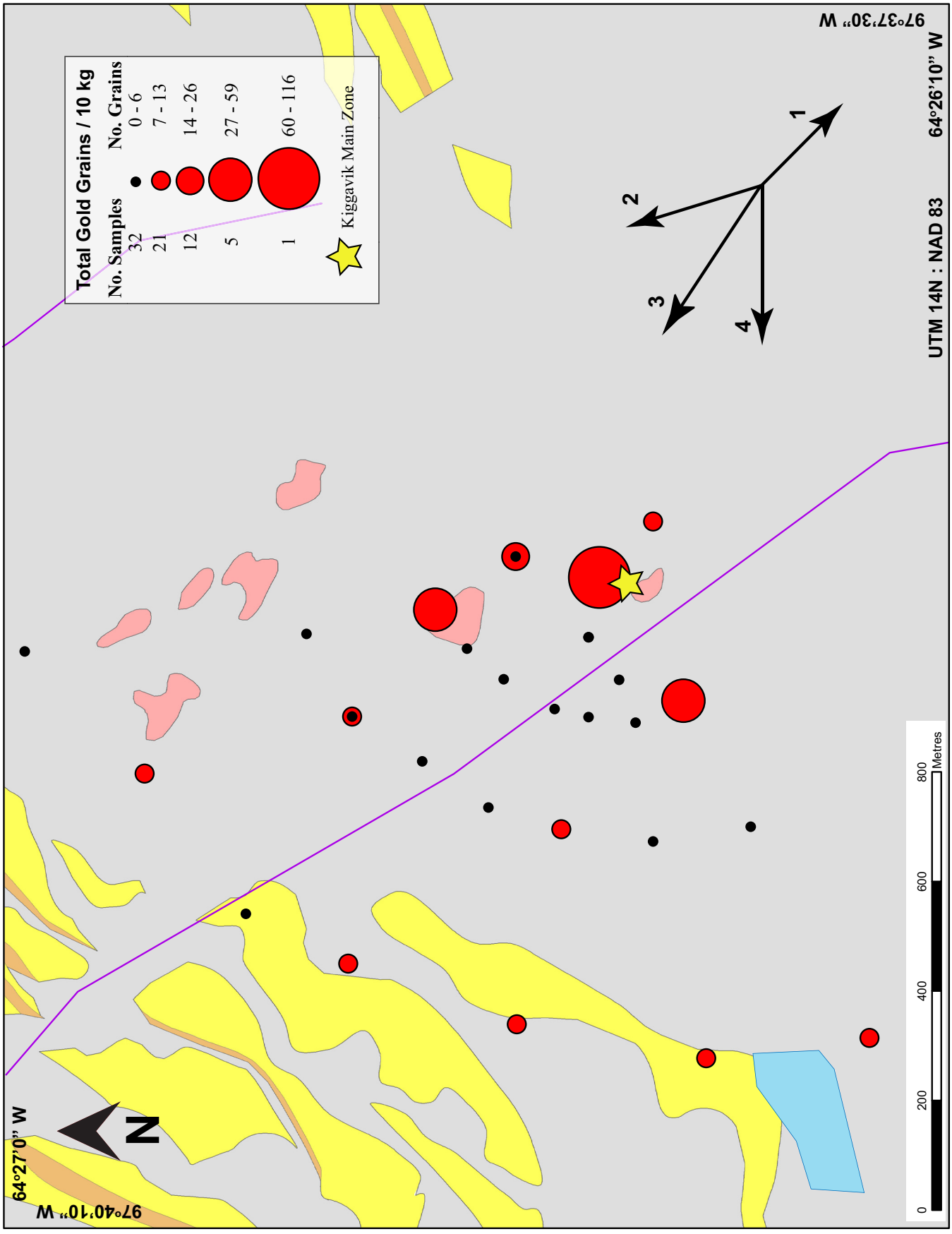

Appendix H3 continued.

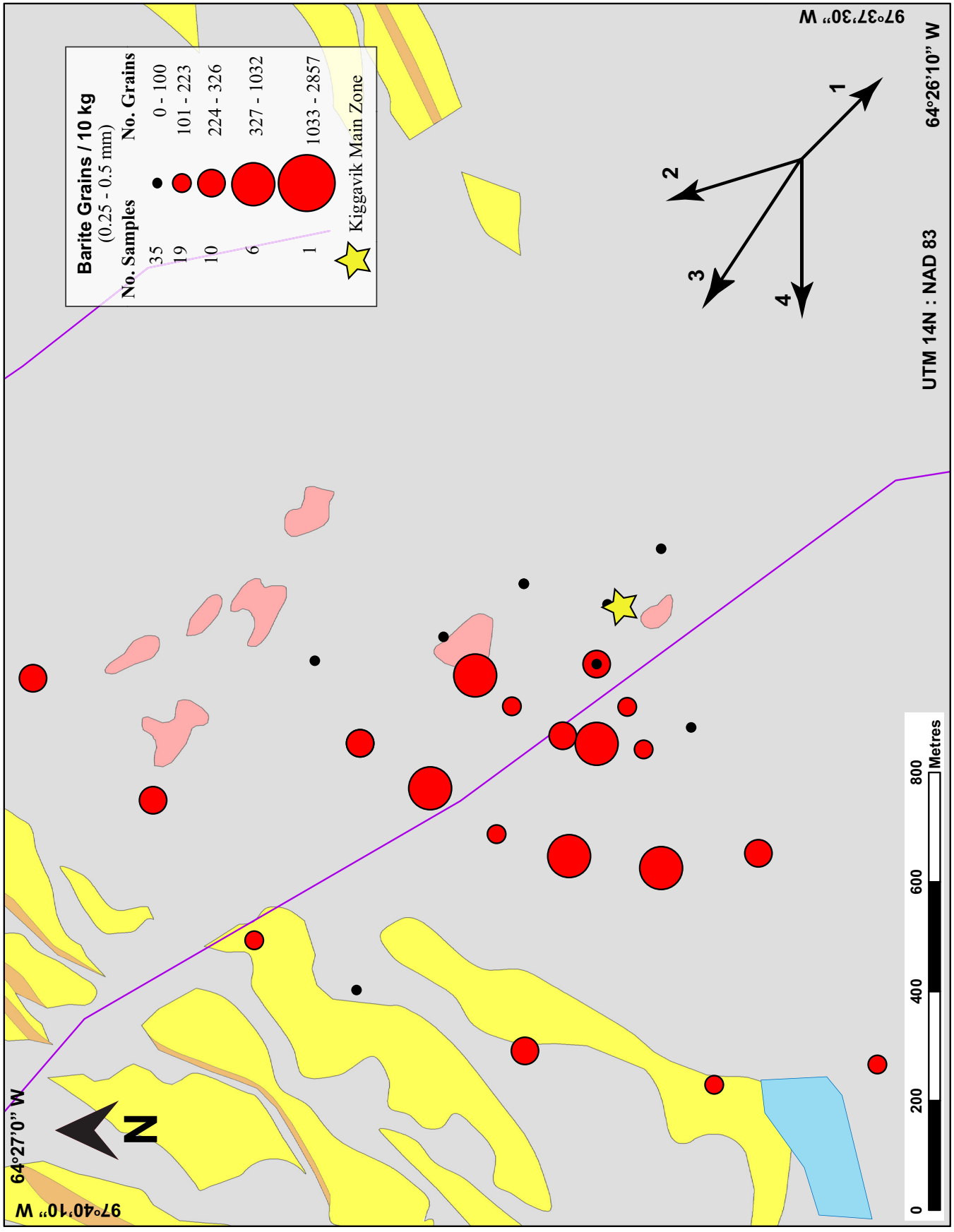

Appendix H3 continued.

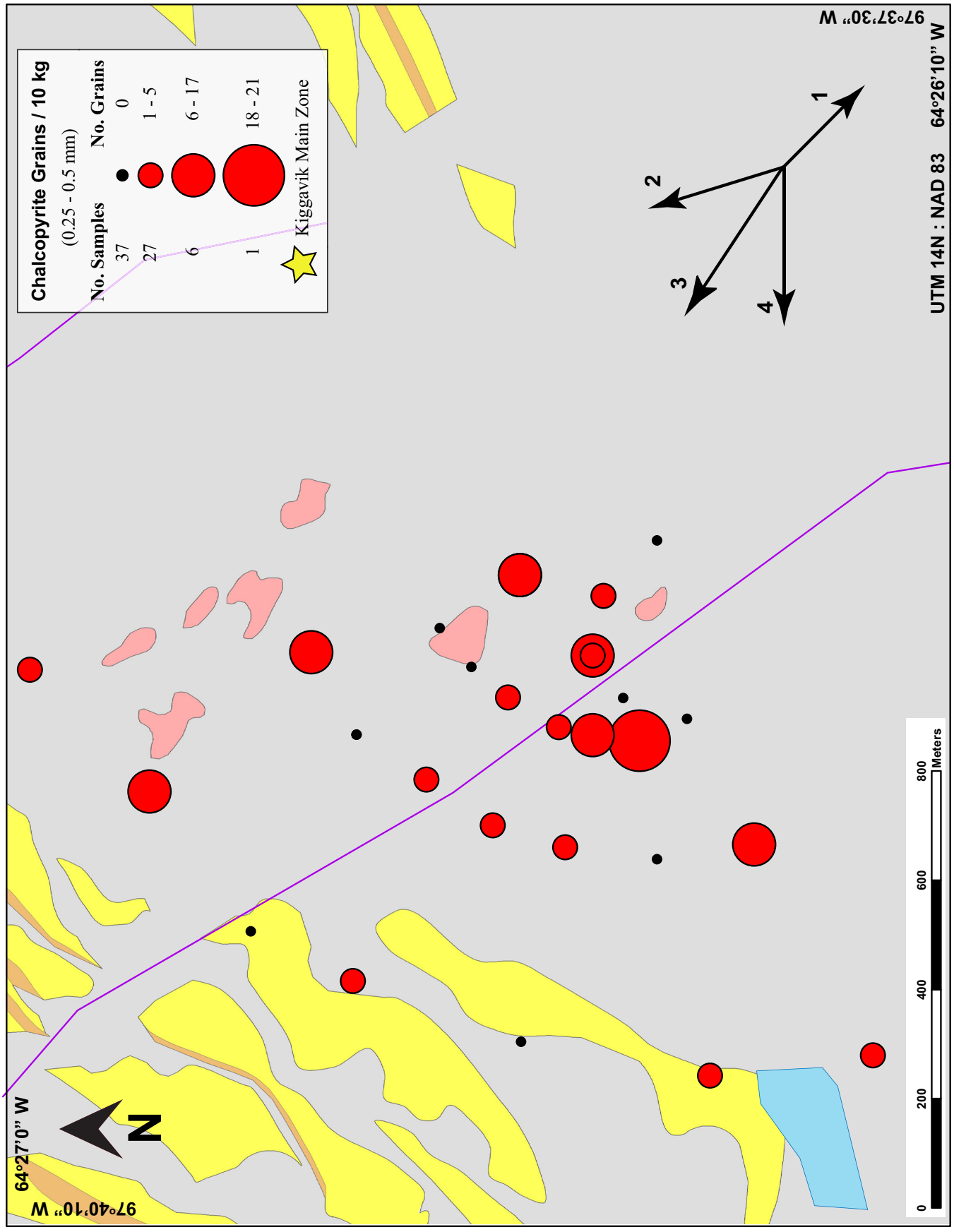

Appendix H3 continued.

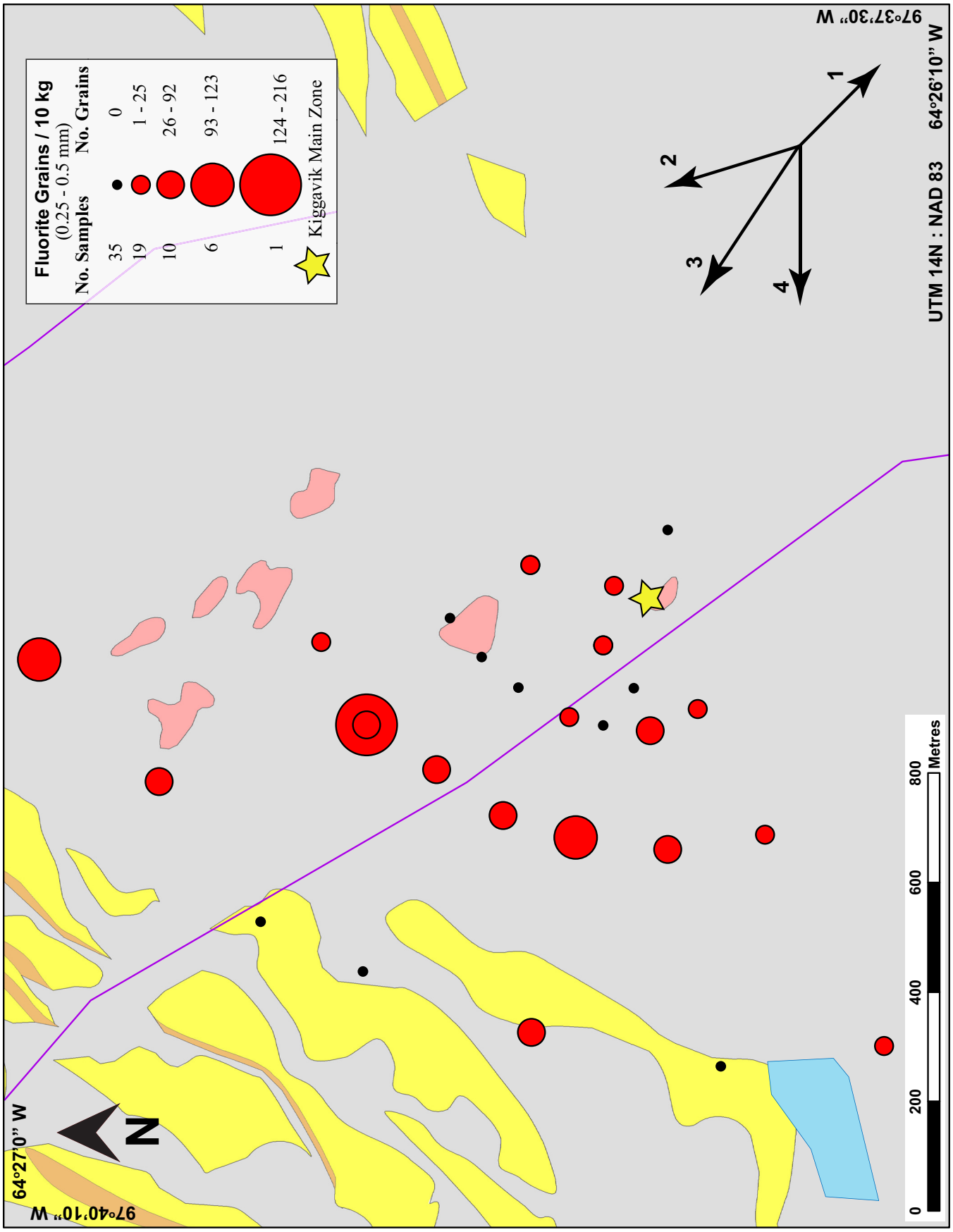

Appendix H3 continued.